Pipeline Defect Growth Prediction and Risk-based Integrity Management

by

Mingjiang Xie

A thesis submitted in partial fulfillment of the requirements for the degree of

Doctor of Philosophy

Department of Mechanical Engineering
University of Alberta

Abstract

Pipelines have been used for several decades, and threats such as corrosion, fatigue crack and erosion increase the danger of leak or rupture. Faulty pipelines could lead to very expensive downtime and environmental damage. Therefore, it is essential to have effective ways to monitor, evaluate and assure the integrity of the pipeline, reduce the risk of leaks and rupture, and subsequently prevent hazards for the environment and population. In-line inspections (ILI) are performed periodically using smart pigging tools to detect pipeline defects such as corrosion and cracks. Significant advances are needed to accurately evaluate defects based on ILI data, predict defect growth and optimize integrity activities to prevent pipeline failures, and pipeline integrity management has drawn extensive and growing research interests.

The aim of this thesis is to develop effective prognostics and risk-based management methods for performing inspection and maintenance activities for pipelines with crack or corrosion defects. This thesis starts with developing an efficient integrated methodology, and finally leads to more accurate predicted failure time distributions, better risk management, and consequently more effective pipeline integrity management system. This thesis provides a comprehensive review and fundamental knowledge on pipeline integrity management based on ILI data. Physics-based models and data-driven methods for predicting defect growth for pipelines with different categories of defects are discussed. Models and methods for risk-based integrity management are reviewed in this thesis.

In the more advanced prognostics strategy, an integrated prognostics model for a pipeline with fatigue crack is proposed to make a better prediction. Rainflow counting method is employed in the proposed method for analyzing time-varying loading conditions of pipelines. We use a

Canadian pipeline operator's field data to demonstrate the effectiveness of the proposed integrated approach. And the proposed method provides more accurate pipeline remaining useful life prediction compared to the traditional physics-based method.

Studies are performed on improving risk-based maintenance strategies, which are currently widely adopted in pipeline industry. A simulation-based approach is developed for cost evaluation for pipelines with corrosion defects. The probability of failure (PoF) threshold is used as input random variable instead of fixed inspection interval. The uncertainties from multiple sources are considered here to make a better and more realistic prediction and that support decision making in industry. Examples are given to illustrate the proposed approach, and parametric studies are performed. The proposed method provides less cost rate results compared to the traditional fixed interval method.

It is also important to determine the impact of ILI tool specifications on pipeline risks and costs, and thus recommend optimal integrity assessment and risk mitigation activities. By investigating the effect of ILI tool uncertainties on life-cycle costs and re-assessment results, suggestions for future improvement of ILI crack detection tools can be given. The effect of ILI tool uncertainties on re-assessment results for pipelines with crack defects is investigated. The long-term run scenario is also investigated considering crack initiation mechanism and probability of detection during each simulation run. Examples are used to illustrate the proposed approach, and sensitivity analysis is performed.

The research in the thesis provides innovative methods for defect growth prediction and risk-based management in the pipeline industry. The developed approaches will contribute to preventing pipeline leak and rupture, unnecessary expensive downtime, and environmental threats.

Preface

This thesis is an original work by Mingjiang Xie. The research topics have been published or submitted for publication under the supervision of Dr. Zhigang Tian. The journal papers and conference papers are with Mingjiang Xie as the lead author and Dr. Zhigang Tian as the corresponding author. Mingjiang Xie was responsible for literature review, methods generation, experimental studies, and results analysis. Dr. Zhigang Tian was involved with manuscript composition and concept formation.

Section 2.1 has been published as Mingjiang Xie and Zhigang Tian. "A review on pipeline integrity management utilizing in-line inspection data". Engineering Failure Analysis. Vol. 92, pp.222-239, 2018 [1].

Chapter 3 has been published as Mingjiang Xie, Steven Bott, Aaron Sutton, Alex Nemeth, and Zhigang Tian. "An integrated prognostics approach for pipeline fatigue crack growth prediction utilizing in-line inspection data". ASME Journal of Pressure Vessel Technology. Vol. 140, No. 3, pp. 03170 (10 pages), 2018 [2].

Chapter 4 has been published as Mingjiang Xie and Zhigang Tian. "Risk-based pipeline re-assessment optimization considering corrosion defects". Sustainable Cities and Society. Vol. 38, pp. 746-757, 2018 [3].

Chapter 5 brings up a submitted journal paper and a conference paper. The journal paper is Mingjiang Xie, Zhigang Tian, Jeff Sutherland, Bingyan Fang, and Bill Gu. "A method to analyze the impact of in-line inspection accuracy on integrity management program planning of pipelines", manuscript completed and under the final review of the co-authors. The conference paper is Mingjiang Xie, Zhigang Tian, Jeff Sutherland, Bingyan Fang, and Bill Gu. "A method to

analyze the impact of in-line inspection accuracy on integrity management program planning of pipelines". 2018 12th International Pipeline Conference. American Society of Mechanical Engineers. pp. V001T03A051-V001T03A051, 2018 [4].

Acknowledgements

First of all, I would like to thank my supervisor, Dr. Zhigang Tian for his constant encouragement, care and guidance through all my Ph.D. study. His great patience and continuous support made my Ph.D.'s study completed in a relaxed and enjoyable atmosphere. I am also very grateful for the valuable academic training and enthusiasm from him. I would also like to thank my supervisor committee members, Dr. Ming J. Zuo and Dr. Ben Jar for their kindness, guidance, and support. And I would like to express my gratitude to Dr. Ming J. Zuo for his help in my career and research studies. I wish them the best in their whole life. I sincerely thank the rest of my Ph.D. examining committee members, Dr. Ahmed Qureshi, and Dr. Jie Liu, for providing their precious time to review and examine my thesis.

Secondly, I am grateful to research fellows in our group for their advice, support, and assistance. I have enjoyed the days and nights we spent together. I wish them all the best and happiness in their whole life.

Finally, I would like to thank my parents for their endless love and support. Their love helped me a lot during the process of my graduate study. I also would like to thank my wife, for her encouragement. Thank her for accompanying and supporting me along the way.

Table of Contents

List of Tables

List of Figures

List of Acronyms

AFOSM	Advanced First Order Second Moment Method
ANN	Artificial Neural Network
API	American Petroleum Institute
ASME	American Society of Mechanical Engineers
CR_{Insp}	Inspection Cost Rate
CR_{Total}	Total Cost Rate
CBM	Condition Based Maintenance
CVN	Charpy V-Notch
EC	External Corrosion
EMAT	Electro Magnetic Acoustic Transducer
ET	Eddy currents Testing
FAD	Failure Assessment Diagram
FE	Finite Element
FFS	Fitness-For-Service
FORM	First Order Reliability Method
FOSM	First Order Second Moment
HPP	Homogeneous Poisson Process
IC	Internal Corrosion
ID	Inside Diameter
ILI	In-Line Inspection

LCC	Life Cycle Cost
LMS	Least Mean Square
LSF	Limit State Function
MC	Monte Carlo
MCMC	Markov Chain Monte Carlo
MFL	Magnetic Flux Leakage
MOP	Maximum Operating Pressure
NDE	Non-Destructive Examination
NHPP	Non-Homogeneous Poisson Process
O&M	Operation and Maintenance
PDAM	Pipeline Defect Assessment Manual
PHM	Proportional Hazard Model
PIM	Pipeline Integrity Management
PoD	Probability of Detection
PoF	Probability of Failure
PoI	Probability of Identification
RBM	Risk-Based Management
RBIM	Risk-Based Integrity Management
RUL	Remaining Useful Life
SCC	Stress Corrosion Cracking
SIF	Stress Intensity Factor
SMYS	Specified Minimum Yield Strength

S-N	Stress-life
SVM	Support Vector Machine
UT	Ultrasonic Testing
WT	Wall Thickness
PV	Present Value

List of Symbols

σ_f	Flow stress
σ_H	Nominal hoop stress
σ_u	Ultimate tensile strength
σ_y	Yield strength
σ_{ILI}	Standard deviation of ILI measurement error
a	Crack length
A_c	Cross-sectional area of the Charpy impact specimen
C	Material parameter in Paris' law
C_v	Upper shelf CVN impact toughness
C_{in}	In-line inspection cost
C_{ev}	Excavation cost
C_{rc}	Recoating cost
C_{rs}	Sleeving cost
C_f	Failure cost
C_{af}	Additional fixed cost
CR(PoF)	Total cost rate with a given PoF threshold
CR_{Insp}	Inspection cost rate
CR_{Total}	Total cost rate
da/dN	The fatigue crack growth rate
d	Crack depth

d_0	Initial crack depth
d_c	Critical crack depth
D	Outside diameter
K_a	Stress intensity factor at the surface point
K_b	Stress intensity factor at the depth point
K_{max}	Maximum stress intensity factor (SIF)
K_{min}	Minimum stress intensity factor (SIF)
L_0	Initial crack length
L	Crack length
m	Material parameter in Paris' law
N	The number of simulation iterations
N_f	The number of features exceeding the failure criteria
N_i	The number of cycles to initiate a crack
N_p	The number of cycles to propagate to the failure state
n_{corr}	The number of correct identification features
n_{rep}	The number of reported features
n_{incorr}	The number of incorrect identification features
n_{unrep}	The number of unreported features
T_0	Last inspection time
T	Inspection time
t	Wall thickness
PF_{defect}	Defect failure probability

PF_{pipe}	Pipeline failure probability
P_{op}	Operating fluid pressure
P_{f}	Failure pressure
PoF_{a}	Acceptable PoF threshold
p	Internal pressure
PV_t	Net present value of total cost at time t
PV_{insp}	Net present value of inspection cost
PV_{repl}	Net present value of replacement cost
PV_{fail}	Net present value of failure cost
PV_{main}	Net present value of maintenance cost
PV_{fixed}	Net present value of additional fixed cost
r	Discount rate
V_{a}	Axial corrosion growth rate
V_{r}	Radial corrosion growth rate
WT	Wall thickness

1 Introduction

1.1 Background

Thanks to the advantages of safety, efficiency and low cost, pipelines are widely used in transporting large quantities of oil and gas products over long distances. According to the Canadian Energy Pipeline Association (CEPA), 94% of the refined petroleum products, and most of the Canadian oil and gas exports were transported by pipelines [5]. Pipelines are subject to different types of defects, such as fatigue cracking, corrosion, etc. [6], [7], [8]. Fatigue cracking refers to crack growth due to fatigue caused by pressure cycling during pipeline operations. And corrosion defects are the most common ones existence in pipelines. Without proper remediation actions, these defects can eventually result in pipeline failures including leaks or ruptures, which lead to public safety issues, i.e. a release of pipeline contents to the environment, and expensive downtime. There are many pipeline incidents every year around the world, and three of the North America pipelines incidents in 2016 resulted in over 2,000 metric tons of oil and gas leak and spill. Integrity is the top priority for pipeline operators to ensure reliable and safe operations of pipelines, to increase productivity, reduce cost, prevent damage to the environment, support future projects, etc. It is essential to find effective ways to monitor, evaluate and assure the integrity of the pipeline, and reduce the risk of leaks and rupture.

For pipelines, we need to ensure safety, security of supply and compliance with relevant codes and legislation. Procedures and practices are implemented to protect, manage and maintain the integrity of pipeline systems. Due to the significant severity of pipeline failures, the core of pipeline integrity management is to keep pipelines in safe operating conditions. Pipeline integrity

tools are developed to improve business performance, manage risks as well as ensure compliance. Proper pipeline integrity management can reduce both the probability and consequences of failure and increase the pipeline companies' benefits, by properly assessing and managing the defects. Pipeline integrity program monitors and predicts defects and thus adjusts when, where, how, and what actions need to be taken, such as inspection, maintenance and repair. A good pipeline integrity program should be able to manage risk successfully, prevent failure from occurring, control damage effectively, and reduce the overall cost.

A pipeline integrity program generally consists of three major steps:

(1) Defects detection and identification, to obtain defect information through inspection, monitoring, testing and analysis techniques.

(2) Defect growth prediction, to predict defect growth based on damage prediction models and the collected data.

(3) Risk-based management, to recommend optimal inspection, maintenance and repair policies and activities.

Defect information is collected using detection and identification tools. Pipeline companies can gather defect information through walking along the pipelines by technical personnel, hydrostatic testing, in-line inspection (ILI), nondestructive evaluation (NDE), etc. ILI tools are currently the most widely used inspection technology for detecting and inspecting various types of pipeline defects. ILI runs are performed periodically using smart pigging tools to detect defects and evaluate pipeline health conditions. In this thesis, only ILI tools will be discussed and other detection techniques will not be covered. Defect growth prediction is to predict defect growth and when a pipeline failure will occur. There are different kinds of threats to pipeline integrity, such as metal loss, cracking, dents, third party damage, weld, etc. Study on different defect prediction

models is the foundation of effective integrity management. The last step, risk-based management, will determine proper inspection intervals, and maintenance and repair actions. The management models will also influence the first step and the second step by possibly changing the inspection actions and defect status. The aim of an integrity program is to achieve accurate defect prediction and balance the reliability and costs in an effective way.

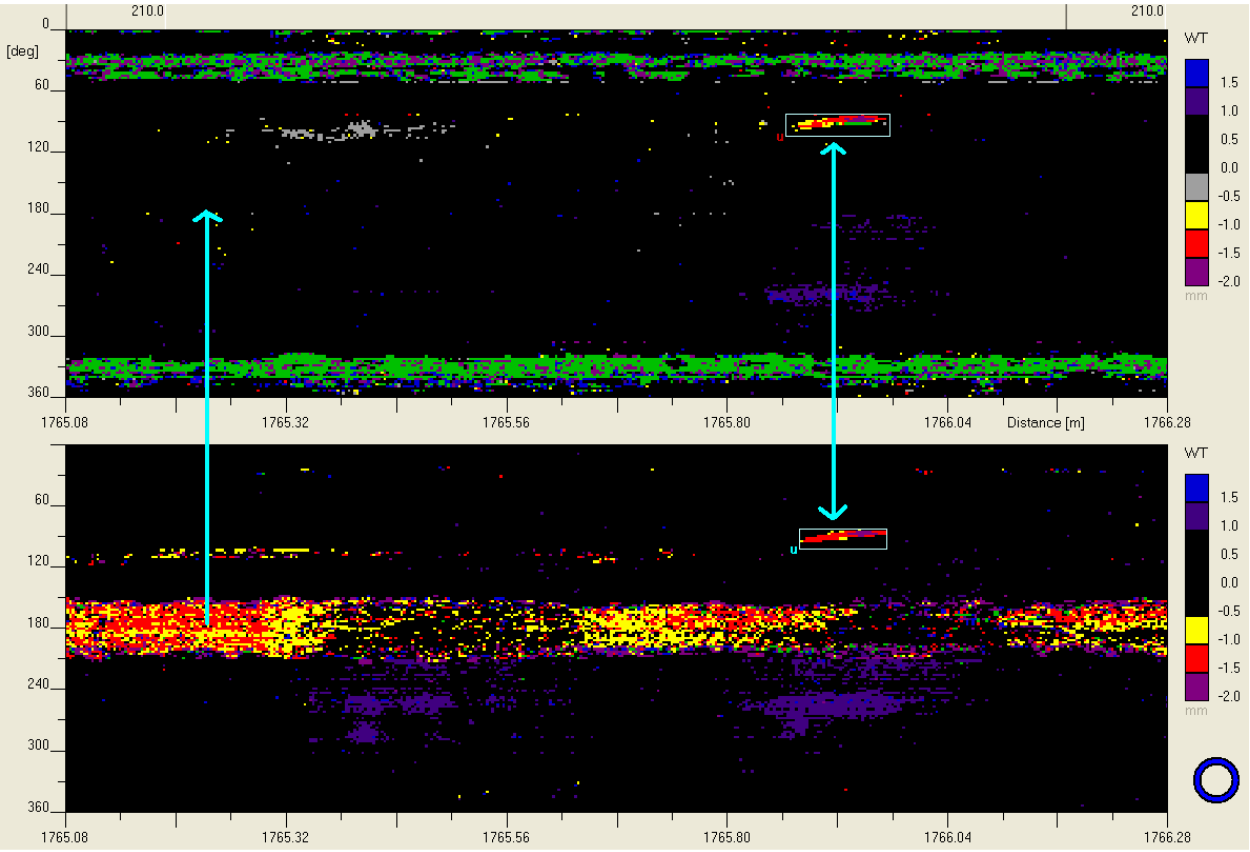

Figure 1.1 A sample screenshot of analyzing corrosion ILI raw data using software PIXUS [9]

Figure 1.1 shows a sample screenshot of analyzing corrosion ILI raw data using software PIXUS [1]. The left blue arrow shows that channeling corrosion has newly developed. And the right arrow indicates a metal loss. Based on this ILI raw data, we could obtain an ILI report. This

ILI report should include a list of corresponding metal loss features. For each defect, it must contain the following items: a) defect location in distance and orientation; b) defect size in width, length and depth. ILI can report defect size in two different types, as shown in Table 1.1. ILI data reported in wall thickness bins in Table 1.1 (a). The defect depth bin is shown as the percentage of the pipe wall thickness (*WT*) Measurement tolerance is 0.5mm on either side of the bin range. And this type of ILI report does not provide discrete depths. The upper bound is normally used for other analysis. And Table 1.1(b) shows the flaw measured properties, we can directly use the defect information to do further analysis.

Table 1.1 An ILI report example

(a) Type 1

Date	ILI *WT* (mm)	Length (mm)	Depth bin (%*WT*)
July 2002	7.5	60	12.5-25%
July 2005	7.5	62	25-37.5%

(b) Type 2

Date	ILI *WT* (mm)	Length (mm)	Peak depth (mm)
July 2002	7.5	60	1.84
July 2005	7.5	62	2.36

Pipeline defect and reliability assessment is a key step to assess the current and future condition of the pipeline with defects. And based on integrity planning strategies, one can make decisions like when to perform the next inspection or when to optimally mitigate potential threats. Defect assessment and management for pipelines is a key part of pipeline integrity management,

and there has been extensive research into this field. A review of pipeline integrity management methods and models utilizing ILI tools was conducted in Ref. [1]. In-line inspection (ILI) tools are developing rapidly these days and are widely used to detect defects in pipelines. The inspection results contain information about types, locations and dimensions of anomalies and they serve as the basis for assessing pipeline system's current condition.

Some reported studies considered the design stage as a part of the pipeline integrity management process [10], [11]. It is true that pipeline integrity management is a life-cycle approach which involves the design phase, and better design practices typically lead to better pipeline integrity assurance. Study on behaviors of different threats in pipelines as well as inspection and maintenance activities can also give a good feedback to the pipeline design stage. Bai and Bai [12] introduced life-cycle cost modeling for the design stage of pipeline integrity management. In this thesis, though, we will not cover the pipeline integrity design stage, and will focus on detection, prediction and management methods and models during the operation stage.

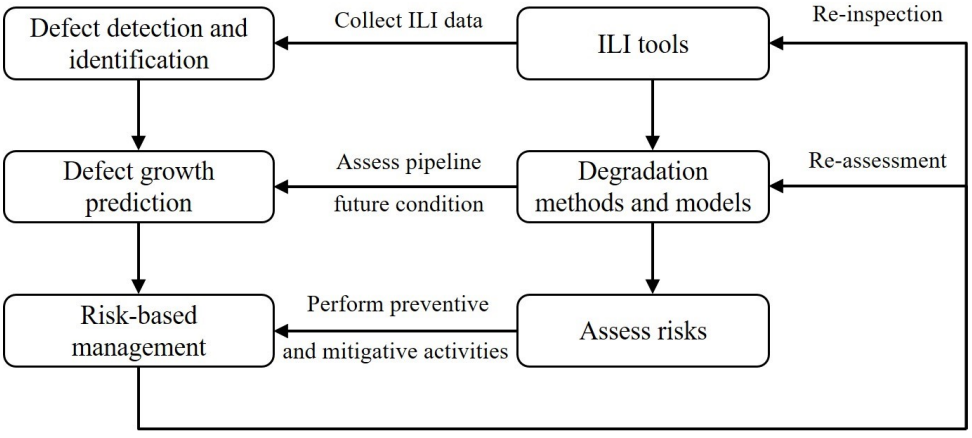

Figure 1.2 A flowchart for a pipeline integrity management program

A flowchart for a pipeline integrity program is shown in Figure 1.2. These main parts included in Figure 1.2 are all critical for preventing pipeline failures and unnecessary downtime. Due to the existence of relatively large measurement error in ILI detection tool, there is a need to make a more accurate defect growth prediction and more effective risk-based management with the consideration of ILI measurement error. With the use of a more accurate prognostics model, we could better assess the current and future condition of pipelines, thus prevent unexpected failure. Then, with the input of reliability assessment, risk-based management can be performed to determine the re-inspection and re-assessment interval. A more effective risk-based management method can result in a better decision on when to perform next ILI tool run. Consequently, we could avoid unnecessary digs and downtime while also ensuring safe operation of pipelines.

1.2 Research motivations

As mentioned in the previous section, it is essential to ensure the integrity of pipelines in pipeline industry. The consequences of accidents in pipelines could be catastrophic to the public and environment. Therefore, the failure probability of pipelines with different kinds of defects is an issue of high concern. These defects need to be managed well. Meanwhile, unnecessary digs could cause unnecessary shutdowns of pipelines, and lead to loss of oil and gas supply and high economic loss. Therefore, we need to try to reduce unnecessary expensive downtime while also ensuring the safety of pipeline operation.

Among these threats to pipeline integrity, fatigue cracks and corrosion defects are two kinds of critical threats. For corrosion and crack defects, the nature of mechanisms are time-dependent. With the use of suitable damage propagation model, the probability of failure can be estimated for

pipelines with particular types of defects. Fatigue cracking is a key type of defect for liquid pipelines, and managing such fatigue cracks continues to be a top priority amongst pipeline integrity management. However, existing ILI tools have relatively large fatigue crack measurement uncertainties, and typically have a specification of about plus/minus 1 millimeter, 80% of the time [6], [13]. Furthermore, currently physics-based methods are mainly used for fatigue crack growth prediction, based on crack growth models governed by the Paris' law [13], [14]. The uncertainty in crack sizing and the Paris' law model is propagated to the predicted time of failure due to fatigue cracks, resulting in large uncertainty which requires a conservative management integrity management approach and risk mitigation strategies, such as repairs, pipe replacement, pressure reductions and hydro-testing. There is an urgent need to develop accurate fatigue crack growth prediction tools, and reduce the uncertainty and conservatism in pipeline integrity management.

For pipeline fatigue crack grow prediction, existing pipeline defect prognosis methods are mainly classified into physics-based methods and data-driven methods [15]. A key disadvantage of the existing physics-based method is that typically the same fixed model parameters are used for all pipes. However, these material dependent model parameters should be different for different pipes, and slight differences in such model parameters can lead to large differences in fatigue crack growth predictions. Due to the measurement errors and cost of an ILI tool, data-driven methods do not work well if the number of ILI tool runs and the amount of data are not sufficient. In this way, there is an urgent need to develop a new method for pipeline defect grow prediction.

Corrosion is the most common integrity threat to oil and gas pipelines. Risk analysis for metal loss corrosion defect is a vital part of pipeline integrity management. Risk is typically defined as the multiplication of probability and consequence, and it can be used as a reliability measure for

pipeline systems. A minimum total cost is expected to achieve while pipeline reliability needs to be larger than its predetermined target to avoid failure damage and unnecessary downtime. This is a tradeoff between reliability and cost. A more accurate cost evaluation policy and cost optimization are also needed. Inspection and maintenance actions are taken for pipeline reliability and safety assurance. As mentioned above, ILI is a typical inspection method for evaluating pipeline conditions and defect sizes using in-line inspection tools such as magnetic flux leakage tools and ultrasonic tools. Repair actions can be taken based on inspection results. Risk-based management policies and models of pipelines with corrosion or crack defects need to be built considering potential activities such as inspection and maintenance actions and uncertainties from many possible sources such as ILI measurement error. It is important to optimize inspection and maintenance activities to improve reliability, reduce risks and minimize the overall costs.

Currently, for pipeline integrity management, the optimal inspection interval is fixed and constant during the whole pipe service time once it is determined. However, pipelines with different defect sizes at the current inspection point lead to different future defect growth and system failure probability, and it is more reasonable to apply different re-assessment intervals depending on pipeline health conditions. Besides, various uncertainty sources such as ILI measurement error need to be considered when making decisions on pipeline integrity management. Therefore, new approaches for cost evaluation and re-assessment interval determination are needed for pipelines subject to corrosion or crack defects. Better risk-based integrity management methods for pipelines with corrosion or crack defects need to be proposed.

A pipeline integrity management program is greatly affected by integrity planning methods and ILI tool performance. In integrity management program planning, inspection and maintenance activities are in common practice, determined from risk and integrity assessment practices with the

objective to reduce risk and effectively exceed a reliability target for the safe operation of the pipeline. An effective integrity planning method can address the most significant risk and optimize operational and maintenance costs. To investigate the perception of large measurement errors in ILI crack detection tools, we need to express value in practical terms for a pipeline integrity program. In this way, it is important to establish a method that addresses reliability targets for the safe operation of pipelines while also addressing operational and maintenance costs. Investigations on the impact of ILI tool accuracy on integrity planning programs would provide a valuable aid in developing more advanced ILI tools and a better understanding of a pipeline integrity program.

1.3 Research scope

Overall, the objective of this thesis study is to develop effective prognostics methods and risk-based management models for pipelines with crack or corrosion defects. Based on the above-mentioned challenges, this Ph.D. thesis study aims to achieve the following specific research objectives:

(a) To propose a comprehensive prognostics model for pipelines with fatigue cracks by integrating physics models and ILI data, providing a valuable aid in more accurate prediction.

(b) To construct effective risk-based models and policies for performing inspection and maintenance activities for pipelines with corrosion or crack defects.

(c) To analyze the impact of ILI tool accuracy on integrity planning programs of pipelines with fatigue cracks.

First of all, a comprehensive review on pipeline integrity management utilizing ILI data is given. Then, prognostics methods for pipelines with fatigue cracks or corrosion defects need to be improved to make a more accurate prediction. After reliability assessment, policies and models for risk-based integrity management can be given. Different uncertainty sources are considered for the prediction models. In this way, more realistic decisions on when to perform next ILI run can be given. And the perception of large measurement errors in ILI crack detection tools can then be analyzed by investigating the impact of ILI tool accuracy on integrity planning programs. Overall, it is expected that a more accurate prognostics model and risk-based management models will contribute to make better decisions regarding when to do the reinspection and re-assessment. And my thesis research will bring major economic, environmental and social benefits to the pipeline industry.

Specifically, three research topics of the thesis are proposed in Figure 1.3. The first row of Figure 1.3 belongs to the area of remaining useful life (RUL) prediction for pipelines with fatigue cracks and corrosion defects. And the second row belongs to risk-based integrity management (RBIM) for pipelines of fatigue cracks and corrosion defects.

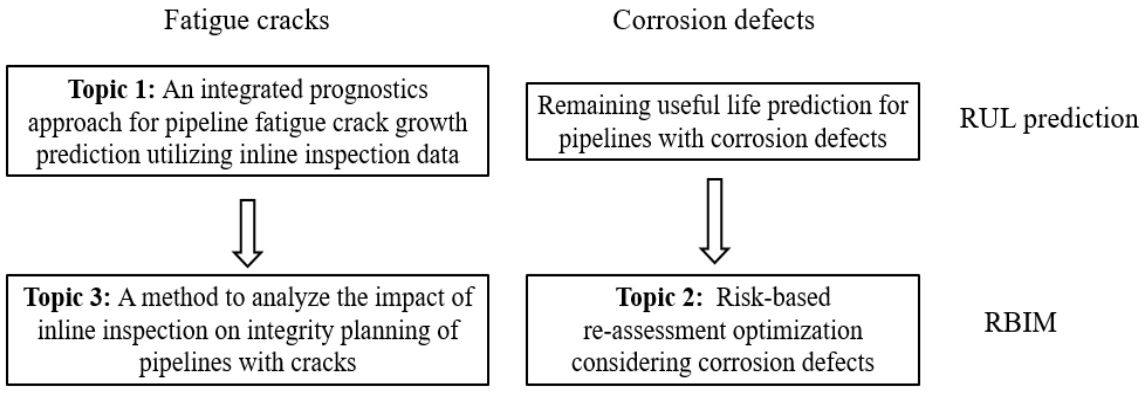

Figure 1.3 Outline of research topics

In the first research topic, an integrated prognostics method is proposed for pipelines with fatigue cracks. Time-varying loading conditions of pipelines are analyzed by using rainflow-counting method. A simulation example is introduced to demonstrate the effectiveness of the proposed method considering the growth on both crack depth and length. And field data provided by a Canadian operator is employed to compare with the traditional physics-based method.

In the second research topic, a simulation-based approach is proposed to determine the optimal inspection interval for pipelines with corrosion defects. This proposed approach is developed for a given re-assessment policy defined by the PoF threshold. The remaining useful life prediction for pipelines with corrosion defects is performed first considering uncertainties from multiple sources including pipe geometry, mechanical properties, growth rates, ILI measurement error, etc. In this way, a more realistic decision can then be made based on RUL prediction results. Multiple examples are given to illustrate the effectiveness of the proposed approach by comparing with fixed interval methods. Sensitivity analysis is performed for several important parameters including growth rates, initial depths, failure cost, ILI tool measurement error, etc.

In the third research topic, a method is proposed to analyze the impact of in-line inspection on integrity planning of pipelines with fatigue cracks. A simulation-based cost evaluation approach is developed with a certain reliability target given. Then, we investigate the impact of ILI tool accuracy on the cost-effectiveness of an integrity planning program. We also investigate the impact of the use and selection of non-zero discounted cash rate and two different inspection cost assumptions. The long-term cost rates are also calculated for the investigations. The crack defects

initiation mechanism and the probability of detection are introduced for the simulation. And parametric analysis is performed at last.

These methods are proposed to make contributions to the pipeline industry by preventing unexpected failures and unnecessary downtime, thus reducing the total life-cycle costs.

1.4 Thesis organization

The thesis is prepared following the guidelines from the Faculty of Graduate Studies and Research (FGSR) at the University of Alberta. The thesis, with six chapters, is organized as follows.

Chapter 2 gives a comprehensive literature review and background knowledge on methods and models in the area of pipeline integrity management. This chapter also devotes to presenting fundamentals of ILI tools, pipeline defect growth prediction and risk-based management for pipelines with defects in the thesis. The materials have been published in a journal paper [1].

Chapter 3 proposes an integrated prognostics method for pipelines with crack defects. Rainflow counting method is employed for analyzing time-varying loading conditions of pipelines. Field data provided by a Canadian pipeline operator is used to validate the effectiveness of the proposed approach. The results of this chapter are published in a journal paper [2].

Chapter 4 presents a simulation-based cost evaluation approach for a given re-assessment policy defined by PoF threshold for pipelines with corrosion defects, which particularly considers uncertainties from different sources to make a better and more realistic decision. The contributions of this chapter are documented in a published journal paper [3].

Chapter 5 investigates the effect of ILI tool uncertainties on re-assessment results for pipelines with crack defects. Different cases are discussed and compared with the consideration of discount

rate, inspection cost assumption, and pressure, etc. The results of this chapter are published in 12th International Pipeline Conference [4] and the manuscript is completed and under the final review of the co-authors for possible journal publication.

Chapter 6 summarizes the contributions of this thesis. Several possible future works are also discussed.

2 Literature review and background knowledge

2.1 Literature review

Pipeline integrity management has drawn extensive and growing research interests, and a large number of studies have been published in conference proceedings and academic journals on methodologies, models and applications. This chapter reviews the research studies on pipeline integrity management based on ILI data, with an emphasis on models and methods developed for more effective defect detection, prediction and management. In this literature review, this section gives more comprehensive and detailed discussions on the methods and models used in the pipeline integrity management framework, and provides an overview on strategies for inspecting, predicting and managing all major pipeline threats. Pipeline integrity management framework and some related case studies were also presented in [16]–[20]. Legal issues and demands for pipeline integrity programs were discussed in [21]. Pipeline integrity management guidelines are developed by American Petroleum Institute (API) [22], which conducts studies on petroleum industry and provides standards for oil and natural gas industry.

2.1.1 In-line inspection tools for defect detection

Due to possible pipeline leakage, environmental damage and high costs of repair and replacement, accurate pipeline monitoring and inspection becomes essential these days. Finding and recording data about pipeline integrity is the first step in pipeline integrity management, and there are a variety of ways to gather information about defects. Varela et al. [23] briefly summarized major methodologies, which are not limited to ILI tools, that are utilized for monitoring and inspecting

external corrosion of pipelines and discussed the pros and cons of major inspection tools. For external corrosion as well as other types of threats, there are various inspection techniques to record data on the defects. Pipeline inspection techniques include potential survey techniques, ILI tools, hydrostatic tests, tools for inspecting non-piggable pipelines like pipeline crawlers, etc. These pipeline inspection techniques were briefly introduced in [24], [25]. ILI tools will be focused on in this thesis.

A high-tech smart pigging device is utilized for in-line inspections, which is inserted in the pipeline and typically pushed through the pipe by the fluid flow from one compressor station to another. Such a smart electronic device is known as a smart pig in pipeline industry. This sophisticated electronic device is essentially a robotic computer that gathers all specific information related to the health condition of the pipeline. The ILI tools can classify the types of defect and their attributes including orientation of defects, size (length, width, depth) and specific location (Internal/External) of the defects [18]. In-line inspection tools can also evaluate pipeline integrity in geohazard areas by mapping techniques [26]. How to get high-quality reports from ILI data was introduced in [27].

Depending on the types of flaws they can detect, ILI tools can be classified as metal loss tools, crack tools, geometry detection tools, etc. Metal loss defects reported from an ILI inspection can be categorized into two main types: pressure based and depth based defects [18]. With depth based defects such as pitting, a pipeline is typically considered failed when the defect depth reaches 80% of the pipe wall thickness in industry, if there are no other specific rules such as NG18, even though sometimes the pipeline doesn't show any failure behavior. For pressure based defects such as corrosion defects, failure is determined by the failure pressure, the model uncertainty and the safety factor [18].

After gathering relevant data through ILI tools, data processing needs to be performed to minimize data errors and extract useful information. There are a variety of signal processing techniques and algorithms for different types of ILI tools. In the following subsections, signal processing technologies and models will also be reviewed for different ILI tools.

2.1.1.1 In-line inspection technologies

With the rapid improvement of signal processing technologies, the accuracies of defect profiling, sizing and mapping and ILI tool performance keep improving. And that leads to more cost-effective decisions on pipeline integrity management. A variety of ILI technologies are widely used in the pipeline field, such as Magnetic flux leakages (MFL), Ultrasonic (UT) tools, Electromagnetic acoustic transducers (EMAT), Eddy currents testing (ET), etc. Cartz [28] presented a review of sensor technologies, and Varela et al. [23] discussed ILI technologies that can detect external defects. In the following subsections, main ILI technologies will be reviewed and compared.

2.1.1.1.1 Magnetic flux leakages (MFL)

The most widely used tools for in-line inspection of pipeline are MFL tools. This technology can detect different types of defects, such as missing material and mechanical damage, and it is particularly widely used for metal loss inspection in a pipeline integrity management program. MFL inspection tools detect pipeline defects by sensing a local change in a saturating magnetic field, which is generated by huge magnets. The center of the MFL tools is the magnetizer. Gloria et al. [29] presented the development of the magnetic sensor. Ireland and Torres [30] provided a

finite element modeling of a circumferential magnetizer under both moving tool and static conditions. The results showed that the magnetic field profile is very complicated and researchers need to pay more attention to studying it in order to further develop MFL tools. Various levels of sensitivity can be chosen based on the testing needs, such as low resolution (standard), high resolution and extra high resolution [28]. The higher the resolution of the MFL tools, the higher the detection capability, which also leads to smaller sensor spacing and higher confidence level of accuracy. But in industry, some companies used standard tools a lot because they believe they are sufficient, faster and cheaper. Kopp and Willems [31] presented a dipole model study of sizing capabilities of MFL tools. As the resolution getting higher, the number of sensors in the system gets bigger. Although it is the most common test and it can meet different testing needs, it may cause the permanent magnetization of pipe after being used and the restriction of the product flow.

Modern, high-resolution MFL inspection tools have the ability to provide very detailed signals. However, most of the MFL data can be easily influenced by various noise sources. To address this problem, many researchers proposed MFL sizing models and analyzed MFL sizing performance. Yeung et al. [32] discussed a technique to improve MFL ILI sizing performance and gave two case studies. Sometimes the sizing performance is more related to the shape of the defects and some sizing algorithms may give bigger sizing error due to the differences of the geometries. To address this problem, Miller and Clouston [33] proposed an MFL sizing model utilizing high-resolution NDE data to give better performance. Signal processing for MFL data is a key element in MFL inspection technique. The primary methods for MFL signal processing are wavelet transform, fast Fourier transform (FFT), Wigner distribution, etc. Mao et al. [34] gave a brief introduction to MFL signal processing, and they proposed to improve the defect recognition ability though integrating neural network, data fusion and expert system techniques. Saha et al. [35]

used wavelet transform to pre-process the raw radial MFL data. Kathirmani et al. [36] proposed a three-stage algorithm for the compression of MFL signals, that is practically feasible and fast. Mean Absolute Deviation, Principal Component Analysis (PCA) and Discrete Wavelet Transform (DWT) were utilized in stage I, II, III respectively. Adaptive algorithms were reported for the processing of MFL signals. Joshi et al. [37] and Afzal and Udpa [38] utilized adaptive wavelets to obtain and process MFL technique signals. Ji et al. [39] employed a fuzzy threshold filter algorithm with adaptive wavelets to process MFL data, and the errors of MFL signals were reduced compared with traditional wavelet transform. Carvalho et al. [40] utilized artificial neural networks (ANNs) to classify MFL signals into signals with defects and signals without defects, and classified the defect signals into external corrosion (EC), internal corrosion (IC), and lack of penetration (LP) with high reliability. Chen et al. [41] presented an empirical mode decomposition (EMD) based method for signal processing of MFL data. Mukherjee et al. [42] proposed a new algorithm of adaptive channel equalization for MFL signal to modify sensor imperfections, which could recover the signal successfully and minimize noises effectively.

2.1.1.1.2 Ultrasonic (UT) tools

Currently, ultrasonic is the most reliable in-line inspection technology compared with the other technologies. Ultrasonic inspection generates ultrasonic pulses of high frequency and short wavelength to detect defects or measure pipeline wall thickness. In general, ultrasonic tools give better results and defect accuracy than MFL. The types of flaws UT can detect include internal/external metal loss, cracking, wall thickness variations, etc. They are widely used for detecting stress corrosion cracking and many forms of corrosion. The corrosion penetration depth measurement detection capabilities of UT tools is around ±0.3 to ±0.6 mm [43], and for

longitudinal and circumferential resolution, it is around 3 mm and 8 mm, respectively. The confidence level is at around 95%, which is more reliable than MFL [44]. As UT crack detection tools require a liquid coupling medium to produce shear waves in the pipe wall, they can be only used for liquid transmission pipelines. As for gas pipelines, EMAT tools can be used instead of UT tools. Lei et al. [45] introduced the ultrasonic in-line inspection pig, which was used for corroded pipelines, and provided the introduction to design stage of the data acquisition system (DAS) as well as the off-line signal processing method. A latest generation of ultrasonic ILI tools was presented in [46], which had high inspection velocity and high resolution, and, as a result, production loss could be avoided and confidence level of inspection results could be improved. In addition, the reported tool generation could deal with higher temperature, higher pressure and bigger speed and wall thickness ranges. UT tools need to be further developed to give more integrity benefits. A brief overview and a case study on ultrasonic phased-array (USCD) technology for the Centennial pipeline stress corrosion cracking were given in [47]. A multilayer data-driven monitoring framework based on signal processing and machine learning techniques was introduced by Ying et al. [48]. Bo et al. [49] gave an introduction to an ultrasonic ILI system for pipelines.

Compared with other tools, UT gives reliable defect depth sizing and good repeatability, and it can deal with very small pipeline wall thickness. Compared with MFL tools, UT tools are also sensitive to a larger variety of features. However, UT tools have the drawback that they require liquid coupling between the pipeline and the transducer (pig), which as a result affects its applications in gas pipelines.

The ultrasonic signals collected by UT tools in pipelines are typically noisy. Effective de-noising techniques are needed to get accurate information regarding defects. The main signal

processing methods used for UT signals are wavelet transform [50], [51], ANNs [52], [53], fast Fourier transform (FFT), etc. Song and Que [50] developed a new technique based on wavelet transform for processing heavily noised ultrasonic signals for the purpose of band-pass filter to get better de-noising results. Martinez et al. [54] employed several digital processing techniques to improve the image quality. Ravanbod [55] employed fuzzy logic and neural networks to improve the algorithm for detecting corrosion defects using the ultrasonic testing technique. Ravanbod and Jalali [56] presented an acquisition system for ultrasonic images and proposed a fuzzy edge detection method. Compared with other methods, the proposed method performed better because it has a constant minimum edge contrast. Shakibi et al. [57] developed a signal processing scheme to increase the time resolution of an ultrasonic system. Cau et al. [58], [59] preprocessed UT signals with DWT, Blind Separation techniques or FFT to be used as input for neural networks models, to classify the information for defect detection. Chen et al. [60] fused the Morlet wavelet with the least mean squares (LMS) adaptive filter to process ultrasonic signals. Iyer et al. [61] also utilized both wavelet transform and neural networks to process ultrasonic signals. Saniie et al. [62] combined a neural network model with split-spectrum processing for ultrasonic target detection and characterization.

2.1.1.1.3 Electromagnetic acoustic transducers (EMAT)

Electromagnetic acoustic transducers (EMAT) are relatively new, and such a sensor consists of a coil at the internal surface of the pipe wall. EMAT generates ultrasound through Lorentz forces without requiring a coupling agent. EMAT is able to detect all kinds of cracks, weld characteristics and wall thickness variations. The mechanism of the EMAT inspection technique was described by Murayama et al. [63]. Salzburger et al. [64] gave a comparison between UT and EMAT and

provided a brief introduction to the development of the probe design. Tappert et al. [65] summarized the evolution of the EMAT techniques from 2002 to 2007. EMAT technology is continuously being developed in order to meet harsh environment and higher performance requirements. Kania et al. [66] described the development of EMAT framework and its corresponding validation for SCC crack inspection, and demonstrated that EMAT technology performed very well when identifying and sizing SCC cracks. Hilvert and Beuker [67] gave an introduction to high-resolution EMAT tools for analyzing cracking defects. Hirao and Ogi [68] presented SH-wave EMAT technique for inspecting corrosion defects in gas pipelines.

Since EMAT does not require couplant, which is its biggest advantage, it is readily applicable to gas pipelines and the risk of overlooking defects is reduced. However, EMAT needs to be located less than 1mm from the test body, which is too close to applying high frequency. In addition, its detection ability and efficiency are not as good as UT.

Signal processing methods and models reported in the literature for EMAT signals are similar to those for UT signals, since the signals are both ultrasound signals. Tucker et al. [69] performed wavelet analysis to classify the EMAT signals. Mazal et al. [70] compared anti-casual IIR and FIR filters, discrete wavelet transform (DWT) and wavelet packets methods for EMAT signal processing. Through numerical tests, they drew a conclusion that wavelet packet filtering technique performed best among these three de-noising methods. Lee et al. [71] utilized wavelet transform to extract meaningful information from EMAT signals. Kercel et al. [72] utilized wavelet packets and genetic algorithm to process EMAT signals. Bolshakov et al. [73] investigated signal processing methods include frequency filtering (FIR), Gaussian wavelet decomposition, synchronous detection and their combination for analyzing EMAT data.

2.1.1.1.4 Eddy current testing (ET)

Eddy current testing is widely used in the automotive, aerospace and manufacturing industries. As an energized coil is brought close to the surface, the impedance of the coil is influenced by the nearness of the induced eddy current. When the eddy currents are affected by the defects, the impedance is also altered, and this change will be measured and used to detect defects. Eddy current testing can only be used on conductive materials. It can detect cracks, and assess wall thickness and laminar defects. It cannot detect external defects because of its limitation of signal through the wall. Detection of SCC using self-excited eddy currents was introduced in [74]. ET does not have any residual effects like MFL, and the test is non-contact. Besides, currents induced by MFL can be detected using ET sensors. However, at current pig speeds, the ILI applications have slow response limits and they are sensitive to coupling variations.

2.1.1.1.5 Comparison of the four main ILI technologies

The comparison of four main ILI technologies is as shown in Table 2.1.

Table 2.1 Comparison of four main ILI technologies [75]

Tool type	Cracks	Metal loss (corrosion, etc.)	Metallurgical changes	Geometry changes	Others (weld characteristics, etc.)
MFL	N	Y	Y	S	S
UT	Y	Y	N	N	S
EMAT	Y	N	N	N	S
ET	Y	N	S	N	S

Y: The tool can detect this type of flaw.

N: The tool cannot detect this type of flaw.

S: Some types of the tool can detect this type of flaw while others can't.

From the observations in Table 2.1, we can find that MFL or UT tools are typically used to detect metal loss (external or internal corrosion) in pipelines. When detecting cracks (fatigue cracks and SCC), one uses UT tools or EMAT tools. Besides, a transverse MFL tool is also possible to be used in detecting cracks.

2.1.1.2 In-line inspection performance and applications

2.1.1.2.1 ILI performance

Understanding the performance of ILI tools is essential for applying them properly. ILI performance is typically characterized by four measures: detection, identification, accuracy, and locating. Detection refers to the capability that a feature is detected by the ILI tool, and the probability of detection (POD) should be usually over 90% for ILI tools. The probability of detection can be defined as:

$$\mathrm{POD} = \frac{n_{rep}}{n_{rep} + n_{unrep}} \tag{2-1}$$

where n_{rep} is the number of reported features, and n_{unrep} is the number of unreported features. By fitting the POD with different feature sizes, we could obtain POD curve for ILI tool. Different ILI detection tools have different POD curves. We can use a specific function, such as exponential function, to describe the POD curve. The probability of detection increases as the feature depth increases. The detection ability of ILI tools has a significant impact on deciding inspection intervals.

Identification indicates the capability to successfully classify and report the type of defects after being detected, and the probability of identification (POI) increases when the size of the

defect increases. The incorrect identification and classification of defects will cause significant inaccuracy when predicting the growth of defects. The probability of identification can be defined as:

$$\mathrm{POI} = \frac{n_{corr}}{n_{corr} + n_{incorr}} \tag{2-2}$$

where n_{corr} is the number of correct identification features, n_{incorr} is the number of incorrect identification features. For common features such as corrosion, cracks, we should utilize suitable identification and classification method to ensure POI is beyond 90%.

The sizing accuracy is the most significant measure to assess the performance of ILI tools, and it has a big impact on integrity management of pipelines. The performance of ILI tools can be specified as a tolerance with the corresponding confidence level. For example, the measurement error of the crack depth can be specified as ±0.5mm at 80% confidence. And it can be easily transferred and represented by the standard deviation of measurement error. And a more accurate ILI tool would produce a more realistic and less-conservative remaining useful life prediction. Hence, as the accuracy increases, the unnecessary excavations will be reduced, selection of the essential features will be improved and failure pressure will be well predicted. Last but not least, the capability of accurately locating a defect can also affect maintenance and repair activities a lot. The validation of ILI tool performance can be achieved through a hypothesis test following API 1163. ILI tools and technologies are being developed to improve their performance, as a result, it will reduce unnecessary repair actions and/or increase inspection interval for better and more cost-effective pipeline integrity management activities.

To assess and improve in-line inspection performance, algorithms regarding sizing, detection and classification are introduced in the literature. Hrncir et al. [47] gave a case study using a

proposed revised sizing algorithms, with which the confidence level of reported feature information was improved. Caleyo et al. [43] presented criteria for assessing the performance of ILI tools. There are three main types of uncertainties in ILI tools which affect performance: systematic error of the ILI tool, measurement noise and random error from the tool and the surface roughness [76]. The effects of combined error on ILI performance were studied in [77], [78]. How to deal with uncertainty effects was introduced in [79]. McCann et al. [80] presented a Bayesian method to estimate the ILI performance. Coleman and Miller [81] discussed normalization of data and analyzed tool tolerance and repeatability. Elucidation of the outcomes is a big challenge when comparing multiple ILI inspection datasets in multiple ILI tool runs [81]. Adianto et al. [82] presented the advantages for pipeline integrity program if the ILI tool performs better.

2.1.1.2.2 ILI applications

ILI data can be further used to assess and predict the conditions of pipelines, and subsequently plan integrity activities. Examples of analyzing and subsequently predicting pipeline defects (wall loss, cracks, and dents) utilizing ILI data were reported by Anderson and Revelle [83], Alexander [84], Lockey and Young [85] and Ferguson [86]. ILI tools are widely used in the integrity management of corroded pipelines. A comprehensive overview of in-line inspection methods for inspecting corrosion was given in [63]. Potential development directions were also discussed in [87]. Methods for assessing corrosion features, and the application of B31G and RSTRENG criteria for ILI data, were introduced in [88]. Lecchi [89] presented defect assessments of corroded pipelines with the use of ILI tools.

Sizing cracks using ILI tools is also discussed in many papers. Bates et al. [90] presented two case studies on detecting and analyzing cracks through ILI tools. Slaughter et al. [91] described the

procedures to analyze the ultrasonic ILI data for cracking and discussed how to improve the crack sizing accuracy. Marr et al. [92] summarized the performance of latest EMAT technology for assessing SCC. Tappert et al. [65] introduced in-line inspection for all kinds of cracks utilizing EMAT based on their operational experience. Hrncir et al. [47] analyzed crack sizing performance of ultrasonic ILI tools. Murayama et al. [93] gave an introduction to the development of the applications of EMAT ILI. Marr et al. [94] described a method to increase the probability of detection and the probability of identification for cracks, and as a result reduce validation costs using EMAT ILI and multiple data sets. Limon-Tapia [95] described a framework for managing crack defects based on ILI tools. Nielsen et al. [96] compared the ILI measurements with field NDE measurements.

Overall, ILI tools have evolved a lot over the past decades in the pipeline industry. Current ILI tools perform relatively reliable in detecting and identifying different types of anomalies. However, the sizing performance of ILI tools needs to be significantly improved to reduce risks and costs. In addition, details of shapes of the corrosion and crack defects need to be captured in the future, which can better assist defect growth prediction and integrity planning. ILI tools also need to be further developed to be suitable for various operating conditions. Signal processing methods need to be further developed within the pipeline industry to remove noise, improve sizing accuracy and provide better performance.

2.1.2 Pipeline defect growth prediction

To predict the remaining useful life of pipelines, methods are developed concerning the following three aspects. First, the number of defects. It can be given through ILI tool run, but the probability of detection cannot be 100%. Some methods can be used for updating the true number of defects,

such as Bayesian and Nonhomogeneous process. Second, the types of defects. The mechanism for different defects are different, and so it is important to correctly identify each defect. Third, the correlation among defects, a study of defect interaction should be provided for better prediction. Last but not least, the degradation models for different types of defects should be well studied. The determination of remaining useful life of pipeline is based on the degradation models and the sizes of defects, which are detected by ILI tools. And there are a lot of papers in the literature that proposed defect prognostics methods and models.

There are mainly two types of methods for predicting pipeline defect growth, data-driven methods and model-based methods. Data-based methods mainly use ILI data or test data to study the defect propagation stage. Applications of ILI data for defect evaluation are discussed in the previous section, and analyzing defects through ILI data can also give key information for predicting the growth of defects. For data-driven methods, we will mainly discuss pipeline defect growth using ILI data, test data or sample inspection data. Schneider et al. [97] predicted the defect growth and remaining useful life of pipelines using sample inspection data. Examples on the application of ANNs models to predict the failure of oil pipelines were discussed by Senouci et al. [98] and Lu et al. [99]. Remaining useful life prediction for pipelines using support vector machines (SVM) was introduced by Lee et al. [100], and Isa and Rajkumar [101]. Model-based methods mainly apply physical models such as finite element models to perform defect prediction. For example, Liu et al. [102] analyzed the probability of damage of offshore pipelines by utilizing Bayesian networks. Based on the failure probability, pipeline remaining useful life could be predicted using physical models like pipeline degradation models.

The pipeline defect assessment manual (PDAM) is a well-known industry project, which gives best available methods to assess pipeline defects like corrosion, dents, etc. Cosham and

Hopkins [103] provided an introduction to PDAM. Cortese et al. [104] proposed a calibration method for ductile damage estimation of pipelines. A variety of methods and models are available in the literature to predict how a defect grows and when a failure occurs. The methodologies and models used for defect growth prediction depend mainly on the types of defects. Prediction algorithms and models for defects like metal loss, cracking, mechanical damage, and others like third party damage are discussed respectively in the following subsections.

2.1.2.1 Metal loss

Metal loss is a major integrity threat to oil and gas pipelines. Serious metal loss can lead to pipeline rupture or collapse. Pipeline metal loss is mainly caused by corrosion and erosion. The prediction methods and models regarding pipelines with corrosion and erosion defects are discussed in this section.

2.1.2.1.1 Corrosion

Corrosion is a most common form of defects in pipelines and it can be easily affected by the surrounding environment. Pipeline corrosion is a natural process that happens when pipe materials interact with the working environment, such as soil and water. Corrosion can be divided into two categories, internal and external corrosion. Nine well-known critical environmental factors are soil resistivity, soil moisture, half-cell potential, pH, concentrations of CO_3^{2-}, HCO_3^-, Cl^- and SO_4^{2-}, and distance between the defect and the nearest cathodic protection station [76]. Alamilla et al. [105] developed a mathematical corrosion damage propagation model considering main environmental parameters that influence the propagation of corrosion defects. A large group of

pipeline corrosion data from 1922 to 1940 was analyzed in [106]. A corrosion growth model can be further generated by fitting the corrosion damage data.

A pipeline failure caused by corrosion defect can occur when either the failure pressure is smaller than operating pressure, or the depth of defect reaches the critical threshold (normally 80% of wall thickness in industry). The failure stress of a corrosion defect can be expressed as a function of the size and shape of the defect and the geometry of the pipe, as well as the material properties such as yield strength and ultimate tensile strength. The effect of corrosion defect on burst pressure of pipelines is studied in many papers. Netto et al. [107] estimated the burst pressure of pipelines with corrosion defects. The comparison between model predictions with burst tests and long-term hydrostatic tests was presented in [108].

Methods for assessing pipelines with corrosion defects have been extensively studied, and popular code-based deterministic methods in the published literature include ASME B31G [109], modified B31G [110], RSTRENG [110], SHELL92 [111], SAFE [112], DNV-RP-F101 (LPC) [113], [114], CPS [115] , PCORRC [116]–[118]. Equations used in these methods are similar and are based on the NG-18 equation [119], except PCORRC. The differences are mainly in the defect shape factor and bulging factor in the NG-18 equation. These methods provide the prediction for corroded pipelines by determining the burst pressure using relevant equations. Defect information such as shape and size and pipeline physical properties such as thickness, diameter and ultimate strength are the main factors that affect the burst pressure. Given the failure criteria, the remaining useful life can be estimated by generating a physics-based model considering the pressure and the defect size versus time. Modified B31G is being verified to be more accurate than B31G, and currently it is the most popular code in the pipeline industry. Cosham et al. [120] presented and compared these various code-based methods used to assess corrosion defects. Caleyo et al. [121]

also gave a study and comparison among some of the above-mentioned methods. Some deterministic defect prediction models were presented in the literature. Engelhardt et al. [122] predicted the growth of corrosion damage in pipelines using several deterministic methods. Li et al. [123] studied correlated corrosion defects in pipelines using modified B31G.

Monte Carlo method, first-order reliability method (FORM), and the first order Taylor series expansion of the limit state functions are the main methods that can be combined with deterministic methods for computing the probability of failure for a corrosion defect. In this way, corrosion propagation model is generated and remaining useful life is predicted. Details of these methods can be found in [124]. Larin et al. [125] and Zhang et al. [126] utilized Monte Carlo simulation and 3D FE models to investigate the reliability of pipeline with corrosion defects. Teixeira et al. [127] utilized FORM to assess the failure probability of corroded pipelines and this could be further used to predict the pipeline remaining useful life.

Calculating the corrosion growth rates is an essential part of corroded pipeline integrity management. Corrosion growth models based on corrosion growth rates are also popular in industry. Corrosion rate can be estimated either through the physics-based corrosion models or using ILI data. It was reported in [18] that the latter one gave a better estimate for those pipelines where multiple ILI data sets are available. Race et al. [128] developed a corrosion prediction model for pipelines using ILI data to determine corrosion growth rates. However, there are typically big uncertainties when measuring corrosion growth rates. Spencer et al. [129] compared successive ILI inspections for reducing the bias, when the same ILI vendor is used or different ILI vendors are used. Bayesian method and Markov Chain Monte Carlo (MCMC) simulation have been applied to build corrosion growth models [130]–[132]. Through combining cluster technique

with a Bayesian approach, Wang et al. [76] proposed a methodology to estimate the real external corrosion depth based on ILI inspection and to represent the impact of soil property variation.

Stochastic process models were also reported to assess corrosion defect of pipelines. Using random process corrosion rate, researchers can develop corrosion growth models that lead to a better fit to the data. Bazán and Beck [133] proposed a nonlinear random process corrosion propagation model for pipelines. Zhou [130], [134] assessed the reliability of corroding pipelines considering the stochastic process. Valor et al. [135] proposed a stochastic model for modeling pitting corrosion initiation and growth. Alamilla and Sosa [136] gave a stochastic modeling of corrosion propagation based on inspection data.

Other models have also been reported for corrosion growth prediction. Weiguo et al. [137] proposed a method for pipeline corrosion prediction under cyclic loads. Medjo [138] employed FEM calculations and Complete Gurson Model to determine the corrosion defect development in pipelines. Das et al. [139] assessed turbulence models for predicting flow-induced corrosion defects. Wang et al. [140] used Bayesian inference to propose an integrated method which employed both Monte Carlo techniques and clustered inspection data in order to assess corroded pipelines.

2.1.2.1.2 Erosion

Sand particles are often produced along with oil and gas in the pipelines, and they can cause erosion defects when they impact pipeline walls because of change in oil or gas flow direction. The erosive failure of pipeline induced by sand particles is introduced in [141]. A detailed review of sand particle erosion modeling for pipelines was given by Parsi et al. [142], where erosion

prediction equations and models were discussed and presented, and further improvements regarding erosion prediction were given.

Erosion prediction models can be categorized into computer fluid dynamics (CFD), experimental and mechanistic models. CFD models were widely used in predicting the erosion damage of pipelines. CFD can be utilized to predict erosion rate and study the impact of different parameters on the erosion rate. CFD tools are accessible, but they are simulation-based and may not be as realistic in some applications. Experimental or empirical methods can be developed by conducting lab tests. They can provide high quality data compared with other methods, but are generally expensive and relatively time-consuming. Mechanistic models such as phenomenological models are analytical ways to predict erosion defects. Although they are fast and inexpensive, the models may be over-simplified and limited in some circumstances. Due to these limitations, researchers proposed a number of erosion prediction models by combining these categories. Ukpai et al. [143] analyzed the impact of sand particle for predicting erosion damage using acoustic emission (AE) technique. Gnanavelu et al. [144] integrated CFD with experimental results to propose a method to predict pipeline erosion. Tang et al. [145] predicted the remaining useful life for a pipe with erosion under multiphase flow condition through CFD modeling techniques. Chen et al. [146] proposed a CFD-DEM coupling method to provide erosion prediction.

2.1.2.2 Cracking

Cracking is a critical time-dependent threat to pipelines. There are mainly two types of cracks, namely fatigue cracks and stress-corrosion cracking, which will be focused on in this section. Fatigue crack propagation is defined as the process of weakening pipe material due to pressure

variation. Stress corrosion cracking, SCC in short, is the growth of a form of environmental assisted cracks in corroded pipelines. We can divide the crack growth process into three stages. Stage I is the crack initiation stage where the crack growth rate is very small and can be influenced by the environment a lot. Stage II is the stable growth stage. And stage III is the unstable crack growth stage that is less influenced by the environment. Stage III is also called rupture to failure stage, which happens so quickly that it is hard to control. Researchers mainly focus on the first two stages, with an emphasis on stage II. The fatigue life of pipeline can be defined as:

$$N_f = N_i + N_p \tag{2-3}$$

where N_{i} is the number of cycles to initiate a crack, and N_{p} is the number of cycles to propagate to the failure state. We are interested in the remaining useful life, defined by the time between the point when the defect is detected by ILI tools in stage II and the failure time.

The initiation stage of fatigue damage in pipes was studied and explained in details in [147]. Zheng et al. [148] assessed the crack initiation life if pre-deformation exists. Stage II is the stage that researchers mainly focused on. Fatigue assessment can be obtained based on the stress-life method (S-N), the local strain method (Ɛ-N), and Paris' law [149]. The S-N method is an approach based on S-N curve, which can be obtained by fatigue tests. The S-N approach can be employed with algorithms such as Minor's rule, which can be used to accumulate different stress components to further assess the remaining useful life. So the key factors for the S-N method are to determine or select S-N curves accurately, to apply a correction factor and to use a suitable algorithm to combine all the stress contributions. Methods utilized to predict the remaining life of the damaged pipelines based on S-N curves were presented by Pinheiro and Pasqualino [150] and Hong et al. [151]. However, there are some limitations associated with the fatigue S-N approach. It fails to

recognize the probabilistic nature of fatigue, and it does not consider the influence of the compressive residual stress resulting from high stress. The Ɛ-N method is another method for fatigue growth assessment, which utilizes ΔƐ-N curves, where N is a function of strain range ΔƐ, and ΔƐ means the total amplitude of strain variations. This method is also similar to S-N approach in some way.

The most popular methods for crack growth models are based on the Paris' law [152]:

$$\frac{\mathrm{d}a}{\mathrm{d}N} = C(\Delta K)^m \tag{2-4}$$

where $\Delta K = K_{max} - K_{min}$, with K_{max} being the maximum stress intensity factor (SIF), and K_{min} being the minimum SIF. $\frac{\mathrm{d}a}{\mathrm{d}N}$ is the fatigue crack growth rate, where a is the crack length and N is the number of fatigue cycles. C and m are two material dependent model parameters. These two coefficients can be obtained through either laboratory experiments or industry recommended practices. Reliability analysis for crack defects is more challenging than corrosion defects due to different parameters need to be addressed. There are three primary modes of fracture. Mode I is called opening mode, mode II is sliding mode and mode III is tearing mode. As a result, SIF should also reflect these three modes. Mode I SIF (K_I) dominates the magnitude of crack propagation, and many papers only calculate K_I to represent the total stress intensity while using Paris' law. In the literature, the majority of physics-based models for predicting cracks in pipelines are based on the Paris' law. To employ the Paris' law, one needs to determine the SIF first. SIF can be determined through standard codes, numerical equations derived by researchers, experiment results and finite element software (ANSYS, ABAQUS, etc.). There are different equations to calculate the SIF for different crack types. The categories of crack shapes in pipelines are surface, embedded, and

through-thickness cracks. Shim and Wilkowski [153] applied FE simulation to calculate bulging factor for a pipeline with cracks in the external surface. The bulging factor could be further utilized to determine SIF and crack-driving force. Beside SIF, other measures such as crack tip opening displacement (CTOD) and crack tip opening angle (CTOA) can also be used to determine the fracture toughness of most materials including pipeline materials. Ben Amara et al. [154] gave a study on how to obtain CTOA in steel pipelines.

The crack defect can be determined as a failure when SIF reaches critical SIF (micro criteria) or predicted failure pressure reaches the maximum operating pressure (macro criteria). In pipeline industry, the macro criteria is more popular than the micro criteria. Researchers have developed methods, standards, software tools to analyze the predicted failure pressure for pipelines with crack defects. After calculating the predicted failure pressure, the macro criteria is then be used. Popular standards for assessing crack defects include API 579 [155], BS 7910 [156] and NG 18 [119], and many pipeline companies follow these standards to make decisions. Software tools such as CorLAS^{TM} [157] are also used to analyze these defects. Some other physics-based approaches are also introduced in the literature. These assessment methods require the inputs as follows: crack sizes (length and depth), material properties (Young's modulus, yield and tensile strength), pipeline dimensions (outside diameter, thickness), and loading conditions. The calculation results will then be compared with a suitable safety factor and help to make corresponding decisions. Popelar et al. [158] developed a theoretical model to simulate and calculate the propagation speed of crack in pipelines. Pipeline crack prediction with strain rate dependent damage model (SRDD) through experiments and simulation were investigated by Oikonomidis et al. [159], [160], and Yu and Ru [161]. Iranpour and Taheri [162] [163] did research on the impact of compressive stress cycles and peak tensile overload cycles on the fatigue life of pipelines. Amaro et al. [164], [165]

proposed a hydrogen-assisted fatigue crack propagation model, which is used to predict crack growth using a function of ΔK and hydrogen pressure. Besides, Sekhar [166] summarized the effects as well as the identifications of the multiple cracks, and more studies were needed to consider multiple cracks in pipeline crack growth prediction. Polasik and Jaske [167] described a crack growth model based on the Paris' law and fracture mechanics principles. Hadjoui et al. [168] studied the behavior of crack growth of double butt weld in two pipeline material, X60 and X70. Nonn and Kalwa [169] analyzed multiple published ductile damage mechanics models including Gurson-Tvergaard-Needelman (GTN), Fracture Locus Curve (FLC) and Cohesive Zone (CZ)) for ductile crack propagation in pipelines.

Experimental testing of pipelines with crack defects was performed and reported by many groups. Kumar et al. [170] used acoustic emission (AE) method to study the behavior of crack propagation in low carbon steels which can be used as the pipeline material. Slifka et al. [171] gave tests on two pipeline steel to get fatigue crack growth rate. Jin et al. [172] performed a test on pipeline steel to assess the propagation of a semi-elliptical surface crack. Hosseini et al. [173] compared the experimental testing results they obtained with the industrially known methods, such as BS 7910 and NG 18. Pumpyanskyi et al. [174] performed full scale tests to look into crack propagation and arrest behavior of pipelines. Chen and Jiang [175] gave experimental investigations on crack growth analysis of pipeline material X60. Naniwadekar et al. [176] predicted flaw growth in various orientations based on frequency measurements.

Physics-based models may not be applicable to all situations due to the complexity of the applications and availability of authentic models, and the challenge in determining model parameters. ILI tools are very expensive to run, and sometimes there are not sufficient data to effectively run data-driven methods. As a result, there are great room and challenges for improving

prognosis methods and models for cracks in pipelines. Hybrid methods are also being investigated, which integrate physics-based models with data-driven methods. An integrated prognosis method for industrial and mechanical structures was introduced by An et al. [177] using Bayesian inference. Xie et al. [2] proposed an integrated method to predict the remaining useful life of pipelines with fatigue cracks and validated it through field data and simulation examples.

A corrosive environment can affect the growth of fatigue crack [149]. We can call this type of crack environmental cracking or SCC. A probabilistic damage model was proposed by Hu et al. [178] to assess local corrosion crack based on Monte Carlo simulation. Lu et al. [179] presented a high pH stress corrosion crack growth model and validated it through experiment. Imanian and Modarres [180] presented an entropy-based method and did experiments to assess the reliability for corrosion fatigue. Chookah et al. [181] proposed a physics-of-failure model for predicting the propagation of SCC. Jaske and Beavers [182] used the available data and employed J-integral fracture mechanism to predict pipeline remaining life subject to SCC.

2.1.2.3 Mechanical damage

Mechanical damage on pipelines also poses threats to pipeline integrity. Two main categories of mechanical damage are dents and gouges. Bai and Bai [183] gave an introduction to dented pipes including limit-state based criteria, fracture mechanism and reliability-based assessment. A mechanical damage integrity management framework was given in [17]. The burst pressure for pipelines with gouges and dents was studied by Lancaster and Palmer [184], Allouti et al. [185] and Ghaednia et al. [186]. Pressure strength of pipelines with dents and cracks were studied in [187]. Macdonald and Cosham [188] discussed the pipeline defect assessment manual (PDAM) and suggested practices for dents and gouges assessment as well as the limitations of these

assessment methods. Cosham and Hopkins [189] analyzed the dents effect in pipelines based on PDAM.

Prognosis algorithms and models are proposed for mechanical damage in pipelines. Ivanov et al. [190] proposed an FE model using MFL signals to predict the growth of mechanical damage in pipelines. Bolton et al. [191] proposed a finite element model for predicting the life for dented pipeline and validated the model by experiment. Dama et al. [192] used a simple S-N approach to assess the structural condition of pipelines with sharp dents. Bolton et al. [193] developed a finite element model for dented pipes to estimate the remaining life. Azadeh and Taheri [194] performed an experimental investigation on dented pipes. Failure prediction of the pipeline with dents based on local strain criteria was studied by Allouti et al. [185] and Noronha et al. [195].

2.1.2.4 Other defects

Other types of defects, such as weld, third party damage, etc., can cause the failure of pipelines. The main differences between corrosion, cracking and the other failure mechanisms (third-party damage, laminations and earth movements) are the nature of mechanism and failure rate tendency. The nature of mechanisms of corrosion and cracking are time-dependent while the others are generally random, or time-independent. The failure tendencies for corrosion and cracking increase with time, while those for the others remain constant. To better control third party damage, regular surveys of the line, good communications, and good protective measures are important. Goodfellow et al. [196] presented the updated distributions of third party damage with the use of historical data. Hsu et al. [197] provided an introduction to weld mechanism and introduced wear prediction models for metals. El-Hussein [198] compared the FE predictions for third party attacks with real field data. Oddy and McDill [199] employed 3D FE analysis of welding on pipelines to

perform predictions. Niu et al. [200] applied FE simulation to give a creep damage prediction of pipelines in the high temperature and high pressure environment.

2.1.3 Risk-based management

The common definition of risk is the multiplication of probability and consequence. Thus, to perform risk-based management, we need to analyze the causes of risks, estimate failure probabilities as well as perform consequence analysis. For pipeline integrity management, probabilities typically refer to probabilities of pipeline failure due to certain defect growth. The consequences are related to the costs incurred by activities like inspection and maintenance, loss of productivity, rehabilitation and investigation, damage to the environment and community, environmental cleaning up, etc.

While conducting risk-based management for pipelines, some related areas need to be studied. First, threats and consequence need to be identified in order for calculating risk. Selecting a proper risk assessment model is critical to determine the structural integrity. Second, pipeline segments and existing threats must be prioritized. In this way, the riskiest pipeline segments and threats will be inspected and repaired prior to others. Third, select suitable mitigation and preventative activities for each threat. Last but not least, determine cost-effective and appropriate re-inspection and re-assessment interval. This re-assessment interval must ensure the safe operation of pipelines and the reliability of pipelines should be beyond the predetermined safety threshold.

2.1.3.1 Activities for RBM

To evaluate the life cycle cost of pipeline risk-based management, potential activities need to be well discussed and studied. Activities for risk mitigation include visual inspection, potential surveys, cathodic-protection inspection, in-line inspection, operational pigging and other maintenance and repair activities. Emergency plans for failure and accidents also need to be considered. The principal objective of risk-based management activities is to efficiently and effectively utilize available resources to ensure the safety of public, surrounding environment protection and pipeline system reliability. The frequency of inspection and maintenance activities depends not only on the defect damage situation and the consequences of failure, but also on the pipeline operating conditions. Besides, risk acceptance criteria need to be determined before risk-based management process, based on industry regulations and codes, operators as well as risk analysis outcomes. Pipeline risk analysis for integrity management was introduced in [201]–[204]. The advantages and disadvantages of pipeline risk analysis were discussed by Bott and Sporns [205].

Inspection activities are well discussed in Section 2.2. The unit inspection cost of ILI tool increases as tool accuracy increases. With the consideration of time effect (discount rate), the re-assessment interval will make a big impact on inspection cost calculation. Besides, sizing uncertainty is non-negligible while conducting cost evaluation. After the inspection activities, types of defects and their significance to pipeline integrity should be studied. The findings from inspections and tests need to be basically aligned with what the prognostics model predicted. If not, the reasons for that need to be investigated. Besides, the causes of these defects need to be investigated for future preventive and mitigate actions.

As for repair activities, repair criterions and methods are well discussed in [22], [206]. For each kind of defect, certain repair criteria can be utilized to determine the corresponding repair actions. Repair methods for pipeline include pipe replacement, recoating, full-encirclement sleeves, composite wrap repairs, mechanical clamps, etc. Repair criteria can be determined based on the severity of ILI indications. There are four types of responses to pipeline in-line inspections: immediate, near term, scheduled and monitored. For each one, there are time and limit state requirements for repair actions, which can be found in [22]. The costs for repair activities depend on the type of repair methods and the number of defects needs to be repaired. The locations of defects and pipeline segments also affect the repair or replacement costs. Industry does not want pipelines to fail that causes damage to population and environment. Therefore, predictive and preventive maintenance activities are better choices than reactive maintenance activities. The most suitable maintenance activities should be arranged based on the probability of failure of pipelines.

2.1.3.2 Methods for RBM

Risk assessment methods can be divided into three types: quantitative methods, qualitative methods and semi-quantitative methods. Quantitative methods require lots of input data which may include some data that the pipeline operators do not have. If the input data is enough, the output will provide very detailed mitigation and inspection options and criterions. These methods are not efficient or cost-effective for upstream pipelines. Qualitative methods are simple decision matrix methods. These types of methods depend on experts and industry practices a lot. These methods are very effective for ranking pipeline risk. However, they are relatively more conservative and they do not provide optimized schedules and actions for mitigation and inspection activities. Semi-quantitative methods can also be called score index methods. These

methods are widely used in industry. The required input data are relatively less than quantitative methods and easy to acquire. Relative risk values and optimized solutions for mitigation problems will provide as the output of these methods.

Analyzing the reliability and risks is the essential job in the preparation stage for risk-based management. Risk can be obtained by calculating the probability of failure and consequence of failure. Many papers discussed the inputs for the risk-based management. Chien and Chen [207] carried out the reliability assessment of pipelines to provide the integrity management strategies, and the reliability analysis method they used was first order second moment (FOSM) method. Kuznetsov et al. [208] implemented Bayesian method to count the number of defects in a pipeline segment, and it can be further utilized in determining the inspection and maintenance activities. Cunha [209] compared and analyzed the failure statistics for pipelines which can also be further utilized as the basis for risk-based management. McCallum et al. [210] developed a corrosion risk management tool using Markov analysis, which can assist corrosion integrity planning. Mihell and Rout [211] proposed an approach to analyze risk and reliability for pipelines. Tuft et al. [212] provided the comparison between reliability-based analysis method and quantitative risk assessment based on historical failure rates.

There are two main objectives in risk-based management models. One objective is to minimize the whole life cycle cost with the constraints of certain reliability and risk level, and the other objective is to minimize the risk. Risk-based management following the first objective has three main steps. First, define and gather information on threats and defects in the pipelines. Second, calculate probability, consequence of failure and life cycle costs. Third, recommend inspection and maintenance activities by solving the optimization problem to minimize total costs while ensuring the system reliability is above a certain level. Various approaches and models were

reported with cost minimization as the main objective. Dawotola et al. [213] proposed a method where the failure rate changes with time following a nonhomogeneous Poisson process. The historical data were fitted to obtain the probability of failure, and maintenance strategies were optimized by minimizing operation and maintenance loss while meeting risk and reliability target. Bai et al. [214] proposed a tree risk-based inspection approach for subsea pipelines to minimize cost for different safety levels. Sinha and McKim [215] utilized Markovian prediction models to construct a cost-effectiveness based prioritization program to develop strategies for maintenance and repair. Life cycle cost optimization was performed using Genetic Algorithm (GA) for pipeline networks by Tee et al. [216]. In addition, inspection, maintenance and repair strategies for different types of defects in pipelines were also reported. Sahraoui et al. [217] provided a review of risk-based management methods that considered the uncertainties in the inspection results for pipelines with corrosion defects. Stephens et al. [218] studied reliability corrosion assessment to develop cost-effective maintenance and inspection planning strategies, and they adopted a random process model to generate new defects when calculating the probability of failure. Hong [219] developed inspection and maintenance schedules based on reliability constraint for corroded pipelines. Moreno et al. [220] extended the inspection interval using a statistically active corrosion (SAC) method. Xie and Tian [3] proposed a method to determine optimal re-inspection and re-assessment interval for pipelines with corrosion defects based on PoF threshold as a random variable. Gomes et al. [221] optimized the inspection planning and repair intervals for pipelines with external corrosion defects. Gomes and Beck [222] also optimized pipeline management subject to random cracks. The number of inspections and the critical crack size were considered as design variables in the models.

The second optimization objective used in many studies is risk minimization, mainly aiming to reduce the likelihood (probability of failure) and/or the consequence (severity). These kinds of methods follow three steps. First, define a risk and the acceptance criteria. Second, assess the risk and determine the risk level. Third, establish inspection, maintenance and assessment plans based on risk assessment results. Some papers in the literature proposed methods following the process above. Kamsu-Foguem [223] presented an introduction to risk-based inspection management, and suggested a methodology based on a colored risk matrix for providing risk acceptance criteria. Tien et al. [224] proposed a method to determine the optimal pigging inspections planning, with information like damage factor, inspection factor, condition factor, process factor, etc., collected and qualified to form the model built in this paper. Khan et al. [19] proposed a method for risk-based inspection and maintenance modeling using gamma distribution and Bayesian method to describe material degradation process. Kallen and van Noortwijk [225] proposed an adaptive Bayesian model for optimal integrity planning, which used gamma stochastic process to describe the degradation mechanism.

Many studies on maintenance planning were reported for pipelines with a specific defect type, particularly corrosion defect. Singh and Markeset [226] proposed a method to estimate corrosion growth rate for pipelines based on fuzzy logic method. A decision support system (DSS) was utilized for assessing risk effects and developing pipeline integrity plans in [227] and [228]. Condition-based maintenance models developed for multi-component systems were introduced in [229], [230]. Seo et al. [231] discussed the development and application of the proposed risk-based inspection method for pipelines with corrosion defects. Fessler and Rapp [232] proposed a method for determining the re-assessment intervals for pipelines with SCC defects. Zarea et al. [233] gave

an introduction to risk management along with integrity management of mechanical damage in pipelines.

2.2 Background knowledge

2.2.1 Monte Carlo simulation

Monte Carlo simulation is widely used for uncertainty propagation in reliability and risk assessment. And it can be used to simulate systems with multiple random variables. This technique can conduct risk analysis by sampling input random variables from probability distributions and substituting these values to the risk model. In this way, for each iteration, we obtain a possible result. After thousands or tens of thousands of recalculations, we can obtain the final outcome.

The general Monte Carlo simulation methods follow certain steps. First, we generate input random variables from probability distributions over the defined domain. Second, we perform a deterministic computation on these input random variables. At last, we aggregate the computation results and obtain the final output results. For example, for pipeline reliability assessment, we could treat physical properties, geometry parameters, defect growth rates, ILI measurement error as input random variables. For Monte Carlo simulation run, we can determine whether this defect is a failure or not. And with a certain number of Monte Carlo simulation runs, the reliability of pipeline can then be determined.

The accuracy of a Monte Carlo simulation has a positive correlation with the total trial numbers. Suppose N is the total trial numbers, the converge rate of Monte Carlo simulation is $O(N^{-1/2})$. Due to the relatively small converge rate, we can find that Monte Carlo simulation method is relatively time-consuming. However, the converge rate is independent of the number of

random variables, so it can be used to deal with a complex system with a number of input random variables.

2.2.2 Bayesian analysis

Bayesian analysis can be used for uncertainty quantification. And it can update the distribution of a parameter of interest as more information is gathered. Hence, Bayesian analysis is widely used to update model parameters for physical models. Consider the prior distribution of the parameter θ is $f_{\text{prior}}(\theta)$. We have gathered a set of data $\mathbf{X}=\{x_1, x_2, ..., x_n\}$, and the marginal density function of $\mathbf{X}$ is $f(\mathbf{X})$. With equation (2-5), we can obtain a posterior distribution $f_{\text{post}}(\theta \mid \mathbf{X})$:

$$f_{\text{post}}(\theta \mid \mathbf{X}) = \frac{l(\mathbf{X} \mid \theta) f_{\text{prior}}(\theta)}{f(\mathbf{X})} \tag{2-5}$$

where $l(\mathbf{X} \mid \theta)$ is the likelihood to obtain these observations given parameter θ.

The core of Bayesian analysis is to estimate a posterior distribution of a parameter of interest. Compared to prior distribution, posterior distribution reflects the data information after the observations. And in this way, Bayesian analysis can be used to reduce the uncertainty in the parameter of the damage propagation model, which leads to more accurate remaining useful life prediction. With historical data collected, the model parameter is updated, thus a more accurate prognostics is achieved. Monte Carlo simulation technique can then be used to obtain the histogram of the posterior distribution. And we can obtain the mean value of the model parameter from fitting the histogram to a specific distribution.

2.2.3 Limit state function

The limit state function (performance function) of a system can be written as:

$$Z = g(X_1, X_2, \dots, X_n) \tag{2-6}$$

where the failure surface is defined as $Z = g(X_1, X_2, \dots, X_n) = 0$. Each X is basic load or resistance variable. A plot of limit state function is shown in Figure 2.1. Limit state functions are widely used in pipeline industry to determine whether this defect is a failure or not. For example, the limit state function for a pipeline with a single defect can be defined as predicted failure pressure minus maximum operating pressure. Maximum operating pressure can be treated as resistance and predicted failure pressure is the load. As degradation of this defect, the load will decrease over time. When it reaches the failure surface, this defect becomes a failure.

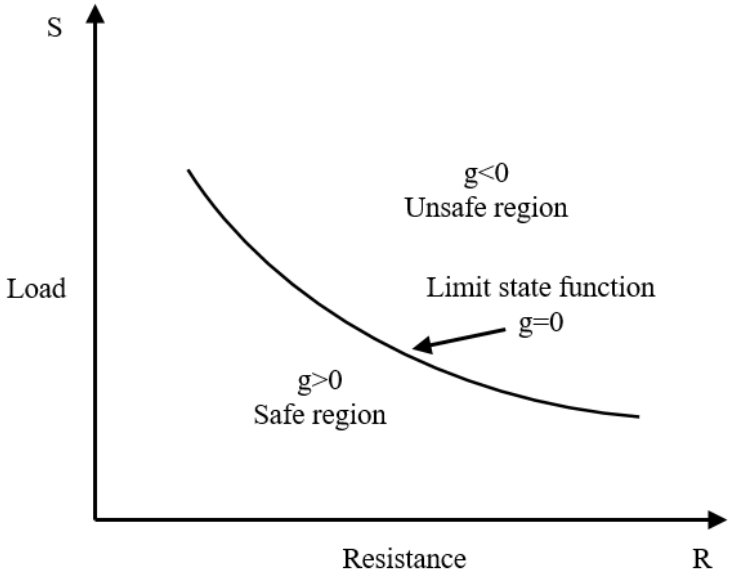

Figure 2.1 Limit state function

2.2.4 Advanced first order second moment method (AFOSM)

Advanced first order second moment method [234], [235] can be used to obtain the points on the failure surface. To use this method, first we transfer these random variables to their standardized forms.

$$x_i'^* = (x_i^* - \mu_{x_i}) / \sigma_{x_i} \tag{2-7}$$

The design point, $\mathbf{X}'^*$ can be found by the following constrained optimization problem:

$$\text{Minimize: } \beta_0 = \sqrt{\mathbf{X}'^T \mathbf{X}'} \text{, subjected to the constraint: } g(\mathbf{X}') = 0 \tag{2-8}$$

The reliability index is called Hasofer-Lind reliability index, and it can be calculated by using the following equations (2-9) to (2-11):

$$\overline{g^*} = -\nabla g(\mathbf{X}'^*)^T \mathbf{X}'^* \tag{2-9}$$

$$\sigma_{g^*}^2 = \nabla g(\mathbf{X}'^*)^T \nabla g(\mathbf{X}'^*) \tag{2-10}$$

$$\beta_{HL} = \frac{\overline{g^*}}{\sigma_{g^*}} = \frac{-\nabla g(\mathbf{X}'^*)^T \mathbf{X}'^*}{\sqrt{\nabla g(\mathbf{X}'^*)^T \nabla g(\mathbf{X}'^*)}} \tag{2-11}$$

With β_{HL}, the design point can be calculated as:

$$\mathbf{X}'^* = \frac{-\nabla g(\mathbf{X}'^*)\beta_{HL}}{\sqrt{\nabla g(\mathbf{X}'^*)^T \nabla g(\mathbf{X}'^*)}} = -\boldsymbol{\alpha}\beta_{HL} \tag{2-12}$$

where α_i is the direction cosine along the axes $x_i'^*$, and it can be written as:

$$\alpha_i = \frac{\frac{\partial g}{\partial x_i}(\mathbf{X}'^*)}{\sqrt{\nabla g(\mathbf{X}'^*)^T \nabla g(\mathbf{X}'^*)}} \tag{2-13}$$

The following steps can be used to compute the optimal solution of $\mathbf{X}'^{*}$.

1. Define the appropriate limit state function $g(\mathbf{X}')$
2. Give initial values of x_i^*, i=1, ,2, … , n and obtain the reduced variates $x_i'^* = (x_i^* - \mu_{x_i}) / \sigma_{x_i}$. And we can set the initial values to be the mean values of these random variables.
3. Evaluate $\nabla g(\mathbf{X}'^*)$ and $\boldsymbol{\alpha}$ at $\mathbf{X}'^*$ using equations (2-9) to (2-11).
4. Update the new design point by using equation (2-12).
5. Calculate $g(\mathbf{X}'^*)$ by substituting the new $\mathbf{X}'^*$, and solve for β_{HL}.
6. Evaluate $\mathbf{X}'^*$ by using the new obtained β_{HL} and equation (2-12).
7. Set a threshold for the acceptable error for β_{HL}. Check if β_{HL} converges or not. If yes, stop. If not, repeat step 3 to 6.

2.2.5 Burst pressure models

2.2.5.1 Corrosion defects

As introduced in the literature review, the following burst pressure models can be used to calculate the burst pressure for pipelines with corrosion defects.

2.2.5.1.1 B31G [109]

The burst pressure P_f can be calculated using equations (2-14) to (2-17).

$$G = 0.893\frac{L(T)}{\sqrt{Dt}} \tag{2-14}$$

$$M = \sqrt{1 + 0.893\frac{L(T)}{Dt}} \tag{2-15}$$

$$P_f = 1.11\frac{2YSt}{D}\left(\frac{1-\frac{2d(T)}{3t}}{1-\frac{2d(T)}{3tM}}\right), \text{ for } G < 4 \tag{2-16}$$

$$P_f = 1.11\frac{2YSt}{D}\left(1-\frac{d(T)}{t}\right), \text{ for } G \geq 4 \tag{2-17}$$

where D is the outside diameter; t is the wall thickness; $L(T)$ is the corrosion length at time T; $d(T)$ is the corrosion depth at time T; YS is the yield strength.

2.2.5.1.2 Modified B31G [110]

Modified B31G is the most popular tool to calculate the burst pressure P_f, the equations are listed as follows:

$$P_f = \frac{2(YS + 68.95)t}{D}\left(\frac{1-\frac{0.85d(T)}{t}}{1-\frac{0.85d(T)}{tM}}\right) \tag{2-18}$$

$$M = \sqrt{1 + 0.6275\frac{L(T)^2}{Dt} - 0.003375\left(\frac{L(T)^2}{Dt}\right)^2}, \text{ for } \frac{L^2}{Dt} \leq 50 \tag{2-19}$$

$$M = 0.032\frac{L(T)^2}{Dt} + 3.3, \text{ for } \frac{L^2}{Dt} > 50 \tag{2-20}$$

2.2.5.1.3 Battelle

The following equations are used as Battelle model to calculate P_f:

$$P_f = \frac{2UTSt}{D}(1-\frac{d(T)}{t}M) \tag{2-21}$$

$$M = 1-\exp(-0.157\frac{L(T)}{\sqrt{D(t-d(T))/2}}) \tag{2-22}$$

where *UTS* is the ultimate tensile strength, the meaning of other parameters can be found in section 2.2.6.1.1.

2.2.5.1.4 DNV-99

The following equations are used as Battelle model to calculate P_f:

$$P_f = \frac{2UTSt}{D-t}(\frac{1-\frac{d(T)}{t}}{1-\frac{d(T)}{tM}}) \tag{2-23}$$

$$M = \sqrt{1+0.31\frac{L(T)^2}{Dt}} \tag{2-24}$$

2.2.5.2 Crack defects

The following models and methodologies are the popular ones used in industry for predicting burst pressure for pipelines with crack defect.

2.2.5.2.1 NG-18 method [119]

The Ln-secant (NG-18) failure criterion is also called Battelle model, which is the basis of many other methods. It gives the relationship between critical flaw size and hoop stress and many other parameters. This equation can be used to calculate the critical stress intensity factor (equation (2-25)) or burst pressure (equation (2-26)).

$$K_{IC} = \sqrt{\frac{8}{\pi} c_{eq} \times {\sigma_f}^2 \times lnsec(\frac{\pi \times M_p \sigma_h}{2\sigma_f})} \tag{2-25}$$

$$P_B = \min\left\{ \frac{2t\sigma_f}{D} \frac{1-\frac{a}{t}}{1-\frac{a}{Mt}}, \frac{4t\sigma_f}{\pi D} \frac{1-\frac{a}{t}}{1-\frac{a}{Mt}} \arccos(\exp(-\frac{\pi K_{mat}^2}{8c{\sigma_f}^2})) \right\} \tag{2-26}$$

$$M_p = \frac{1-\frac{d}{t}(\frac{1}{M_t})}{1-\frac{d}{t}} \tag{2-27}$$

$$M_t = \begin{cases} \sqrt{1+0.6275z-0.003375z^2}, \text{if } z = L_e^{\ 2}/(Dt) \le 50 \\ 0.032z+3.3, \text{if } z > 50 \end{cases} \tag{2-28}$$

2.2.5.2.2 Failure assessment diagram (FAD) methods [155], [156]

The FAD methods are widely used for assessing cracks in pipelines. There are three levels of FAD approaches. Level 1 FAD is the most conservative one, and it is used when the known material properties and load conditions are limited. Level 2 gives a better prediction and Level 3 provides the best estimate of burst pressure. In this study, API 579 Level III and BS 7910 Level III are used to predict burst pressures. The FAD approach is based on two failure criteria which are brittle

fracture (K_r) and plastic collapse (L_r). Figure 2.2 is an example of FAD, from this figure, all assessment points using API 579 and BS 7910 are under the assessment line, so they are considered to be safe.

To obtain the assessment points, we can use Level 3 FAD through API 579 and BS 7910 separately to get the L_r and K_r:

$$L_r = \frac{\sigma_{ref}}{\sigma_y} \tag{2-29}$$

$$K_r = [\frac{E\varepsilon_{ref}}{L_r\sigma_y} + \frac{L_r^3\sigma_y}{2E\varepsilon_{ref}}]^{-0.5} \tag{2-30}$$

And we can use the Ramberg-Osgood equation to determine the reference strain:

$$\varepsilon_{ref} = \frac{\sigma_{ref}}{E} + \alpha(\frac{\sigma_{ref}}{\sigma_y})^n \frac{\sigma_{ref}}{E} \tag{2-31}$$

API 579-Cylinder Approach gives the reference stress as follows:

$$\sigma_{ref} = M_S\sigma_h \tag{2-32}$$

where σ_h is the hoop stress; Folios bulging factor M_S is given by:

$$M_S = \frac{1-0.67\dfrac{d}{tM_t}}{1-0.67\dfrac{d}{t}} \tag{2-33}$$

$$M_t = \frac{1.02+0.4411\lambda^2+0.006124\lambda^4}{1+0.02642\lambda^2+1.533\times10^{-6}\lambda^4} \tag{2-34}$$

$$\lambda = \frac{1.818C}{\sqrt{dR_i}} \tag{2-35}$$

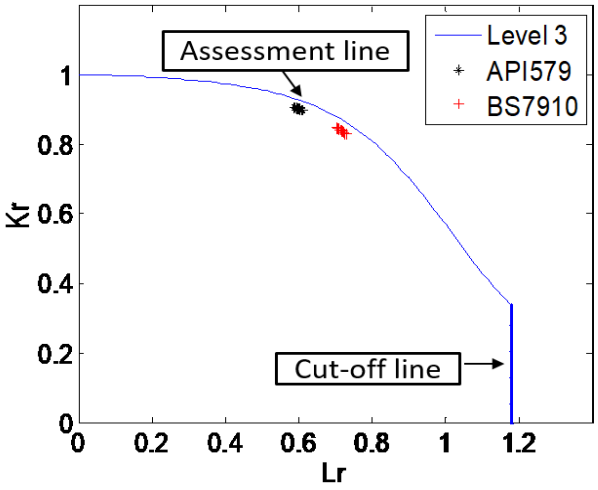

Figure 2.2 One example of FAD

BS 7910-Cylinder Approach gives the reference stress as follows:

$$\sigma_{ref} = 1.2 M_S \sigma_h \tag{2-36}$$

where σ_h is the hoop stress; Folios bulging factor M_S is given by:

$$M_S = \frac{1 - \frac{d}{tM_t}}{1 - \frac{d}{t}} \tag{2-37}$$

$$M_t = [1 + 1.6\left(\frac{c_{eq}{}^2}{Rt}\right)]^{0.5} \tag{2-38}$$

2.2.5.2.3 CorLAS^{TM} model [157]

CorLAS^{TM} is a popular software tool used in industry, it can assess a detailed crack depth profile rather than other methods. The CorLAS^{TM} model uses the effective area method to calculate the burst pressure.

3 An integrated prognostics approach for pipeline fatigue crack growth prediction utilizing in-line inspection data

3.1 Introduction

Fatigue cracking is a key type of defect for liquid pipelines, and managing such fatigue cracks continues to be a top priority amongst pipeline integrity management. However, existing ILI tools have relatively large fatigue crack measurement uncertainties, and typically have a specification of about plus/minus 1 millimeter, 80% of the time [6], [13]. Furthermore, currently physics-based methods are mainly used for fatigue crack growth prediction, based on crack growth models governed by the Paris' law [13], [14]. The uncertainty in crack sizing and the Paris' law model grows to the predicted time of failure due to fatigue cracks, resulting in uncertainty which requires a conservative management integrity management approach and risk mitigation strategies, such as repairs, pipe replacement, pressure reductions and hydro-testing. There is an urgent need to develop accurate fatigue crack growth prediction tools, and reduce the uncertainty and hence the conservatism in pipeline integrity management.

Existing pipeline defect prognosis methods are mainly classified into physics-based methods and data-driven methods[15]. The physics-based methods for pipelines mainly include stress-life method (S-N), local strain method (ε-N), and Paris' law based methods [149]. Among them, the physics-based method governed by the Paris' law is currently the dominant method used for

pipeline fatigue crack growth prediction [6], [13], [14]. The Paris' law is generally used for describing fatigue crack growth [13], [14], [236], [205]:

$$\frac{\mathrm{d}a}{\mathrm{d}N} = C(\Delta K)^m \tag{3-1}$$

where $\mathrm{d}a/\mathrm{d}N$ is the crack growth rate, a is crack size, N is the number of loading cycles, ΔK is the range of the Safety Intensity Factor (SIF), and C and m are material related uncertainty model parameters. C and m can be estimated via experiments, and are set as fixed constants in the physics-based method. Many studies have been published on using physical models, such as FE models, and crack growth models based on *S-N* curves or some forms of Paris' law. Hong et al. [151] estimated the fatigue life by using the *S-N* curves of the ASTM standard specimens, curved plate specimens and wall-thinned curved plate specimens. Pinheiro and Pasqualino [150] proposed a pipeline fatigue analysis based on a finite element model and S-N curve with the validation of small-scale fatigue tests. Oikonomidis et al. [159], [160] predicted the crack growth through experiments and simulation based on a strain rate dependent damage model (SRDD). Crack arrest length and velocity can be predicted through the proposed model. A key disadvantage of the existing physics-based method is that typically the same fixed model parameters are used for all pipes (i.e. m=3). However, these material dependent model parameters should be different for different pipes, and slight differences in such model parameters can lead to large differences in fatigue crack growth predictions. As an example, a 10% change in parameter m may lead to a change of 100% in the predicted failure time.

Data-driven methods use the experimental data or monitoring data rather than physical models for prognosis. Varela et al. [23] discussed major methodologies used to produce condition monitoring data. Among these pipeline inspection techniques, ILI tools are the most reliable for

pipeline integrity management. A review of ILI tools for detecting and sizing cracks was conducted in reference [90]. Slaughter et al. [91] analyzed the ILI data for cracking and gave an introduction to how to improve the crack sizing accuracy. Systematic error of the ILI tool, measurement noise and random error from the tool, and the surface roughness are three main sources of ILI tool uncertainties [76]. Due to the measurement errors and cost of an ILI tool, data driven methods do not work well if the number of ILI tool runs and the amount of data are not sufficient.

In this section, an integrated approach for pipeline fatigue crack growth prediction with the presence of large crack sizing uncertainty is proposed, which integrates the physical models and the ILI data. With the proposed integrated approach, the FE model of cracked pipe is built and stress analysis is performed. ILI data is employed to update the uncertain material parameters for the individual pipe being considered so that a more accurate fatigue crack growth prediction can be achieved. The proposed integrated approach is compared with the existing physics-based method using examples based on simulated data. And real NDE and ILI data provided by a Canadian pipeline company is used for the validation of the proposed integrated approach.

Time-varying operating conditions are considered in the proposed integrated method. When oil and gas content is transported with pipelines, the internal pressure of the operating pipelines varies with time, which presents a challenge for applying integrated prognostics methodology. Zhao et al. [237] proposed an integrated prognostics method for a gear under time-varying conditions. The load changes history considered in [237] is the combination of several constant loading conditions, while in pipeline operations, the internal pressure changes continuously. In this study, we employ the rainflow counting method to deal with time-varying operating conditions. A key advantage of using the rainflow counting method within the proposed integrated method is to

directly link the environmental and human factors which affected the loading conditions to the degradation model. Also, it is proven by Roshanfar and Salimi [238] that rainflow counting method is more accurate compared with other cycles counting methods, such as range counting, level crossing counting, and peak counting methods.

Section 3.2 presents a pipe finite element model considering a single fatigue crack. The proposed integrated method for fatigue crack growth prediction of pipeline is discussed in Section 3.3. Section 3.4 gives examples based on simulated data and Section 3.5 presents a case study to demonstrate the proposed method. Section 3.6 gives the conclusions.

3.2 Pipe finite element modeling considering fatigue cracks

In this section, the pipe finite element model considering a single fatigue crack is built, based on information and methods presented in [239]–[241]. The ANSYS software is used for pipe FE modeling, and a single semi-elliptical type of crack is considered. Stress analysis is performed, and SIF can be calculated.

3.2.1 Pipe FE modeling

Test data 157-1 presented in [242] on line pipes was used. The material is X70 grade pipe steel. Table 3.1 shows the line pipe's physical properties. These parameters of pipeline geometry and mechanical properties shown in Table 3.1 are used as input parameters to build the pipeline finite element model.

Table 3.1 Physical properties of the line pipe

Parameters	Pipe
API 5L Grade	X70
Yield Strength Min. (MPa)	483
Tensile Strength Min. (MPa)	565
Yield to Tensile Ratio Max.	0.93
Elongation Min.	17
Outside Diameter (mm)	914.4
Wall Thickness (mm)	15.875
Length (mm)	5000
Internal Pressure (MPa)	10

Software ANSYS Workbench is used to build the FE model. The crack shape is set to Semi-Elliptical, which is the most common type of fatigue cracks found in pipelines. The crack size and shape are defined by the major radius (crack length a=2r) and the minor radius (crack depth b), which are shown in Figure 3.1. ANSYS Workbench was used to build a pipeline model with a semi-elliptical crack, with the input of major radius and minor radius.

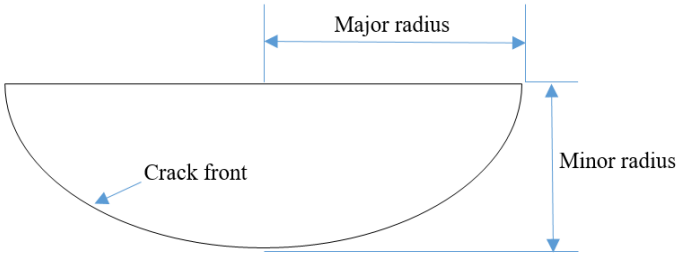

Figure 3.1 Crack shape

The pipe parameters are entered using the fracture tool. The pipe is divided into two parts: one is the fracture affected zone which uses the tetrahedrons method, and the other is the rest of the pipe which uses the hex-dominant method. Figure 3.2 shows the built FE model, where the base mesh without cracks and the region involving the crack are modeled using the two different modeling methods.

Stress intensity factor (SIF) is the key output of pipe finite element analysis. The crack length *a* increases from 4 to 30mm with a step size of 2mm, and the crack depth *b* is varied from 2mm to 12mm with 1mm increments, and obtain the corresponding SIF values through stress analysis. To model the relationship between SIF values at the surface point (K_a), at the deepest point (K_b), along with the crack length and depth, a curve fitting tool with polynomial function in Matlab was used. The results are presented in Figure 3.3. The curve fitting results show that the two adjusted R-squares are both very close to 1, indicating good goodness of fit.

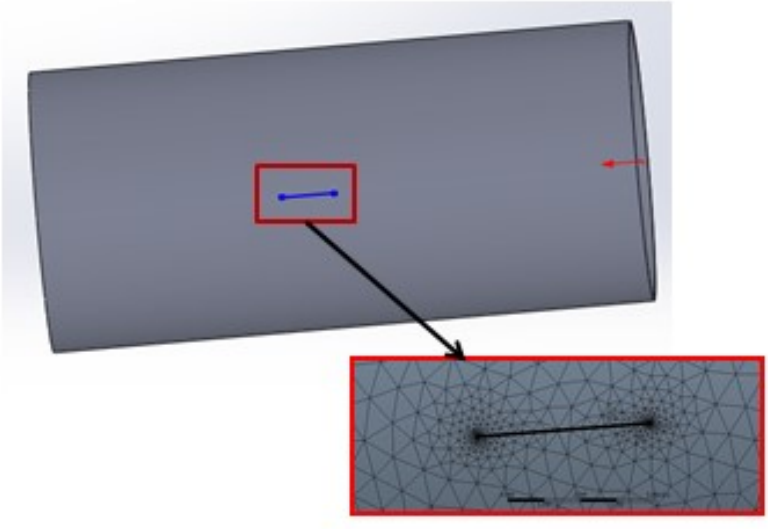

Figure 3.2 Crack built in ANSYS workbench

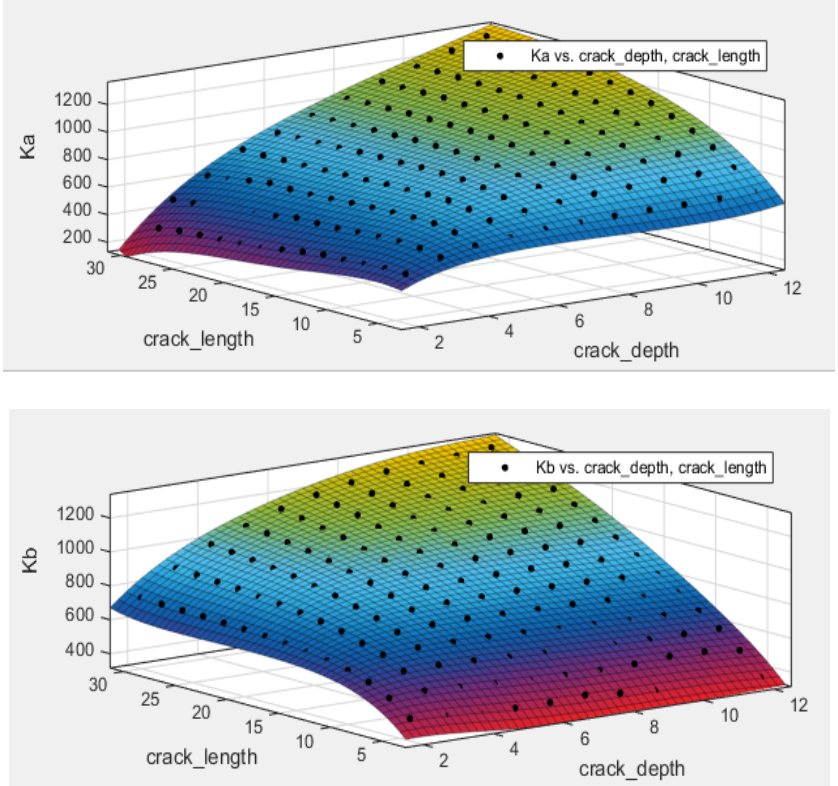

Figure 3.3 The fitted SIF functions

The internal pressure is varied from 0.69MPa to 2.76MPa in 0.69Mpa increments to find the SIF values at the surface point and those at the deepest point, which are displayed in Table 3.2. It can be concluded that the SIF is proportional to pressure. It can also be verified through the technique by Raju and Newman [243], which is widely applied to evaluate pipe stress considering fatigue cracks:

$$\Delta K = \Delta\sigma f\sqrt{\pi\frac{a}{Q}} = \Delta P\frac{D}{2t}f\sqrt{\pi\frac{a}{Q}} \tag{3-2}$$

where $\Delta\sigma$ is the range of the hoop stress, ΔP is the size of the pressure cycle, a is the instantaneous crack depth, and f and Q are constants that depend on pipe geometry and defect

length, respectively. Given that SIF is proportional to pressure, the SIF can be calculated at a certain pressure to obtain the SIF value at a different pressure by scaling the SIF value proportional to the pressure level [237].

Table 3.2 Pressure influence on SIF

P(MPa)	a(mm)	b(mm)	K_a	K_b
0.69	15.2	2.54	653.36	1187.6
1.38	15.2	2.54	1306.7	2375.2
2.07	15.2	2.54	1960.1	3562.7
2.76	15.2	2.54	2613.4	4750.3
0.69	15.2	5.08	1193.6	2340.9
1.38	15.2	5.08	2387.1	4681.9
2.07	15.2	5.08	3580.7	7022.8
2.76	15.2	5.08	4774.3	9363.8
0.69	50.8	5.08	792.33	2219.7
1.38	50.8	5.08	1584.7	4439.4
2.07	50.8	5.08	2377	6659
2.76	50.8	5.08	3169.3	8878.7

3.2.2 Pipe FE model verification

The pipe FE model is partially verified by comparing with the Raju and Newman method [243], outlined in “OPS TTO5 – Low Frequency ERW and Lap Welded Longitudinal Seam Evaluation”

[244]. The Raju and Newman method for calculating SIF for a semi-elliptical surface flaw is implemented in this project based on the following equations (3-3)-(3-8).

$$\Delta K = \Delta\sigma f\sqrt{\pi\frac{a}{Q}} = \Delta P\frac{D}{2t}f\sqrt{\pi\frac{a}{Q}} \tag{3-3}$$

$$Q = 1 + 4.595(\frac{a}{L}) \tag{3-4}$$

$$f = M_1 + M_2(\frac{a}{t})^2 + M_3(\frac{a}{t})^4 \tag{3-5}$$

$$M_1 = 1.13 - 0.18(\frac{a}{L}) \tag{3-6}$$

$$M_2 = \frac{0.445}{0.1 + \frac{a}{L}} - 0.54 \tag{3-7}$$

$$M_3 = 0.5 - \frac{0.5}{0.325 + \frac{a}{L}} + 14\left(0.5 - 2(\frac{a}{L})\right)^{24} \tag{3-8}$$

ΔP is the size of the pressure cycle, a is the depth of crack from the pipe surface, L is the length of the crack, D is outside diameter, and t is the pipe wall thickness.

The results by the Raju & Newman's method are compared with those obtained using the FE model, when the flaw length is 150mm (5.9in.). Length 150mm (5.9in.) is used because it corresponds to the case study in Section 3.5.The two curves are shown in Figure 3.4. As can be observed, the values calculated using these two methods are pretty close for a large portion of the crack depth range. The FE method is also compared with two other methods for cracked pipe SIF calculations: API 579 and BS 7910, which are outlined in Section 3.4.

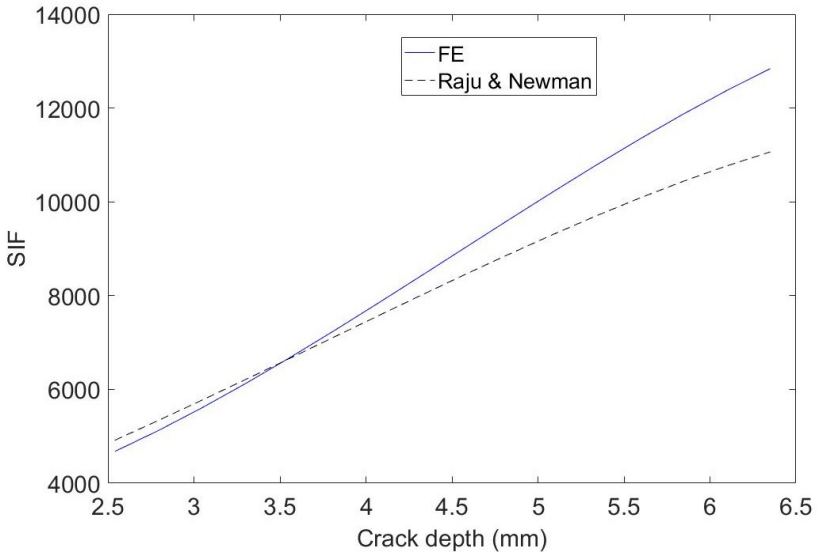

Figure 3.4 Comparison of SIF results between the Raju & Newman method and the FE method

3.3 The proposed integrated method for fatigue crack growth prediction

In the proposed integrated method for fatigue crack growth prediction, the pipe FE model calculates the SIF values for given crack sizes, which are utilized in the crack growth model governed by the Paris' Law for propagating the fatigue. The distributions of the uncertain model parameters are updated through Bayesian approach using the current fatigue crack size [245]. The estimate is based on ILI or nondestructive evaluation (NDE) data to get the uncertain model parameters to approach the real values for the specific unit being monitored. With the updated uncertain model parameters, the crack growth model can be applied to predict future crack growth and subsequently the failure time distribution. As part of the proposed approach, the pipe FE models are described in Section 3.2, and can be used for SIF computation.

3.3.1 Crack growth model

The fatigue propagation of a semi-elliptical surface crack considering two crack growth directions was analyzed. Newman and Raju [243] indicate that the aspect ratio change of surface cracks should be calculated by assuming that a semi-elliptical profile is always maintained, and that it is adequate to use two coupled Paris fatigue laws known as "two-point plus semi-ellipse" method:

$$\frac{da}{dN} = C_{\mathrm{A}}(\Delta K_{\mathrm{A}})^{m_{\mathrm{A}}} \tag{3-9}$$

$$\frac{db}{dN} = C_{\mathrm{B}}(\Delta K_{\mathrm{B}})^{m_{\mathrm{B}}} \tag{3-10}$$

where ΔK_{A} and ΔK_{B} are the ranges of the stress intensity factor at the surface points and the deepest point of the surface crack, and C_{A}, C_{B}, m_{A} and m_{B} are material constants.

The simulated crack growth paths using the evolution equations considering $C_{\mathrm{A}} = C_{\mathrm{B}}$, $m_{\mathrm{A}} = m_{\mathrm{B}}$ is more in accordance to the actual fatigue tests results reported in [246]. A semi-elliptical crack can propagate to a new semi-elliptical one based on the "two-point plus semi-ellipse" method [247], [248].

3.3.2 Bayesian inference for uncertain model parameter updating

In this section, the degradation model adopts two basic coupled Paris' law formulas as the crack growth model. On the right-hand side of the formula, a model uncertainty term ε is added to make the propagation model more accurate. The modified Paris' law can be represented by the following equations after considering the model uncertainty:

$$\frac{da}{dN} = C(\Delta K_A)^m \varepsilon \tag{3-11}$$

$$\frac{db}{dN} = C(\Delta K_B)^m \varepsilon \tag{3-12}$$

In addition, we assume that the measurement error $e = a_{\text{real}} - a_{\text{meas}} = b_{\text{real}} - b_{\text{meas}}$ has the following distribution:

$$e \sim N(0, \sigma^2) \tag{3-13}$$

The measured crack length and crack depth a_{meas} anf b_{meas}, respectively follow normal distributions centered at a_{real} and b_{real} as follows:

$$a_{\text{meas}} \sim N(a_{\text{real}}, \sigma^2) \tag{3-14}$$

$$b_{\text{meas}} \sim N(b_{\text{real}}, \sigma^2) \tag{3-15}$$

In physics-based methods, researchers use physical models for prognostics without considering the uncertainty of ILI data. In some papers, they only used the ILI data as a new starting point instead of updating model parameters of physics-based models. In this section, ILI data is used to update the uncertain material parameters using the Bayesian inference method. Because parameter *m* affects the degradation path and the predicted results more than parameter *C* based on the Paris' law, only the distribution of *m* is updated, while maintaining other model parameters unchanged. Thus, the posterior distribution $f_{\text{post}}(m \mid a, b)$ can be obtained through the Bayesian inference method:

$$f_{\text{post}}\left(m \mid a,b\right) = \frac{l(a,b \mid m) f_{\text{prior}}(m)}{\int l(a,b \mid m) f_{\text{prior}}(m) dm} \tag{3-16}$$

where $f_{\text{prior}}(m)$ represents the prior distribution of m; $l(a,b \mid m)$ represents the probability of detecting measured crack sizes, including length a and depth b.

Paris' law is employed to propagate the crack from the current ILI measured crack size to the ones at next inspection point with given value of m. Due to uncertainties in ILI tool and Paris' law, there exists the possibility to detect a certain crack length and crack depth at the next inspection point. The possibility can be denoted by a likelihood function $l(a,b \mid m)$.

3.3.3 The integrated method considering crack depth only

In most cases, the pipe fatigue crack does not propagate much along the crack length direction. If only growth along the crack depth direction is considered, the Paris' law model can be simplified to [249]:

$$\frac{da}{dN} = C(\Delta K)^m \varepsilon \tag{3-17}$$

And the equation for Bayesian updating is:

$$f_{\text{post}}\left(m \mid a\right) = \frac{l(a \mid m) f_{\text{prior}}(m)}{\int l(a \mid m) f_{\text{prior}}(m) dm} \tag{3-18}$$

3.4 Examples based on simulated data

3.4.1 Simulation example with the same starting point

In the example in this section, the proposed prognostics approach is verified based on simulated data. It is assumed that the standard deviation of ILI tool error equals to 0.15, C=5e-12, m~(2.5,0.2^2), and ε~N(1,0.2^2). We also set the initial crack length as 4mm and initial crack depth as 2mm.

Ten degradation paths are generated, as shown in Figure 3.5. The ten degradation paths are obtained based on the two Paris' law formulas, one for crack length and the other for crack depth, based on the above-mentioned model parameters. The initial crack length and depth are the same for all the ten degradation paths. The generated paths are separated into two sets: a training set, which is to derive a prior distribution of uncertain material parameter m, and a test set. The prediction performance of the proposed approach can be evaluated based on the test set.

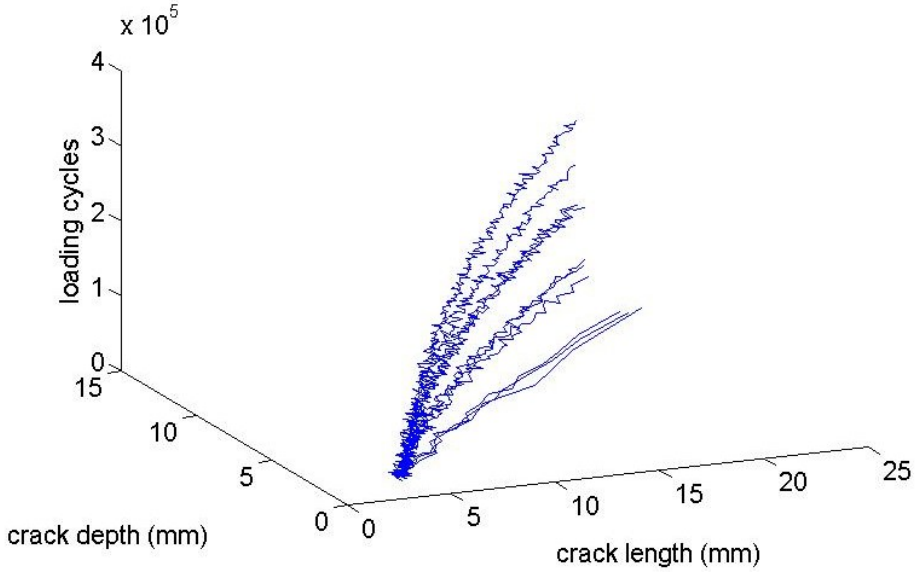

Figure 3.5 Ten simulated degradation paths

We select path 1 to 5 as the training set and 6 to 10 as the test set. Table 3.3 shows the ten real m values, since these real values are known during the simulated degradation path generation process. For the five degradation paths in the training set, a procedure based on least-square optimization, which was reported in Ref. [9], are used to estimate the m value for each training degradation path. These trained m values are subsequently used to fit the prior distribution parameters. We select normal distribution to fit them and the prior distribution of m is:

$$f(m)=\mathrm{N}(2.5439,0.1557^2) \tag{3-19}$$

Paths #6, #7, #8 are selected for testing the prediction accuracy of the proposed prognostics approach. During the updating process, the posterior distribution of m will serve as the prior distribution to update parameter m at the next inspection point. In path #6, a total of 2.4×10^4 cycles are taken to meet the failure criteria. All useful information in the updating process for path #6 is shown in Table 3.4. In path #7, the failure time is 3.1×10^4 cycles, and it is 2.8×10^4 cycles for path #8. The updating histories for mean and standard deviation values of parameter m in path #7 and path #8 are shown in Tables 3.5 and 3.6, respectively. The results show that for all these paths, their material parameter m is gradually updated from prior distribution to approach its own unique real value. Figure 3.6 shows the plots for updated distribution of parameter m for path #6. The plots for updated distribution of predicted failure time for path #6, #7, #8 are shown in Figures 3.7, 3.8, and 3.9, respectively. As can be seen from the results, the updated m values can approach the real m values through updating using the observed data. The failure time predictions also approach the real failure times. The uncertainty is reduced during the updating processes.

Table 3.3 The real values and trained values of *m*

Path#	Real m	Trained m
1	2.3888	2.3890
2	2.5968	2.5968
3	2.7886	2.7838
4	2.4787	2.4792
5	2.4667	2.4662
6	2.8027	-
7	2.7588	-
8	2.7805	-
9	2.5850	-
10	2.5447	-

Table 3.4 Validation results with path #6 (real *m*=2.8027)

Loading cycles	Crack	Crack	Mean of *m*	Std of *m*
0	4	2	2.5439	0.1557
0.6×10^4	5.4811	2.9010	2.7854	0.0358
1.2×10^4	7.6330	4.4793	2.7925	0.0148
1.8×10^4	11.9190	7.3864	2.8001	0.0069
2.4×10^4	22.6406	13.4753	2.8040	0.0036

Table 3.5 Validation results with path #7 (real m=2.7588)

Loading cycles	Crack length(mm)	Crack depth(mm)	Mean of m	Std of m
0	4	2	2.5439	0.1557
0.7×10^4	5.1763	2.8022	2.7239	0.0477
1.4×10^4	6.8845	4.0574	2.7428	0.0201
2.1×10^4	10.3283	6.0624	2.7617	0.0094
2.8×10^4	15.8216	9.5424	2.7546	0.0049

Table 3.6 Validation results with path #8 (real m=2.7805)

Loading cycles	Crack	Crack	Mean of m	Std of m
0	4	2	2.5439	0.1557
0.7×10^4	5.3408	2.9543	2.7527	0.0382
1.4×10^4	7.5956	4.4904	2.7703	0.0152
2.1×10^4	11.8729	7.1897	2.7760	0.0072
2.8×10^4	21.7281	12.7277	2.7777	0.0035

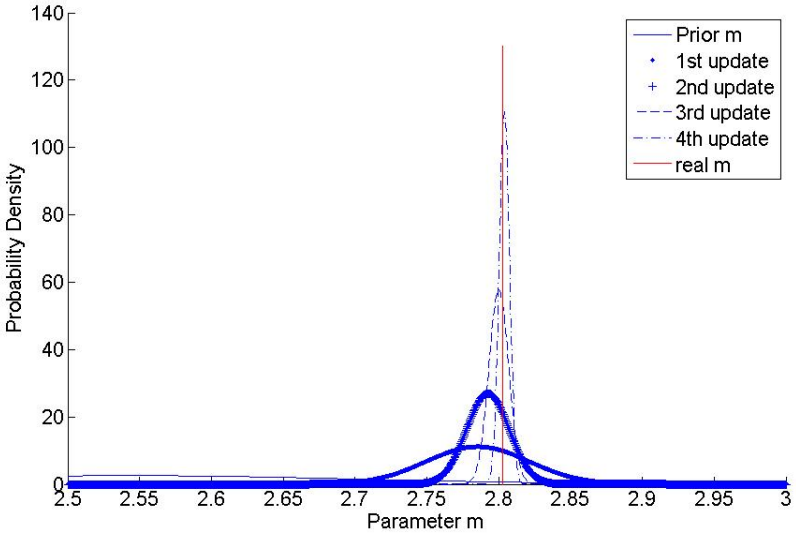

Figure 3.6 Distributions of parameter m for path #6

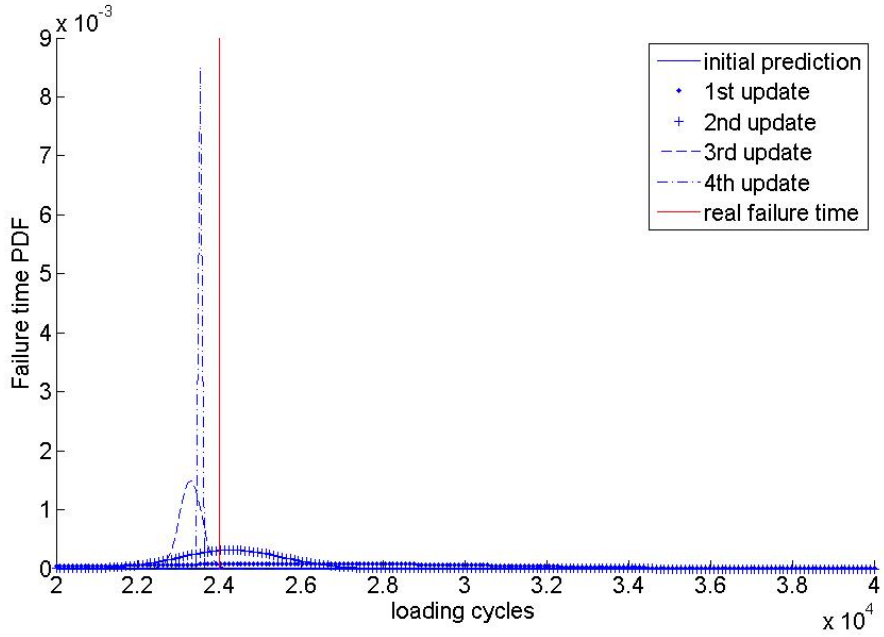

Figure 3.7 Distributions of predicted failure time for path #6

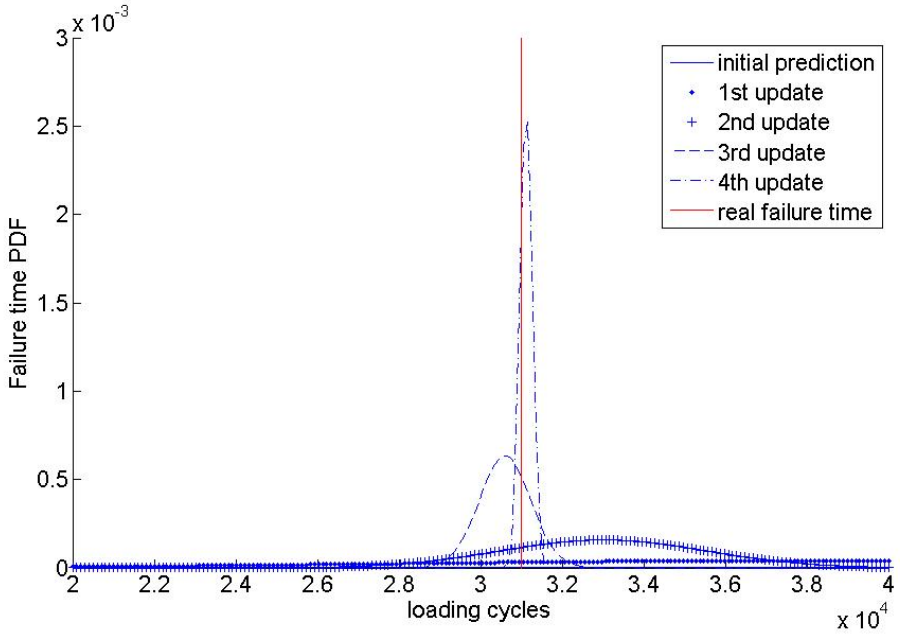

Figure 3.8 Distributions of predicted failure time for path #7

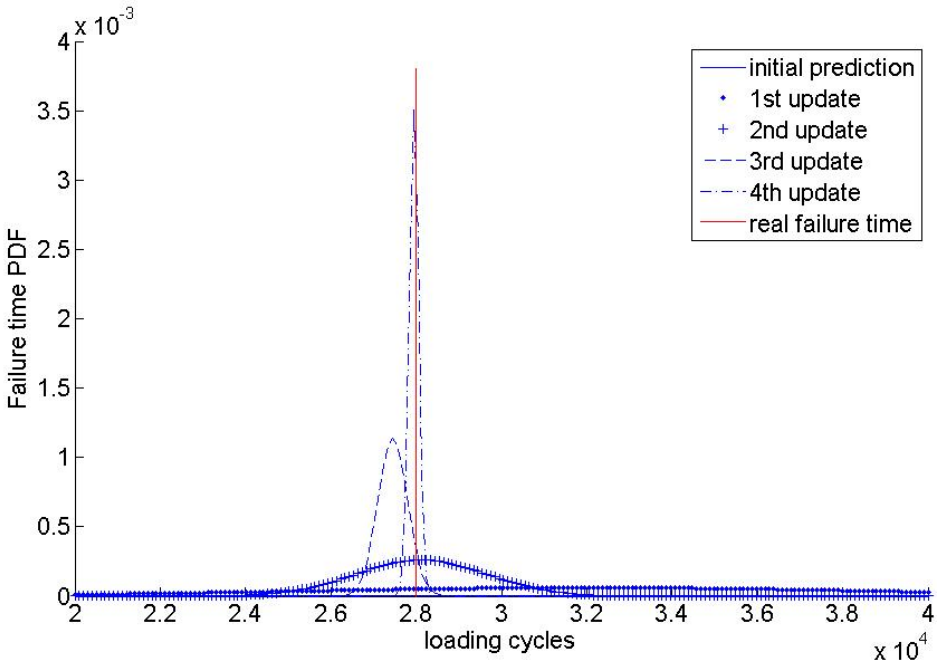

Figure 3.9 Distributions of predicted failure time for path #8

3.4.2 Sensitivity analysis

In this section, we study the sensitivity of the results to the variation of the initial crack sizes and the ILI tool measurement error. We use the same m values, as those listed in Table 3.3 in Section 3.4.1, to generate the ten degradation paths, and use path #6 as the test set. We change the initial crack length a_0 and/or initial crack depth b_0 while maintaining all the other parameters unchanged. In the comparison, three scenarios are considered, where initial crack length is much bigger than crack depth, much smaller than depth, or close to depth, respectively. Table 3.7 is then obtained with three different input sizes combinations. It should be noted that in each of the three initial crack size scenarios in Table 3.7, the initial crack sizes are the same for all the 10 paths in this sensitivity analysis. From the comparison results in Table 3.7, we can find that if we use the same inspection interval, the inspection times decrease from four times to two times or one time, as

crack lengths and/or depths increase. However, even with shorter inspection times, the mean values of *m* are all approaching the real value (2.8027), and this shows that the proposed approach works well under all these different initial conditions.

Table 3.7 Sensitivity analysis for initial crack depths and lengths (real *m*=2.8027)

(1) a_0=8mm, b_0=2mm

Loading cycles	Crack length(mm)	Crack depth(mm)	Mean of *m*	Std of *m*
0	8	2	2.5439	0.1557
0.6×10^4	9.8382	4.3728	2.7611	0.0383
1.2×10^4	15.1176	8.2462	2.7980	0.0110

(2) a_0=4mm, b_0=6mm

Loading cycles	Crack length(mm)	Crack depth(mm)	Mean of *m*	Std of *m*
0	4	6	2.5439	0.1557
0.6×10^4	7.1640	6.9937	2.7707	0.0342
1.2×10^4	13.9725	10.0862	2.8054	0.0096

(3) a_0=8mm, b_0=6mm

Loading cycles	Crack length(mm)	Crack depth(mm)	Mean of *m*	Std of *m*
0	8	6	2.5439	0.1557
0.6×10^4	13.9012	8.9284	2.7960	0.0121

Beside initial condition analysis, we also investigate the impact of measurement errors of the ILI tools on the results. We increase σ_{ILI} from 0.15mm to 0.3mm and 0.5mm, respectively. The results are shown in Table 3.8. The inspection times don't change as σ_{ILI} increases. For both cases

with larger measurement errors, the mean values of m are all approaching the real value (2.8027), which shows the effectiveness of the approach. As expected, the performance of the proposed approach becomes worse as the measurement error of ILI tool increases. This also implies that with the development of more accurate ILI tools, the lower measurement error will result in better performance for the proposed approach.

Table 3.8 Sensitivity analysis for measurement errors of ILI tools (real m=2.8027)

(1) σ_{ILI}=0.3mm

Loading cycles	Crack length(mm)	Crack depth(mm)	Mean of m	Std of m
0	4	2	2.5439	0.1557
0.6×10^4	5.0333	3.4444	2.7343	0.0756
1.2×10^4	8.1987	4.0964	2.7958	0.0218
1.8×10^4	11.8189	7.7472	2.7988	0.0098
2.4×10^4	22.3269	12.9847	2.7985	0.0045

(2) σ_{ILI}=0.5mm

Loading cycles	Crack length(mm)	Crack depth(mm)	Mean of m	Std of m
0	4	2	2.5439	0.1557
0.6×10^4	5.1455	3.5268	2.5728	0.0847
1.2×10^4	7.4150	4.2182	2.5919	0.0450
1.8×10^4	12.9044	8.0734	2.6383	0.0258
2.4×10^4	21.7774	12.4770	2.6829	0.0133

3.4.3 Simulation example with different starting points

In the example in this section, we assume that the standard deviation of ILI tool error equals to 0.15, C=5e-12, m~(2.5,0.2^2), and ε~N(0,0.2^2), which are the same as those in Section 3.4.1. The initial crack lengths and depths are uniformly random generated in the range of 4mm to 10mm, and 2mm to 6mm, respectively. In this way, we have different starting points, i.e. initial crack length and depth values, for the ten simulated degradation paths. The ten new degradation paths are generated, and shown in Figure 3.10.

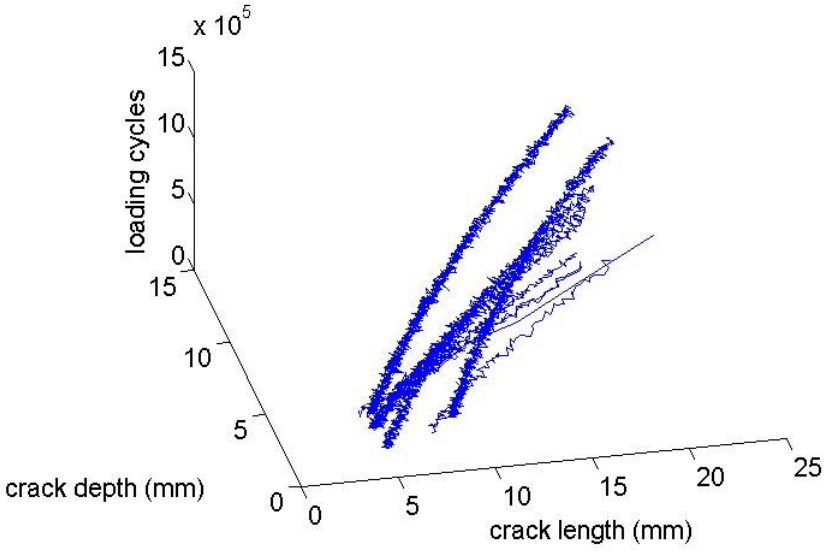

Figure 3.10 Ten simulated degradation paths with different starting points

Following the same procedure as Section 3.4.1, the real values and trained values of m are obtained in Table 3.9, and then we can obtain the prior distribution of m as:

$$f(m)=\mathrm{N}(2.3814,0.1352^2) \tag{3-20}$$

Paths #6, #7, #8 are then selected for testing the prediction accuracy of the proposed prognostics approach. In path #6, a total of 6×10^3 cycles are taken to meet the failure criteria. All useful information in the updating process for path #6 is shown in Table 3.10. The updating histories for mean and standard deviation values of parameter *m* in path #7 and path #8 are shown in Tables 3.11 and 3.12, respectively. From the results in these tables, *m* is gradually updated from the prior distribution to approach its own unique real value. The plots for updated distribution of parameter *m* and predicted failure time for path #6 are shown in Figures 3.11 and 3.12.

As can be seen from the results, the updated *m* values can approach the real *m* values through updating using the observed data. The failure time predictions also approach the real failure times. The uncertainty is reduced during the updating processes. In this example, it shows that the proposed approach works well for the case with different starting points.

Table 3.9 The real values and trained values of *m*

Path#	Real m	Trained m
1	2.5095	2.5096
2	2.2656	2.2653
3	2.2867	2.2864
4	2.5470	2.5468
5	2.2982	2.2979
6	2.9076	-
7	2.1310	-
8	2.3654	-
9	2.1309	-
10	2.5185	-

Table 3.10 Validation results with path #6 (real *m*=2.9076)

Loading cycles	Crack length(mm)	Crack depth(mm)	Mean of *m*	Std of *m*
0	5.6680	5.2929	2.3814	0.1352
2×10^3	8.1578	6.5013	2.7713	0.0161
4×10^3	11.5583	8.3144	2.8079	0.0083
6×10^3	18.3856	11.5141	2.8810	0.0011

Table 3.11 Validation results with path #8 (real *m*=2.3654)

Loading cycles	Crack length(mm)	Crack depth(mm)	Mean of *m*	Std of *m*
0	7.5834	5.9807	2.3814	0.1352
5×10^4	9.6401	7.2315	2.3464	0.0262
1.0×10^5	12.4980	8.3614	2.3579	0.0084
1.5×10^5	15.8673	10.3980	2.3593	0.0028

Table 3.12 Validation results with path #10 (real *m*=2.5185)

Loading cycles	Crack length(mm)	Crack depth(mm)	Mean of *m*	Std of *m*
0	7.0101	5.5680	2.3814	0.1352
2×10^4	9.4881	6.5740	2.5352	0.0332
4×10^4	12.0497	8.2202	2.5151	0.0137
6×10^4	15.9555	10.0877	2.5162	0.0071

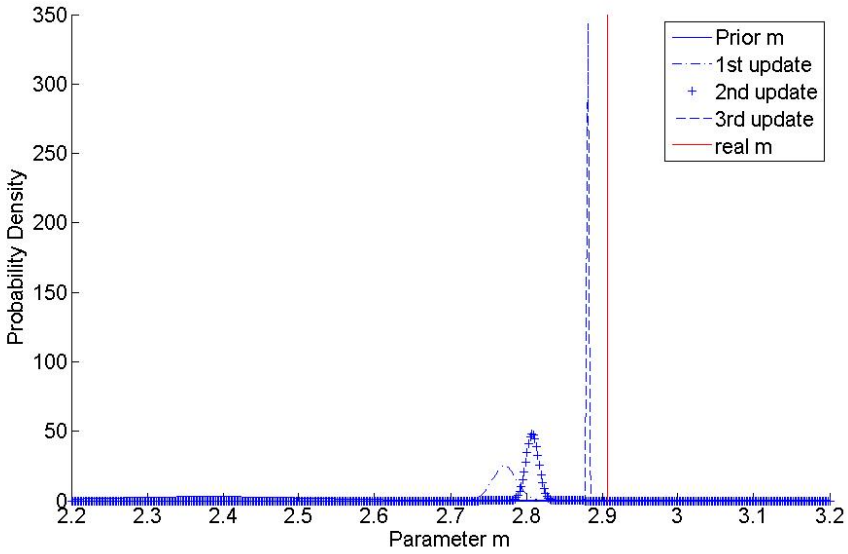

Figure 3.11 Distributions of parameter *m* for path #6

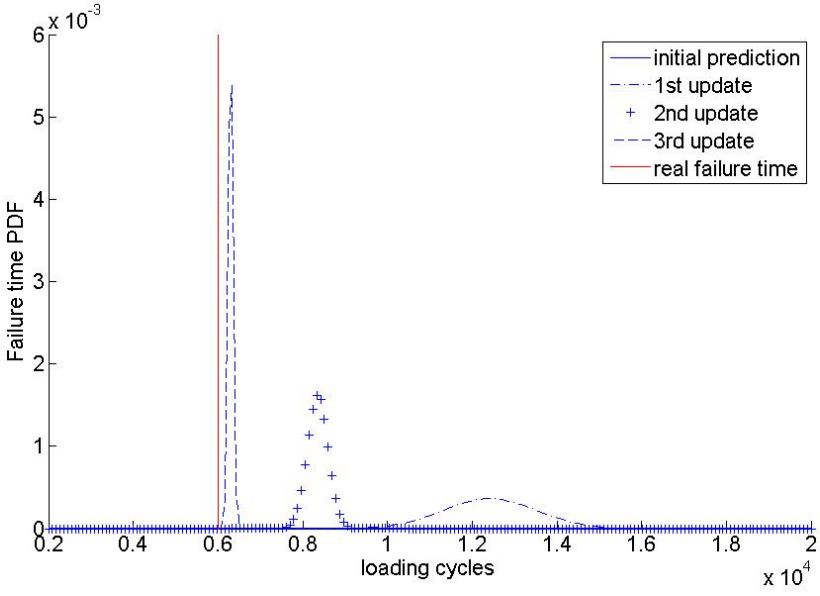

Figure 3.12 Distributions of predicted failure time for path #6

3.5 Comparative study and validation using ILI/NDE field data

In this section, a comparative study is performed between the proposed integrated method and the existing physics-based method using the ILI/NDE field data supplied by a Canadian pipeline operator. In addition, the performance of the proposed method under different ILI tool accuracy is also studied. A summary of the pipe properties and the flaw measured properties are given in the following Tables 3.13 and 3.14. These field data can then be used to validate the effectiveness of the proposed integrated method. And the limitations of the traditional physics based methods are given in this subsection.

Table 3.13 Pipe properties

Property	Value
Diameter	863.6mm (34in.)
Nominal Wall Thickness	7.1mm (0.281in.)
Grade	X52
Maximum operating pressure	4.5MPa (649psi)

Table 3.14 Flaw measured properties

Date of Size	Growth Length	Peak Depth
February 2002	150mm (5.9in.)	2.95mm (0.116in.)
April 2007	150mm (5.9in.)	6.40mm (0.252in.)

3.5.1 Pressure data processing using rainflow counting

The internal pressure keeps changing during the life cycle of pipelines. There are multiple reasons that can cause the change of pressure, such as the transportation of different products, the close and open of valves, etc. Pressure cycling drives pipe fatigue crack growth, and pressure data is used to calculate the SIF values. Figure 3.13 is a plot of the pressure data from February 6, 2003 to March 31, 2007. It can be seen that the pipeline operations change in November 2005, and the pressure cycling also changes at that time. The rainflow-counting method is used to count the number of discrete pressure cycling ranges, which will subsequently be used in pipe stress analysis. Two output matrices, namely matrix 1 and matrix 2, are generated. Matrix 1 contains information for each individual cycle including cycle number, time information, and range of pressure. Matrix 2 organizes the individual cycles into different range limits, with the range increment set to 5 psi (0.034MPa). The rainflow-counting result is shown in Figure 3.14. As can be seen, there are a large number of small cycles with small pressure ranges, and a small number of large cycles.

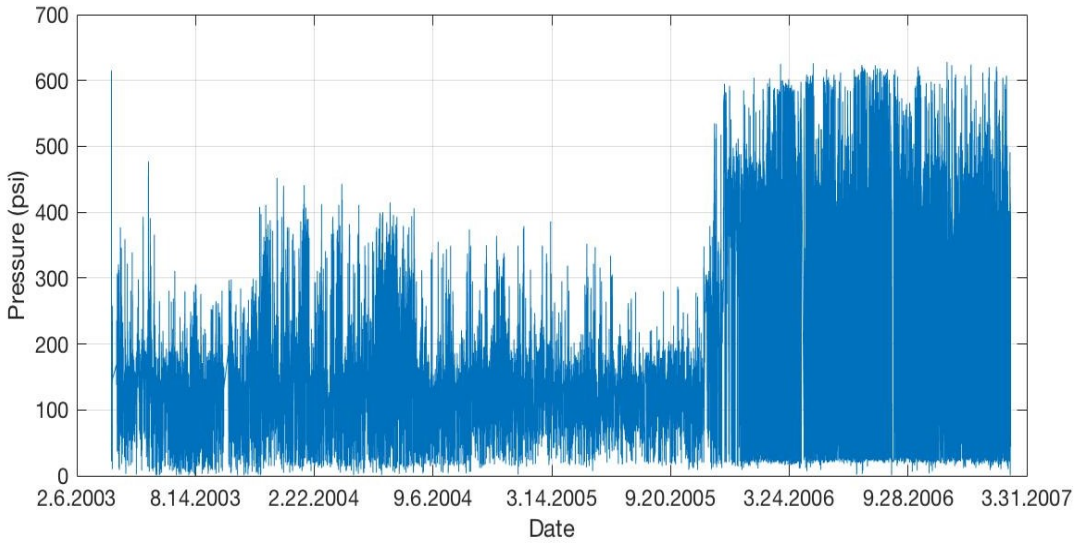

Figure 3.13 Total pressure data from February 6, 2003 to March 31, 2007

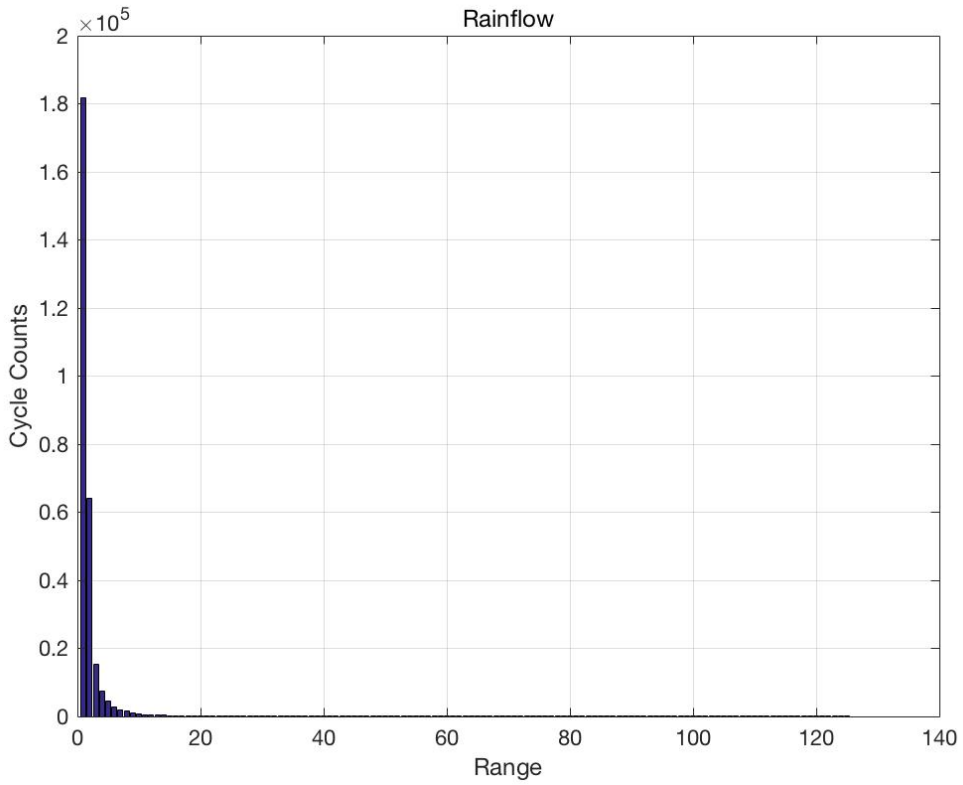

Figure 3.14 Rainflow counting result

3.5.2 Fatigue crack propagation based on the rainflow counting results

As mentioned in the previous subsection, we can obtain two different output matrices from the rainflow-counting method, namely matrix 1 and matrix 2. The two matrices are based on the pressure data from February 6, 2002 to March 10, 2007. It is assumed that prior to February 6, 2003, the pressure data is the same from 2003-2004 since the operation had been the same during the period. It is obvious that matrix 1 should give more accurate results than matrix 2, but can be more computationally intensive to use to calculate fatigue crack propagation. Figure 3.15 shows degradation paths generated using matrix 1 and the FE method. By using matrix 2, the pressure ranges can be ranked in an increasing or decreasing order. Depending on the order, the upper bound or the lower bound can be used to represent each range limit. The investigations show that

using matrix 2 by ordering the pressure ranges increasingly or decreasingly give very close degradation path results. It can also be found that matrix 1 and matrix 2 give relatively close crack depth values on both February 6, 2003 and Mar. 10, 2007.

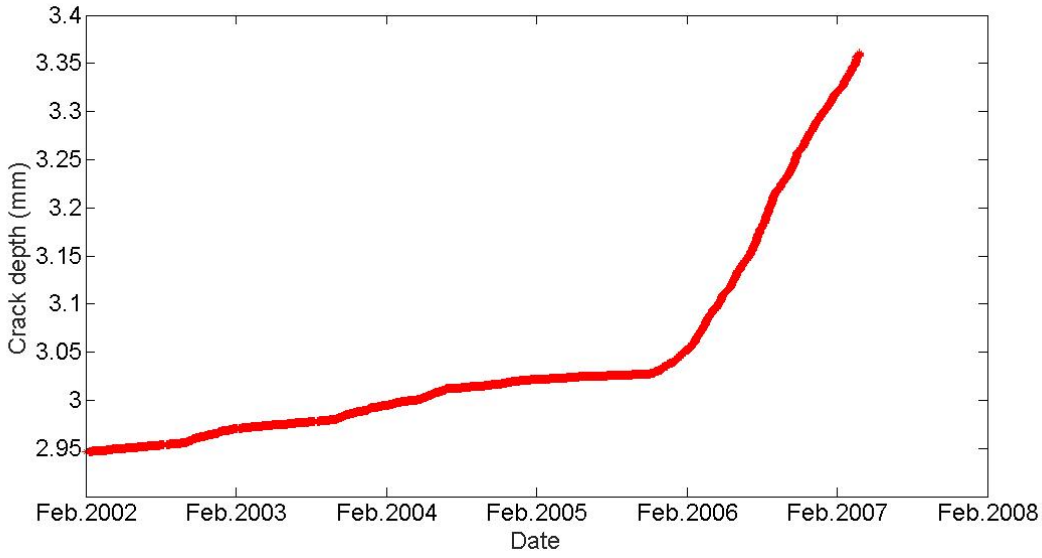

Figure 3.15 Degradation paths generated using matrix 1

3.5.3 Critical crack depth determination

Once the critical crack size is reached, the pipe is considered failed, and thus the failure time and the remaining useful life can be determined. The critical flaw size depends on the nominal stress, the material strength, and the fracture toughness. The relationship between these parameters for a longitudinally oriented defect in a pressurized cylinder is expressed by the NG-18 "ln-secant" equation [244]:

$$\frac{C_V \pi E}{4 A_C L_e \sigma_f^{\,2}} = ln\left[sec\left(\frac{\pi M_S \sigma_H}{2\sigma_f} \right) \right] \tag{3-21}$$

where

$$M_S = \frac{1 - \frac{a}{tM_t}}{\frac{a}{t}} \tag{3-22}$$

$$M_t = [1 + 0.6275z - 0.003375z^2]^{\frac{1}{2}}, z = \frac{L_e^{\ 2}}{Dt} \le 50 \tag{3-23}$$

$$\text{or} \quad M_t = 0.032z + 3.3, z > 50 \tag{3-24}$$

The values used in the equations are further explained as follows: a is flaw depth; t is the pipe wall thickness, and t=7.1mm(0.281in.); E is the elastic modulus, and E=206GPa; L_e is an effective flaw length, equal to the total flaw length multiplied by π/4 for a semi-elliptical flaw shape common in fatigue. In our study, L_e=150×$\frac{\pi}{4}$=117.8mm; σ_f is the flow stress typically taken as the yield strength plus 68MPa, or as the average of yield and ultimate tensile strengths. σ_f=σ_y+10=403+68=471MPa(68.42ksi); σ_H is the nominal hoop stress due to internal pressure. σ_H=p×$\frac{D}{2t}$; C_V is the upper shelf CVN impact toughness. C_V=4.9m·kg (35.8ft·lbs); A_c is the cross-sectional area of the Charpy impact specimen. A_c=80mm^2(0.124 in.^{2}).

The field data is applied to these equations, and the resulting relationship is shown in Figure 3.16. Given the crack length of 150mm (5.9in.), if the internal pressure is equal to the Maximum Operating Pressure (MOP) of 4.5MPa (649psi), the critical depth-to-thickness ratio will be 0.6688. Thus, the critical crack depth is 0.6688×7.1=4.8mm (0.188 in.). The discrepancies from the NDE depth in April, 2007 (6.4mm) is because this way to determine the critical depth is relatively conservative.

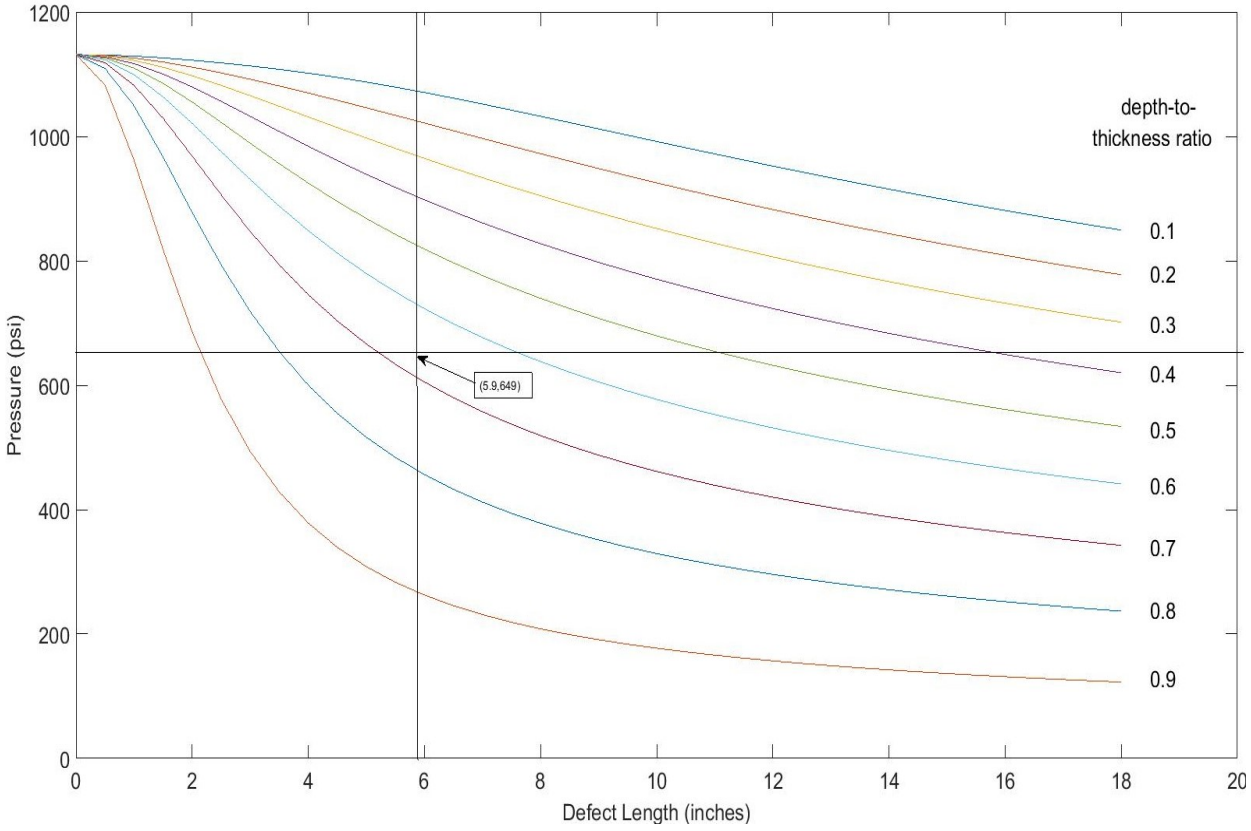

Figure 3.16 Relationship between failure stress and flaw size

3.5.4 ILI-NDE depth distribution

NDE fatigue crack depth is considered as accurate for the purposes of this case study. ILI-NDE depth data give the differences between the collected ILI depth values and the corresponding NDE depth values, and thus can represent the accuracy of the ILI tool in measuring fatigue crack depth. With all the 16 sample field depths provided by the industry partner, a normal distribution is used to fit the ILI-NDE depth data, with the estimated mean 0.6669 mm (0.026 in.), and standard deviation 0.4795 mm (0.0189 in.). This can be further used as the measurement error of ILI tool by considering NDE as a relatively accurate examination tool.

3.5.5 Limitations of the existing physics-based method

The fatigue crack growth results by the existing physics-based method are briefly discussed in Section 3.5.2 and presented in Figure 3.15. With the physics-based method based on the Paris' law, fixed model parameters are used: m=3 and C=3.0×10^{-20}MPa$\sqrt{\text{mm}}$ (8.6×10^{-19}psi$\sqrt{\text{in}}$). The finite element method and Raju and Newman method are employed in stress intensity factor calculations. As can be seen in Figure 3.15, the crack depth in April 2007 is 3.37mm (0.1325 in.), which is far from the actual crack depth of 6.40mm (0.252 in.) which is measured using the NDE tool. The crack growth results show that the existing physics-based method does not perform well in this case study. However, physics-based methods are were much better aligned to observed growth using more common conservative industry approaches to calculate SIF such as BS 7910 and API 579.

3.5.6 The integrated method and its performance under different ILI tool accuracy

With this dataset, 2 NDE measurements are available, and are used to find the real m value by trying different m values. It is found that an m value of 3.11 will give the crack depth of 0.252 inch in April 2007, meaning that 3.11 is the real m value for the pipe. The crack growth curves for m=3.11 and m=3 are shown in the following figure, Fig. 3.17. With the real m value, the real crack depth value can be obtained at any given point in time.

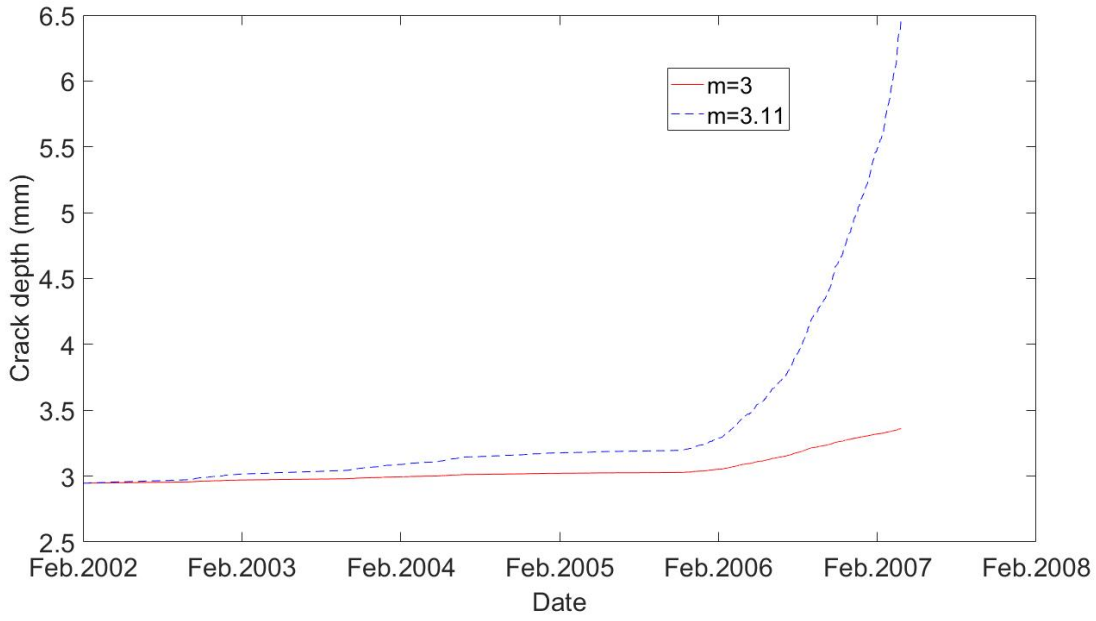

Figure 3.17 Real crack growth curve

The prediction performance of the proposed integrated method is investigated under different ILI tool accuracy, measured by the ILI tool measurement uncertainty. In this thesis, we investigate the integrated method's performance when the ILI tool measurement uncertainty standard deviation is equal to 0.25mm (0.01in.), 0.38mm (0.015in.), and 0.50mm (0.02in.), respectively.

Feb. 2002 is set as the starting point for crack growth, where the crack depth is 2.95mm (0.116in.). Jun. 2006 is used as the first inspection point because ILI data is available from that time. Nov. 2006 is used as the second inspection point. The crack depth will be predicted for Apr. 2007, and compared with the NDE depth measurement of 6.40mm. As can be seen from the real crack growth curve shown in Figure 3.17, the real crack depth is 3.96mm in Jun. 2006 and 5.13mm in Nov. 2006. The first case that was investigated was when the ILI measurement uncertainty standard deviation is 0.25mm. To try to fully assess the prediction performance of the integrated method for the Jun. 2006 inspection point, five ILI data points were sampled from a normal

distribution with a mean of 3.96mm (real crack depth) and standard deviation of 0.25mm. For each of the sampled ILI data points, parameter *m* is updated using Bayesian inference, and the mean of the five updated *m* values is 3.129 for Jun. 2006, as shown in Tables 3.15 (a-c). The same approach is done for the Nov. 2006 inspection point, and the mean of the updated *m* value is 3.101. The mean predicted crack depth values for Apr. 2007 are also obtained and recorded in Table 3.15(a). As can be seen, the updated *m* value gets closer to the real *m* value of 3.11, and the predicted crack depth for Apr. 2007 gets closer to the real crack depth 6.40mm.

Next we investigate the cases where the ILI tool measurement uncertainty standard deviation is equal to 0.38mm and 0.50mm. The same procedure as mentioned above is followed, and the results are recorded in Tables 3.15(b) and 3.15(c). From the results in Table 3.15, it can be seen that the best prediction performance is achieved when the measurement uncertainty is the smallest (0.25mm), and the prediction performance becomes worse when the measurement uncertainty is larger, as expected. It can also be observed that for all three ILI measurement uncertainty cases, the integrated method outperforms the existing physics-based method. Note that for the "ILI-NDE Depth sample" data, the ILI tool measurement uncertainty standard deviation is 0.48mm, which is between the case ($\sigma_{ILI} = 0.38$) and the case ($\sigma_{ILI} = 0.50$). It is expected that the ILI tool accuracy will keep improving in the future, which will result in more accurate predictions of crack depth using the integrated method. And with a more advanced ILI crack detection tool, the proposed integrated prognostics method can greatly improve the accuracy of the remaining useful life prediction for pipelines with fatigue cracks, and consequently that would lead to a more efficient pipeline integraty management program.

Table 3.15 Update results for different ILI tool measurement error

(a) σ_{ILI}=0.25mm

Inspection year	Feb. 2002	Jun. 2006	Nov. 2006
Crack depth (mm)	2.95	3.96	5.13
Mean of m	3	3.129	3.101
Std of m	0.15	0.019	0.008
Predicted crack depth for Apr. 2007	3.37	Reaching 6.40mm in Dec. 2006	5.64

(b) σ_{ILI}=0.38mm

Inspection year	Feb. 2002	Jun. 2006	Nov. 2006
Crack depth(mm)	2.95	3.96	5.13
Mean of m	3	3.097	3.098
Std of m	0.15	0.054	0.018
Predicted crack depth for Apr. 2007	3.37	5.23	5.31

(c) σ_{ILI}=0.50mm

Inspection year	Feb. 2002	Jun. 2006	Nov. 2006
Crack depth(mm)	2.95	3.96	5.13
Mean of m	3	3.029	3.074
Std of m	0.15	0.106	0.042
Predicted crack depth for Apr. 2007	3.37	3.58	4.27

3.6 Conclusions

Managing fatigue cracks has been a top priority for liquid pipeline operators. Existing ILI tools for pipeline defect evaluation have fatigue crack measurement uncertainties. Furthermore, current physics-based methods are mainly used for fatigue crack growth prediction, where the same or similar fixed model parameters are used for all pipes. They result in uncertainty that requires a conservative approach for integrity management approach and management and risk mitigation strategies. In this chapter, an integrated approach is designed to predict pipeline fatigue crack growth with the presence of crack sizing uncertainty. The proposed approach is carried out by integrating the physical models, including the stress analysis models, the damage propagation model governed by the Paris' law, and the ILI data. With the proposed integrated approach, the FE model of a pipe with fatigue crack is constructed. ILI data are applied to update the uncertain material parameters for the individual pipe being considered, so that a more accurate fatigue crack growth prediction can be achieved. The rainflow counting method is used to count the loading cycles for the proposed integrated method under time-varying operating conditions. Furthermore, we compare the proposed integrated approach with the existing physics-based method using examples based on simulated data. Field data provided by a Canadian pipeline operator is also used to validate the proposed integrated approach. At the end, the examples and case studies in this thesis demonstrate the limitations of the existing physics-based method, and the promise of the proposed integrated approach for achieving accurate fatigue crack growth prediction as ILI tool measurement uncertainty further improves. Enbridge recently announced a multi-year collaboration agreement with NDT Global, to build a new generation of improved crack ILI to further improve measurement uncertainty [32]. The developed methods can contribute to a more

efficient pipeline integrity management approach for managing crack threats by reducing unnecessary maintenance work and downtime.

4 Risk-based pipeline re-assessment optimization considering corrosion defects

4.1 Introduction

Pipelines are critical assets for gathering and transporting different crucial items such as oil, natural gas, and water, and they are critical for a city's reliable, safe and secure operations. Research studies have been conducted on various topics to ensure pipeline reliability and safety, such as qualitative and quantitative risk assessment methods for urban natural gas pipeline network [250], risk-based maintenance of petroleum pipeline systems [213], and optimized maintenance scheduling for water pipeline networks [251]. Pipelines in the system are easily affected by surrounding environment, construction errors, natural disasters and human activities. Different kinds of defects, such as corrosion, crack, mechanical damage and third party damage, may result in reduced strength in pipeline segments, and present threat to the whole system. Hence, these defects need to be managed properly to avoid environmental hazards and costly downtime.

For some threats to pipeline integrity, like corrosion, crack and dents, the nature of the growth mechanisms are time-dependent. With the use of suitable damage propagation model, the probability of failure can be estimated for pipelines with particular types of defects. Corrosion is a major integrity threat to oil and gas pipelines. Risk analysis for metal loss corrosion defect is a vital part of pipeline integrity management. Risk is typically defined as the multiplication of probability and consequence, and it can be used as a reliability measure for pipeline systems. Qualitative and quantitative risk assessment methods are two ways for pipeline integrity

management. Qualitative risk assessment methods are based on a risk analysis index system, which contains few essential data and leads to a rough estimation without giving a numerical value. However, a final descriptive ranking is given based on the index system and the results are easily presented and understood. Quantitative methods use physics models and numerical simulation to obtain quantitative assessment of risks. Han and Weng [250] compared proposed qualitative and quantitative risk assessment methods for the natural gas pipeline system. The results for two methods were close and they could both be used in practical applications. Zhang and Zhou [252] proposed a method to evaluate the reliability of corroding pipeline systems.

ILI is a typical inspection method for evaluating pipeline conditions and defect sizes using ILI tools such as magnetic flux leakage tools and ultrasonic tools. It is important to optimize maintenance activities to improve reliability, reduce risks and minimize the overall costs. Li et al. [253] proposed a quantitative risk analysis model for leakage failure using Bayesian networks. Optimal inspection planning for pipelines with corrosion defects has drawn lots of research attention due to its key role and the significant cost of performing ILI inspections. Gomes [221], [222] optimized the inspection schedule for pipelines with corrosion and crack defects respectively. All the methods used in these papers considered the inspection interval as the design variable, and the optimal inspection interval is fixed and constant during the whole pipeline service time once it is determined. However, pipeline defect sizes are different at different inspection points, resulting in different future defect growth and system failure probability, and thus it is more reasonable to apply different re-assessment intervals depending on pipeline health conditions.

In this chapter, we develop an approach to find the optimal re-assessment intervals for pipelines subject to multiple corrosion defects, where the probability of failure (PoF) threshold is

used as the decision variable for this optimization problem. Re-assessment is performed for the entire line when the predicted system PoF reaches the PoF threshold. The re-assessment interval is not constant, because it varies due to different predicted defect growth and failure probability during different stages of pipes in their life cycles, or combinations of pipes with different conditions. The framework of this study is shown in Figure 4.1. First, through using detection and inspection tools like ILI tools, defects for different pipeline segments can be detected. Damage prediction models are used for predicting the growth of these defects. The entire line with multiple corrosion defects can be treated as a series system with multiple components, because it will fail if any defect meets its limit states or failure criteria. The system failure probability can be evaluated based on the structure of pipeline system and each defect's failure probability. When the failure probability for the entire line reaches the PoF threshold, different options of maintenance and rehabilitation activities may be implemented based on the corresponding criteria to ensure the safety of the whole pipeline system. Cost rate evaluation at the re-assessment point needs to be determined considering inspection cost, repair cost, potential failure cost, etc. Lastly, optimization is conducted for the pipeline system to find the optimal PoF threshold with respect to the lowest cost rate. The optimal re-assessment intervals will be determined by implementing the re-assessment policy defined by the optimal PoF.

Monte Carlo simulation technique is utilized to analyze the re-assessment policy, and uncertainties need to be considered and quantified in the simulation process. Defect identification and classification are critical for pipeline system integrity management. ILI tools have been evolving rapidly and these tools are widely used for detecting and inspecting corrosion, erosion, cracks, etc. The accuracy of ILI tools affects inspection results a lot. The inspection results contain information about types, locations and dimensions of defects and they serve as the

basis for assessing a pipeline system's current condition. Therefore, the measurement error of ILI tools is necessary to be considered in the pipeline system integrity management. In this study, uncertainties in pipe geometry and material properties are also considered as important uncertainty factors in addition to the tool measurement error.

The remainder of the chapter is organized as follows. Section 4.2 describes the damage propagation models including the limit state functions for corrosion defects as well as uncertainty quantification. Section 4.3 introduces the proposed re-assessment and maintenance policies, and presents the proposed pipeline re-assessment optimization approach. Section 4.4 presents examples to implement the proposed approach, investigates the impact of relevant parameters on the results, and compares with fixed interval method. Conclusions are presented in Section 4.5.

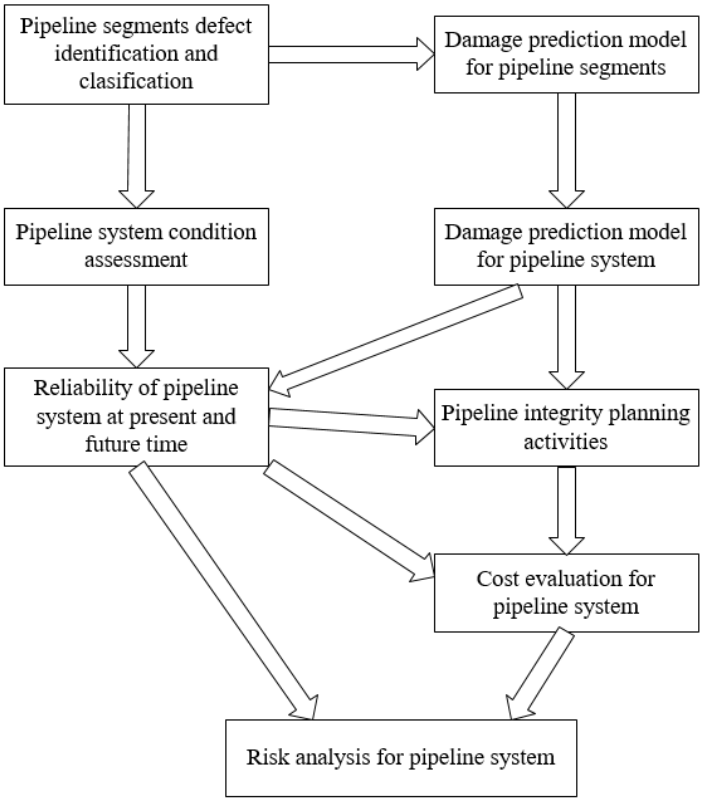

Figure 4.1 Framework for the pipeline system risk assessment

4.2 Damage prediction models

4.2.1 Limit state functions for failure due to corrosion

For pipelines with active corrosion defects, failure caused by the defects is determined by calculating the limit state functions (LSFs). There are two limit state functions representing the failure criteria for pipelines with corrosion defects. The corrosion defects are considered to be safe only when the two limit state functions are both positive.

The first LSF is defined as the difference between the burst pressure P_f and the operating pressure P_{op}, and the general form of the *LSF* is：

$$LSF_1 (P_f, T) = P_f (D, t, YS, UTS, d(T), L(T)) - P_{op} \quad (4\text{-}1)$$

where D is the pipeline diameter; t is the pipeline wall thickness; *YS* and *UTS* are the pipeline material yield strength and ultimate tensile strength, respectively; L is the axial length of the defect; d is the depth of the defect and T is the elapsed time. This limit state function is time-dependent, and the burst pressure P_f depends on the above-mentioned parameters.

As for burst pressure calculation, in the literature, various burst pressure models, including B31G [88], [109], modified B31G [110], Battelle [116], DNV-99 [113, p. 101], Shell-92 [111], can be used to calculate P_f in Eq. (4-1). Equations for all these methods are similar and they are all based on the NG-18 equation [119]. Cosham et al. [120] presented and compared these burst pressure models in the literature used to assess corrosion defects. Caleyo et al. [121] compared these burst pressure models when conducting the reliability assessment of corroded pipelines. Among these burst pressure models, modified B31G is the most popular one and it is relatively

accurate. Hence, in this thesis, we use modified B31G model to calculate burst pressure, which is shown as follows:

$$P_f = \frac{2(YS + 68.95)t}{D}\left(\frac{1-\frac{0.85d(T)}{t}}{1-\frac{0.85d(T)}{tM}}\right) \tag{4-2}$$

$$M = \sqrt{1 + 0.6275\frac{L(T)^2}{Dt} - 0.003375\left(\frac{L(T)^2}{Dt}\right)^2}, \text{ if } \frac{L^2}{Dt} \le 50$$
$$M = 0.032\frac{L(T)^2}{Dt} + 3.3, \text{ if } \frac{L^2}{Dt} > 50. \tag{4-3}$$

In industry practice, often times 80% of the wall thickness is used as the threshold of the defect depth. It is a conservative maximum allowable value though, which means the leaks will not occur when the defect depth reaches 80% of the wall thickness, and there is no tolerance when considering a serious pipeline integrity issue. This leads to the second LSF, which is defined using the following equation:

$$LSF_2\,(d,\ T) = 0.8t - \ d(T). \tag{4-4}$$

As indicated before, a defect failure occurs if one of the LSFs is negative. Therefore, the probability of failure associated with an individual corrosion defect PF_{defect} is computed by:

$$PF_{\text{defect}} = \Pr\,(LSF_1 \le 0 \ OR \ LSF_2 \le 0) \tag{4-5}$$

The corrosion growth model needs to be determined to calculate the probability of failure for a single corrosion defect. The widely used corrosion degradation models for defect depth with respect to time are shown in the following equations [121], [254], [255].

$$d(T) = d_0 + V_r(T - T_0) \tag{4-6}$$

$$L(T)=L_0+V_a(T-T_0) \quad (4\text{-}7)$$

where d_0 and L_0 are initial defect depth and length, respectively; V_r and V_a are radial and axial corrosion growth rate, respectively; T_0 is the time of last inspection and T is the exposure time. Substituting Eq. (4-1)-(4-4), (4-6), (4-7) into Eq. (4-5), we can predict the failure probability of a single corrosion defect at any future time. Thus, reliability can be calculated based on pipe geometry, defect geometry, material properties, growth rates and time.

There are many pipeline segments in a pipeline system, inspected by ILI tools. Therefore, it is very likely there are multiple corrosion defects in the pipeline. The entire pipeline is considered in this study, which is consistent with industry practice in ILI planning. Major pipelines are typically series systems over very long distance without complex network structure, and a pipeline system for which ILI assessments are planned for is typically a series system. It is also assumed that all these corrosion defects are independent, and they typically occur at different locations. The probability of failure for a pipeline segment with multiple corrosion defects PF_{pipe} is calculated by:

$$PF_{pipe}=1-\prod_{i=1}^{n}(1-PF_{defect,i}) \quad (4\text{-}8)$$

where PF_{pipe} is failure probability of the pipeline, and n is the number of corrosion defects.

4.2.2 Uncertainties quantification

There are uncertainties both on load and resistance parameters, which the two limit state functions depend on due to tool performance and measurement errors. The relationship among risks, costs and tool performance need to be investigated. The information about pipe geometry and mechanical properties may have some uncertainties when measuring and testing them.

Material uncertainty and geometry uncertainty will affect the burst capacity model, and as a result, will cause uncertainties in determining the limit state of corroded pipelines. Uncertainties associated with the ILI tool can be represented by the measurement error. In general, the measurement error will be affected by the resolution of ILI tool. It will affect the predicted depth a lot if the measurement error is big. σ_{ILI} is used to denote standard deviation of the measurement error in this thesis.

Besides, model uncertainty of corrosion growth model should also be investigated. In the corrosion growth model, the two major parameters, corrosion growth rates V_r and V_a, depend on the surrounding environment and pipe materials. These random variables are assumed to follow normal distributions. The mean and standard deviation used for the basic variables in each analysis can be seen in Table 4.1. Some parameters of these variables were reported in [4].

Table 4.1 Random variables [4]

Random variables	Mean	Standard deviation
Pipeline diameter (D)	914.4mm	18.288
Pipeline thickness (t)	20.6mm	0.412
Operating fluid pressure (P_{op})	7.8MPa	1.56
Material yield stress (YS)	358MPa	25.06
Ultimate tensile strength (UTS)	455MPa	31.85
Defect length (L_0)	200mm	20
Defect depth (D_0)	(10%-20%)t	0.5
Radial corrosion growth rate (V_r)	0.3mm/year	0.03
Axial corrosion growth rate (V_a)	10mm/year	0.5

4.3 The proposed risk-based re-assessment optimization approach

4.3.1 Re-assessment and maintenance policy

The proposed risk-based pipeline re-assessment and maintenance policies are described in this section. The proposed risk-based re-assessment optimization approach is used to find the optimal PoF threshold. At the current pipeline assessment point, defect information is collected based on the pipeline assessment results. Corrosion defect growth can be predicted based on the current defect information and defect growth models. Considering uncertainties in defect measurement, defect growth, pipe properties, future defect failure probability, and thus pipeline system PoF, can be predicted. The re-assessment interval is the point when the predicted system PoF first exceeds the optimal PoF threshold. Inspection cost is incurred at the predicted re-assessment interval.

In addition, at a pipeline assessment point, maintenance actions, including possible excavation and repair actions, may be taken based on the collected defect information. There are mainly two types of maintenance activities: predictive maintenance and corrective maintenance. Maintenance option selection is based on the risk estimation, which means we need to calculate the probability of failure of the whole system and quantify the total consequence of the failure hazards. If a failure occurs in pipelines at any time, the corrective maintenance or replacement needs to be performed immediately. In industry, pipeline failure is highly undesirable due to the potential damage to human life and environment and huge economic loss, and it is characterized by very high failure cost in this study. As to predictive maintenance activities, it is typically performed at an inspection point and there are two main repair activities, sleeving and recoating.

If a corrosion defect is successfully detected, we can utilize certain criterion to determine repair actions. Based on monitoring programs, the mitigation programs are initiated including pipeline excavations and different repair activities if a defect meets a certain criterion. A defect will be repaired immediately after inspection if any of the following limit state functions, described in equations (4-9) and (4-10), is smaller than zero [206]. Here, we call it as repair criteria 1. If a defect doesn't meet the repair criteria 1, neither excavation nor repair activities need to be performed at the inspection point.

$$LSF\,(d) = 0.5t - d \leq 0 \tag{4-9}$$

$$LSF\,(P_f) = P_f - 1.39P_{\text{op}} \leq 0 \tag{4-10}$$

If a corrosion defect meets repair criteria 1, excavation needs to be performed at the inspection point and we need to check whether it meets repair criteria 2 or not. Repair criteria 2 is described by the following two equations, described in equations (4-11) and (4-12). If any of the following limit state functions is smaller than zero, the corrosion defect meets repair criteria 2, and this corrosion defect is repaired with a full encirclement sleeve. And if the corrosion defect doesn't meet the repair criteria 2, the defect will be recoated.

$$LSF\,(d) = 0.75t - d \leq 0 \tag{4-11}$$

$$LSF\,(P_f) = P_f - 1.1P_{\text{op}} \leq 0 \tag{4-12}$$

The proposed policy, defined by the system PoF threshold, leads to varying pipeline re-assessment intervals. But generally speaking, with the increase of PoF threshold, the average re-assessment interval increases, because the system failure probability that can be tolerated becomes larger. Figure 4.2 is an example plot of failure probability of pipelines versus time. With the design variable PoF threshold given, we can find the re-assessment interval for next tool run. For example,

if PoF threshold is 1×10^{-6}, the PoF of pipelines is smaller than the threshold until T=6 years. In this way, for different PoF thresholds, we can record the corresponding re-assessment intervals and calculate the average re-assessment intervals, which is shown in Table 4.2. We can find that the number of years to perform next tool run increases with the increase of PoF threshold.

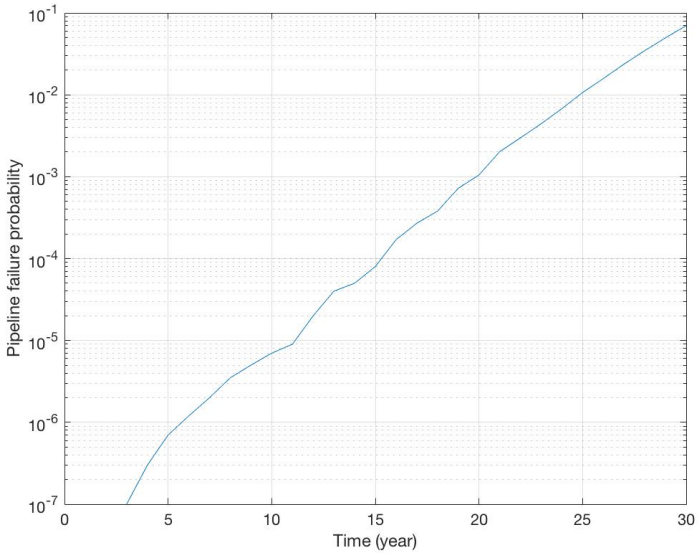

Figure 4.2 Example failure probability of pipelines versus time

Table 4.2 Example average re-assessment interval

Probability of Failure	Average re-assessment
1×10^{-7}	3
1×10^{-6}	6
5×10^{-6}	8
1×10^{-5}	12
5×10^{-5}	14
1×10^{-4}	15
1×10^{-3}	20
1×10^{-2}	25

4.3.2 Cost rate evaluation

An optimal risk-based pipeline re-assessment policy is defined by the optimal PoF threshold corresponding to the lowest cost rate, e.g. cost per year. The optimization problem can be generally formulated as follows:

$$\begin{aligned} &\min CR(\text{PoF}) \\ &\text{s.t. PoF} < \text{PoF}_a \end{aligned} \tag{4-13}$$

where CR(PoF) is the total cost rate with a given PoF threshold; PoF_a is the acceptable threshold. In the optimization model, only the PoF threshold is the decision variable. The re-assessment or inspection intervals can be subsequently determined by the PoF threshold, using the methods described in Section 4.3.1. That is, at a certain inspection point, the corrosion defects are evaluated and future pipeline system failure probability is predicted. The next re-assessment time is the time when the predicted failure probability reaches the PoF threshold. In industry, there is an acceptable failure probability for pipelines defined before risk assessment. According to [256], the acceptable failure probability is defined based on safety class. The value is typically between 10^{-5} and 10^{-3} for different safety class.

In the risk-based pipeline re-assessment optimization, cost rate evaluation is a critical step. The problem is quite complex though, due to the consideration of multiple random variables, failure criteria, maintenance actions and corrosion defects. A simulation-based method is developed for cost rate evaluation given a certain PoF threshold value. The detailed procedure for cost evaluation and re-assessment interval optimization is given in the rest of the section.

4.3.2.1 Step 1: Simulation initiation

In this stage, we consider the current inspection time at the beginning of the inspection cycle (with the predicted re-assessment time as the end of the inspection cycle). We can gather information on the size of each defect, namely depth $d_{0,i}$ and length $L_{0,i}$, pipeline geometry (OD, t), pipeline mechanical strengths (*YS*, *UTS*), etc. We need to consider defect measurement uncertainty, growth rate uncertainty and all the other uncertainties in load and resistant parameters. Then we generate all the load and resistant parameters with the consideration of uncertainties. Suppose the number of detected corrosion defect is k. Generate k initial corrosion defects considering the ILI tool measurement error. An example for uncertainties quantification is shown in Table 4.1. Specify the cost values, including in-line inspection C_{in}, corrosion defect excavation cost C_{ev}, recoating cost C_{rc}, sleeving cost, C_{rs}, failure cost, C_f and additional fixed cost C_{af}.

4.3.2.2 Step 2: Failure probability calculation

In each simulation iteration, grow each corrosion defect with uncertainty using Eqs. (6) and (7). With the use of corrosion growth model and limit state functions described in Section 4.2.1, PoF of the entire line at time T, i.e. PoF(T), can be calculated using first order reliability method (FORM) or Monte Carlo simulation method.

4.3.2.3 Step 3: Cost evaluation in each iteration

When PoF(T) reaches the PoF threshold, the re-assessment point is reached. Record the total time. Costs include inspection costs, repair costs, and failure costs. The net present value (PV) evaluation is performed for the re-assessment interval to account for the time value of money.

The net present value of total cost for pipeline with multiple corrosion defects when re-assessment interval is t^* can be determined as follows:

$$PV_{t^*}=PV_{insp,t^*}+PV_{repl,t^*}+PV_{fail,t^*}+PV_{main,t^*}+PV_{fixed,t^*} \tag{4-14}$$

where $PV_{insp,t^*}, PV_{repl,t^*}, PV_{fail,t^*}, PV_{main,t^*}, PV_{fixed,t^*}$ are net present values of inspection cost, replacement cost, failure cost, maintenance cost and additional fixed cost for entire line at year t^*.

The inspection cost is given by:

$$PV_{insp,t^*}=\frac{C_{in}}{(1+r)^{t^*}}=\frac{l_i \times C_{insp}}{(1+r)^{t^*}} \tag{4-15}$$

where C_{in} is the inspection cost; r is the discount rate; l_i is the distance of the ILI tool run; C_{insp} is the unit inspection cost. In this study, the entire line is inspected when using ILI tools.

The replacement cost is given by [251]:

$$PV_{repl,t^*}=\frac{C_{rp}}{(1+r)^{t^*}} \times PF_{pipe}=\frac{CL_i \times l_i+(CM_i+CSL_i)+CT_i \times s_i}{(1+r)^{t^*}} \times PF_{pipe} \tag{4-16}$$

where C_{rp} is the replacement cost; CL_i is the length cost rate; CM_i and CSL_i are cost of machinery and skilled labor, respectively; CT_i is unit transportation cost; s_i is the transportation distance for replacing pipes; PF_{pipe} is the failure probability of pipeline.

The failure cost considering risk to human and environmental is given by:

$$PV_{fail,t^*}=\frac{C_{fa}}{(1+r)^{t^*}} \times PF_{pipe}=\frac{C_{po}+C_{en}}{(1+r)^{t^*}} \times PF_{pipe} \tag{4-17}$$

where C_{fa} is the failure cost due to damage to population and environment; C_{po} and C_{en} represent the cost converted from the damage to population and environment, respectively. The consequences of potential hazards are hard to estimate. Human safety, environmental damage, and economic loss consequences need to be quantified for further analysis. Total risk is the summation of human safety, environmental and economic risks. After converting damage to population and environment to economic loss, we can calculate the cost due to failure, $C_f = C_{fa} + C_{rp}$.

The maintenance cost is given by:

$$PV_{main,t^*} = \frac{\sum_{j=1}^{k} (C_{main,j} \times z_{t^*,j})}{(1+r)^{t^*}} \tag{4-18}$$

$$z_{t^*,j} = \begin{cases} 1, \text{ if meet repair criteria 1} \\ 0, \text{ otherwise} \end{cases}$$

$C_{main,j}$ is the repair cost; k is the number of corrosion defects. And $C_{main,j}$ can be calculated based on repair criteria 2, which is shown as follows:

$$C_{main,j} = \begin{cases} C_{ev} + C_{rs}, \text{ if meet repair criteria 2} \\ C_{ev} + C_{rc}, \text{ otherwise} \end{cases} \tag{4-19}$$

where C_{ev} is the excavation cost; C_{rs} and C_{rc} represent sleeving cost and recoating cost, respectively.

4.3.2.4 Step 4: Cost rate calculation and optimization

With the Monte Carlo simulation, in each iteration (say i), we can obtain the total net present value PV_i and total time T_i. Suppose we run N simulation iterations. The cost rate with respect to a given PoF threshold can be calculated as:

$$CR(PoF) = \frac{\sum_{i=1}^{N} PV_i}{\sum_{i=1}^{N} T_i} \tag{4-20}$$

We may also be interested in the average re-assessment interval corresponding to the optimal re-assessment policy by taking the average of each re-assessment time:

$$\bar{T} = \frac{\sum_{i=1}^{N} T_i}{N} \tag{4-21}$$

With different PoF thresholds, the total cost rate $CR(\text{PoF})$ are calculated. Based on the results, we can obtain the relationship between cost rate and PoF threshold, with the PoF threshold as the single variable. Due to the computation time required by the simulation procedure, we obtain *CR* values at a set of discrete PoF points, and use a spline to fit the *CR*(PoF) function. A simple optimization procedure can be performed subsequently to find the optimal PoF threshold. Once the optimal PoF threshold is found, the re-assessment intervals can be predicted at each assessment point using the proposed re-assessment policy, based on the inspection results, defect growth prediction and the optimal PoF threshold.

4.4 Examples

In this example, a pipeline with a length of 10km will be inspected by ILI tools. The proposed methodology is utilized for assessing the entire line and finding the optimal PoF threshold value and ILI re-assessment time. The mean and standard deviation of geometry parameters and mechanical properties of the line are shown in Table 4.1. Ten initial corrosion defects are considered in the line within the defect depth range of 10% to 20% of wall thickness, at the beginning of inspection cycle, and later other ranges are also investigated in further analyses. Such

assumptions are used in modeling the inspection cycles by considering various stages during the lives of pipe segments, and the fact that the pipeline might be a combination of pipes with different ages and lives. The ILI tool accuracy is assumed to be σ_{ILI} =0.5mm. And the axial and radial growth rate is set to be 10mm/year and 0.3mm/year in the example. The uncertainties are considered in all these parameters and they are normally distributed with the mean and standard deviation provided in Table 4.1. These parameters in Table 4.1 are set to be the baseline and will be compared with other scenarios in Section 4.4.2. FORM method is implemented here to calculate the probabilities that these limit state functions, described in equations (4-5), (4-9), (4-10), (4-11) and (4-12), are smaller than 0, and then calculate the probabilities of sleeving, recoating, and failure associated with each corrosion defect. FORM is a reliability method that can provide accurate results but less time-consuming compared with the Monte Carlo simulation method.

The summary of costs of inspection, excavation, repair, failure is shown in Table 4.3 [257]. Additional fixed costs such as costs for skilled labor and transportation fees are also considered here. The relative costs are utilized in this example. The cost data is simplified in this example. For instance, the failure cost is assumed to be 200 (corresponding to $4 million), which takes all the human, environmental, and economic loss factors into consideration. And the additional fixed cost will not change with the change of the re-assessment interval, same for the inspection cost. So in this example, the fixed cost is added to inspection cost to better compare with other cost items since they are both non-changing. We assume l_i is equal to the length of the entire line=10km and C_{insp}=$4,000/km, and thus the inspection cost is $40,000. C_f is assumed to be $4,000,000 as the baseline. Table 4.3 is utilized as the baseline to compare with other scenarios in the sensitivity analysis.

Table 4.3 Summary of costs [257]

Cost item	Absolute cost (CAD$)	Relative cost
In-line inspection C_{in}	40,000	2
Corrosion defect excavation C_{ev}	70,000	3.5
Recoating C_{rc}	20,000	1
Sleeving C_{rs}	35,000	1.75
Failure cost C_f	4,000,000	200
Fixed cost (labor, transportation, etc.)	10,000	0.5

4.4.1 Results with the proposed approach

In this study, the total cost rate is broken down into different cost rate components, including inspection, repair and failure cost rates, respectively. It should be pointed out that the additional fixed cost is included in the inspection cost, the excavation cost is included in the failure cost, and the replacement cost is included in the failure cost. The cost evaluation and optimization results are shown in Figure 4.3. The results for the comparison of different cost rate components in term of different discount rate r are shown in Figures 4.3a, 4.3b, 4.3c, respectively. The results indicate that the inspection cost rate decreases with the increase of the PoF threshold, while it is the opposite for both repair cost rate and failure cost rate. It is reasonable because the inspection cost is a fixed cost in this example, and the inspection cost rate will decrease as T and PoF increase. And with the increase of PoF threshold, the possibility of repair actions and failure damage is increasing, which results in the increase of relevant cost rate. Besides, from the observation of these three figures, the inspection cost rate has the highest contribution to the total cost rate when

the PoF threshold is smaller than around 5×10^{-3}, followed by repair cost rate and failure cost rate. The failure cost rate is negligible compared with other components of the total cost rate. This is because when the PoF threshold is small, pipeline is unlikely to fail and the corresponding inspection interval is also small, which gives a relatively big inspection cost rate and low repair and failure cost rate. When the PoF threshold becomes bigger, repair cost rate becomes higher and eventually the highest one. The comparison result for total cost rate of r=0, 2%, 5% is shown in Figure 4.3d. The figures show that the shapes of total cost rate plots with different discount rate are similar and the cost rate increases with the decrease of the discount rate. The optimal solutions for the PoF threshold, and the corresponding average re-assessment intervals and cost rates are shown in Table 4.4. And the results suggest that the optimal solution for the PoF threshold and average re-assessment interval doesn't change much with the discount rate. r is assumed to be 2% in all following studies. And the results for r=2% with the parameters described previously will set to be the baseline and utilized in the parametric analysis. All the horizontal axis in the following figures are in logarithmic scale.

Table 4.4 Comparison of optimal solutions with different discount rate r

r	Optimal PoF threshold	Cost rate	Average re-assessment interval
0	1.83×10^{-4}	0.2272	13.8
2%	1.63×10^{-4}	0.1741	14.5
5%	2.21×10^{-4}	0.1073	14.8

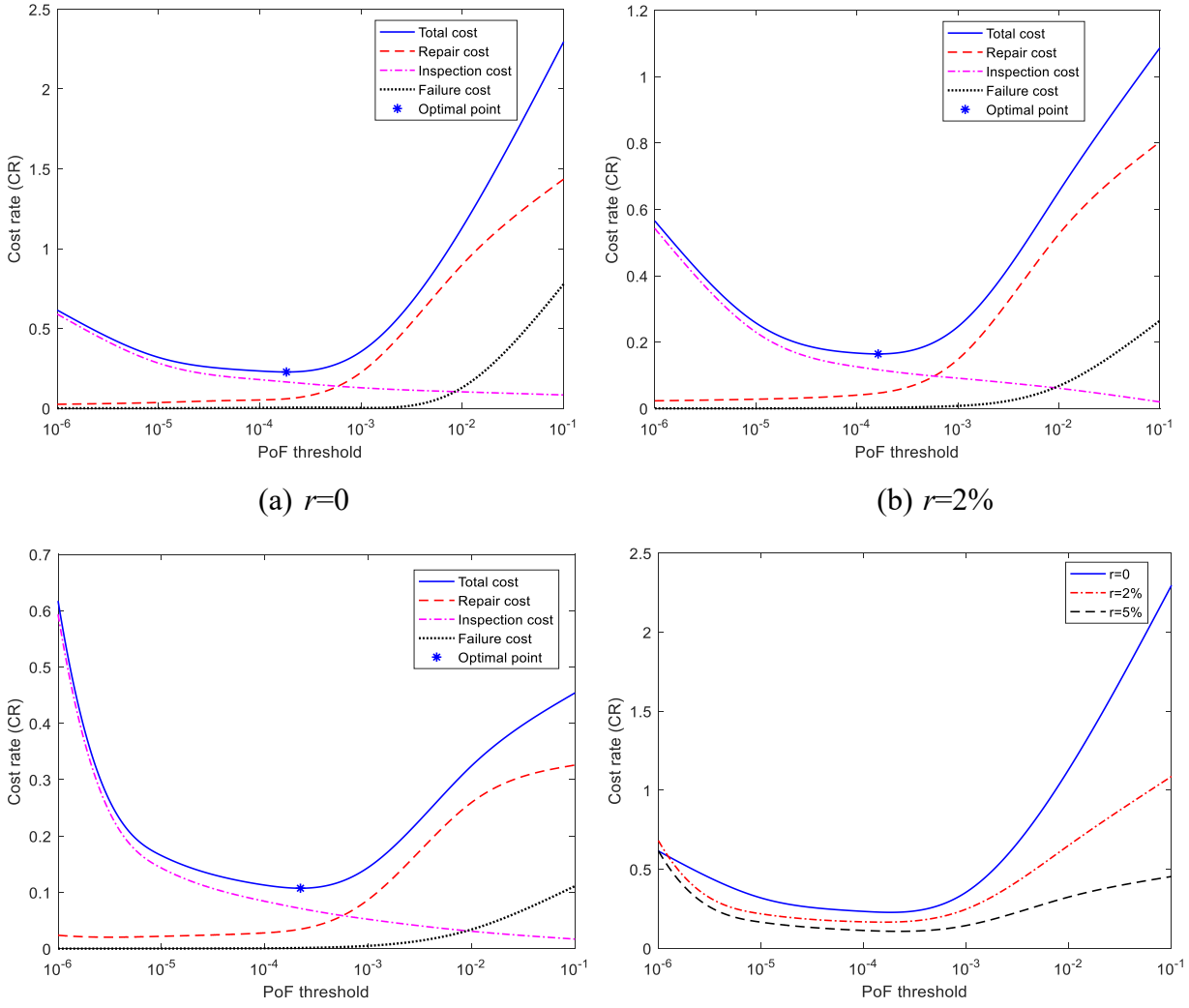

(a) r=0 (b) r=2%

(c) r=5% (d) Comparison of r=0, 2%, 5%

Figure 4.3 Comparison of the expected cost rates associated with different cost items

4.4.2 Sensitivity analysis

There are four scenarios considered in sensitivity analysis, and the studied parameters are failure cost, initial defect depths, corrosion radial growth rate, and measurement error of ILI tools, respectively. For each scenario, three different values of that parameter are chosen. The values of total cost rate and its components as functions of PoF threshold are plotted for each scenario and

the results for the cost rate vs. PoF threshold are studied and compared. The plots for comparison results are depicted in Figures 4.4-4.7, and the optimal solutions are shown in Table 4.5. Note that the optimal PoF threshold and its corresponding re-assessment interval are further summarized and discussed in Section 4.2.5.

Table 4.5 Comparison results of optimal solutions for each scenario

Scenario #	Parameter Value	Optimal PoF threshold	Cost rate
Scenario 1: Failure cost	100	1.46×10^{-4}	0.1687
	200	1.63×10^{-4}	0.1741
	2,000	1.29×10^{-4}	0.1868
Scenario 2: Initial defect depth	(10%~20%)t	1.63×10^{-4}	0.1741
	(20%~30%)t	1.36×10^{-4}	0.2850
	(10%~40%)t	0.85×10^{-4}	0.4526
Scenario 3: Corrosion radial growth rate	0.2 mm/yr.	2.20×10^{-4}	0.1188
	0.3 mm/yr.	1.63×10^{-4}	0.1741
	0.4 mm/yr.	1.30×10^{-4}	0.2206
Scenario 4: ILI tool measurement error	0.3 mm	1.40×10^{-4}	0.1704
	0.5 mm	1.63×10^{-4}	0.1741
	0.7 mm	1.61×10^{-4}	0.1786

4.4.2.1 Scenario 1: Failure cost

Because it is difficult to convert the failure damage of population and environment into economic loss, the value for failure cost is difficult to determine. It depends on many factors such as the

density of population, the recovery time of environmental damage, etc. Different risk factors, like stringent and conservative, may result in a very big difference in the value of failure cost. Hence, it is necessary to investigate the influence of failure cost on the results.

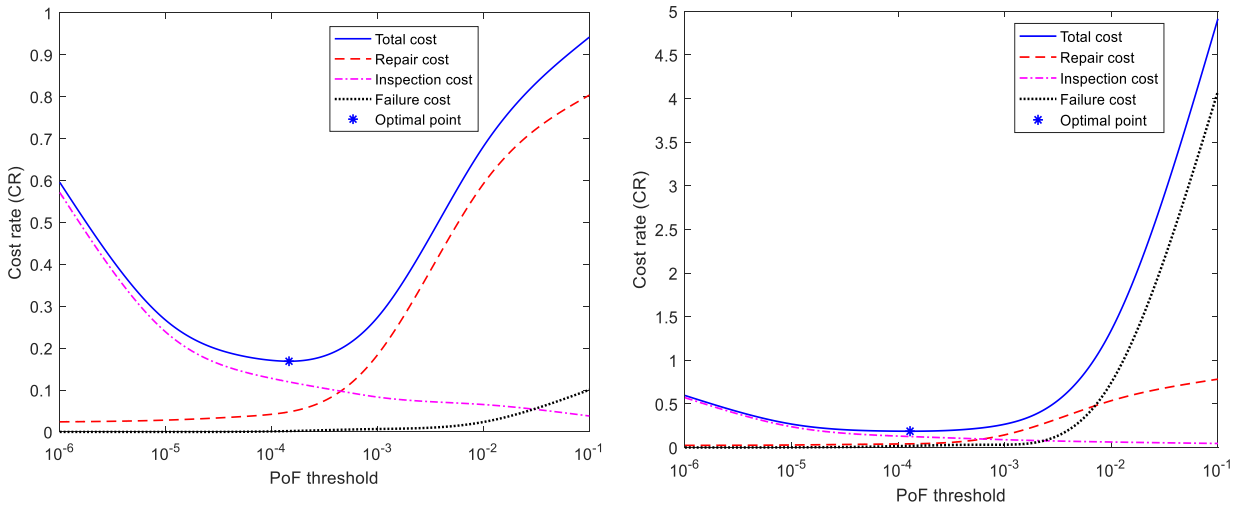

(a) C_f=100 (b) C_f=2000

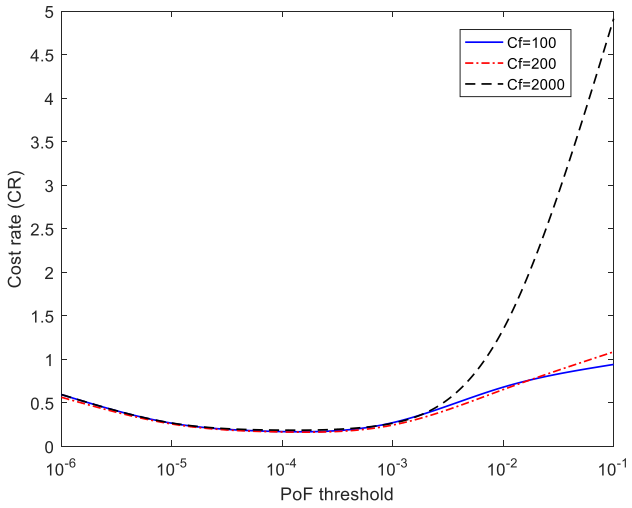

(c) Comparison results

Figure 4.4 Cost rate vs. PoF threshold in term of C_f=100, 200, 2000

Three different values are selected for analyzing the impact of failure cost, with relative cost 100, 200, 2000, respectively. The failure cost equal to 200 is the baseline and the result is shown in Figure 4.3b. The plots for the total cost rate along with different components as functions of PoF threshold for C_f=100 and C_f=2000 are shown in Figure 4.4a and Figure 4.4b, respectively. The failure cost rate increases as C_f increases. And for C_f=2000, the failure cost rate has the highest contribution to total cost rate when PoF threshold is bigger than around 10^{-2} while the repair cost rate is the highest components for the other two. Figure 4.4c suggests that the optimal PoF remains close. And the total cost rates are close when the PoF threshold is smaller, the one with C_f=2000 differs notably from the rest when the PoF threshold becomes big.

4.4.2.2 Scenario 2: Initial defect depth

Three initial defect depths scenarios are chosen for comparison, 10%~20%, 20%~30%, 10%~40% of the wall thickness, respectively. And the values corresponding to (10%~20%)t, (20%~30%)t, (30%~40%)t are shown in Figure 4.3b, Figure 4.5a, Figure 4.5b, respectively. The shapes of curves for repair cost rate and total cost rate are different with the change of the initial defect depths. The PoF threshold at the intersection point of repair cost rate and inspection cost rate decreases as initial defect depths increase. Figure 4.5c suggests that initial defect depths have a large impact on the total cost rate. Higher initial defect depths lead to higher probability of repair actions and failure damage. Therefore, less time will be needed for higher defect depths to reach the certain threshold, and it results in higher repair cost rate, failure cost rate and total cost rate.

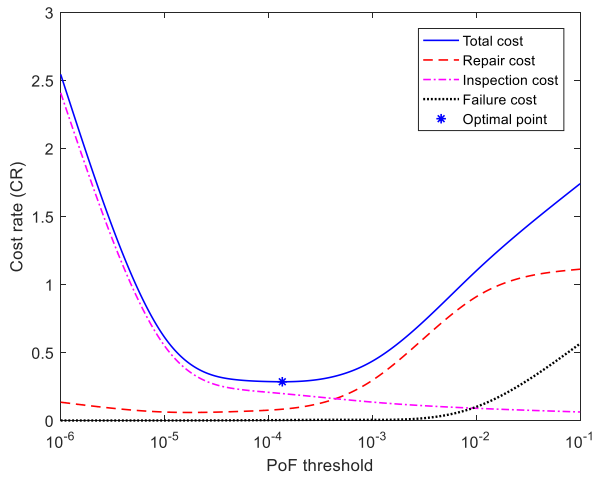

(a) d_0=10%t~20%t

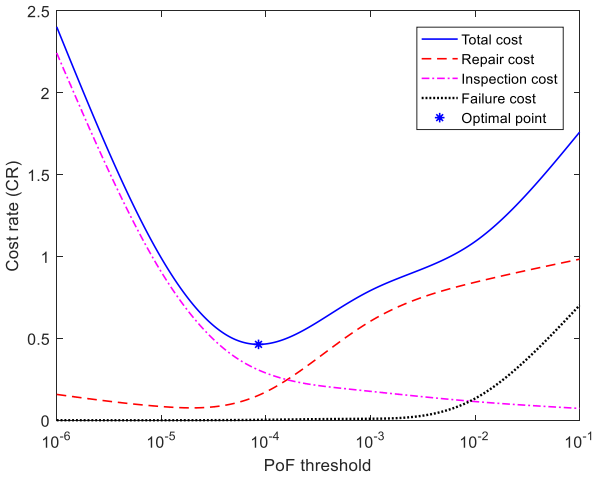

(b) d_0=10%t~40%t

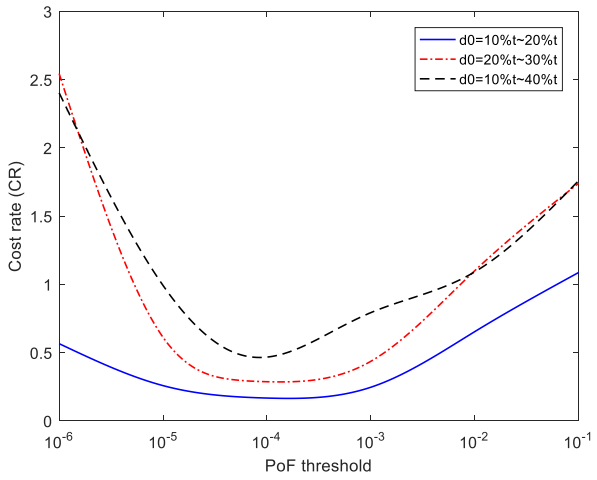

(c) Comparison results

Figure 4.5 Cost rate vs. PoF threshold in term of d_0=10%t~20%t, 20%t~30%t, 10%t~40%t

4.4.2.3 Scenario 3: Corrosion radial growth rate

Three cases are considered in this scenario, namely 0.2, 0.3, 0.4 mm/year, respectively. The results shown in Figure 4.6 illustrate the impact of corrosion radial growth rate on total cost rate and its components. The corrosion radial growth rate affects failure cost rate and repair cost rate a lot, and with the increase of growth rate, the repair, failure and total cost rates increase at a given re-assessment interval. The failure cost rate increases significantly as the growth rate increases

from 0.3 to 0.4mm/year. It is mainly due to the fact that a higher corrosion radial growth rate leads to larger corrosion depth, and therefore, shorter time to reach the PoF threshold, which leads to higher cost rate with the same PoF threshold. From Figure 4.6c, when the PoF threshold is small, the shapes of curves for the total cost rate are similar, and it can reach a higher total cost rate with a higher depth growth rate, as expected. The differences among three curves keep increasing as the PoF threshold increases.

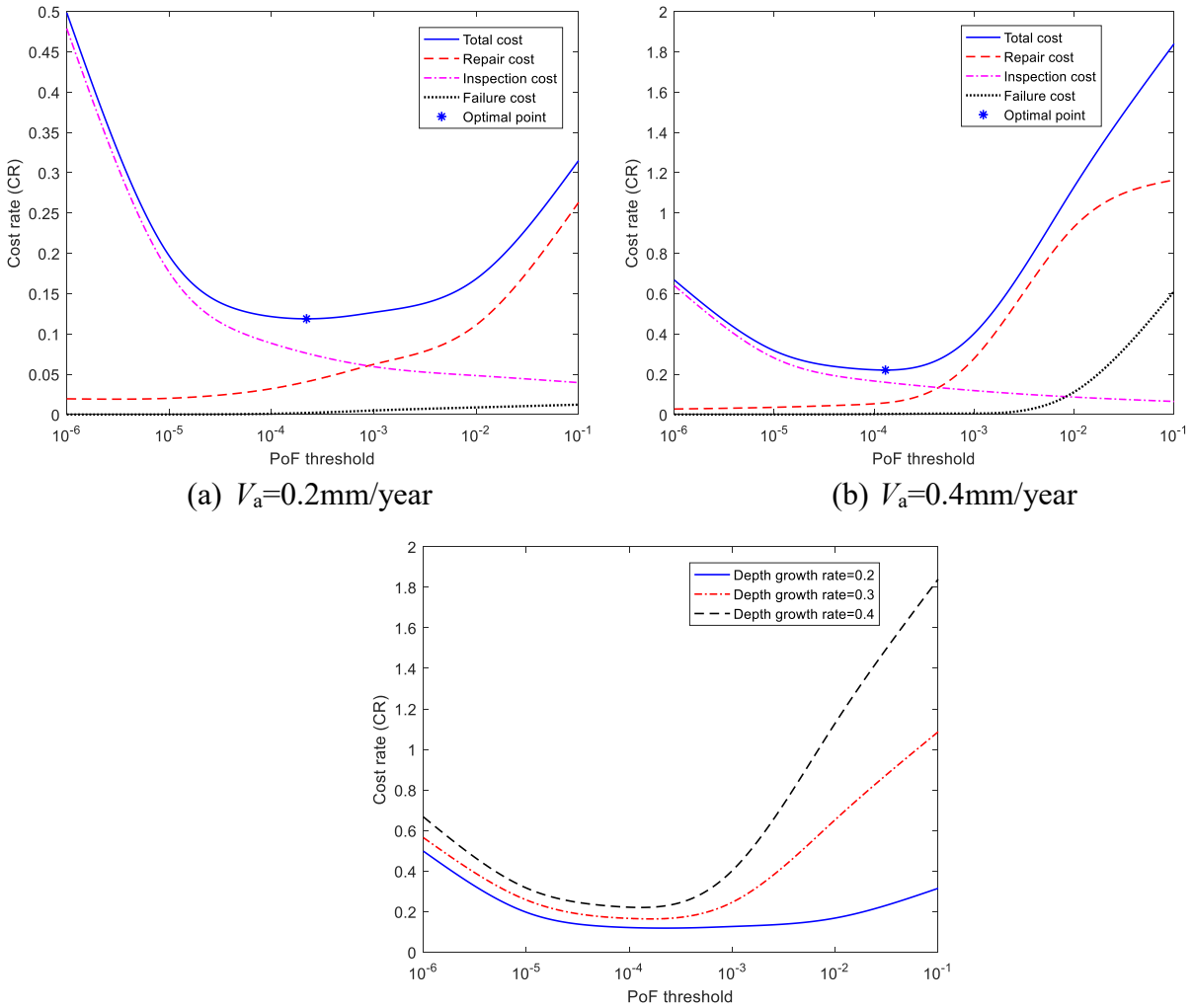

(a) V_a=0.2mm/year

(b) V_a=0.4mm/year

(c) Comparison results

Figure 4.6 Cost rate vs. PoF threshold in term of V_a=0.2, 0.3, 0.4mm/year

4.4.2.4 Scenario 4: ILI tool measurement error

The impact of ILI tool measurement error on cost rate items is illustrated in Figure 4.7.

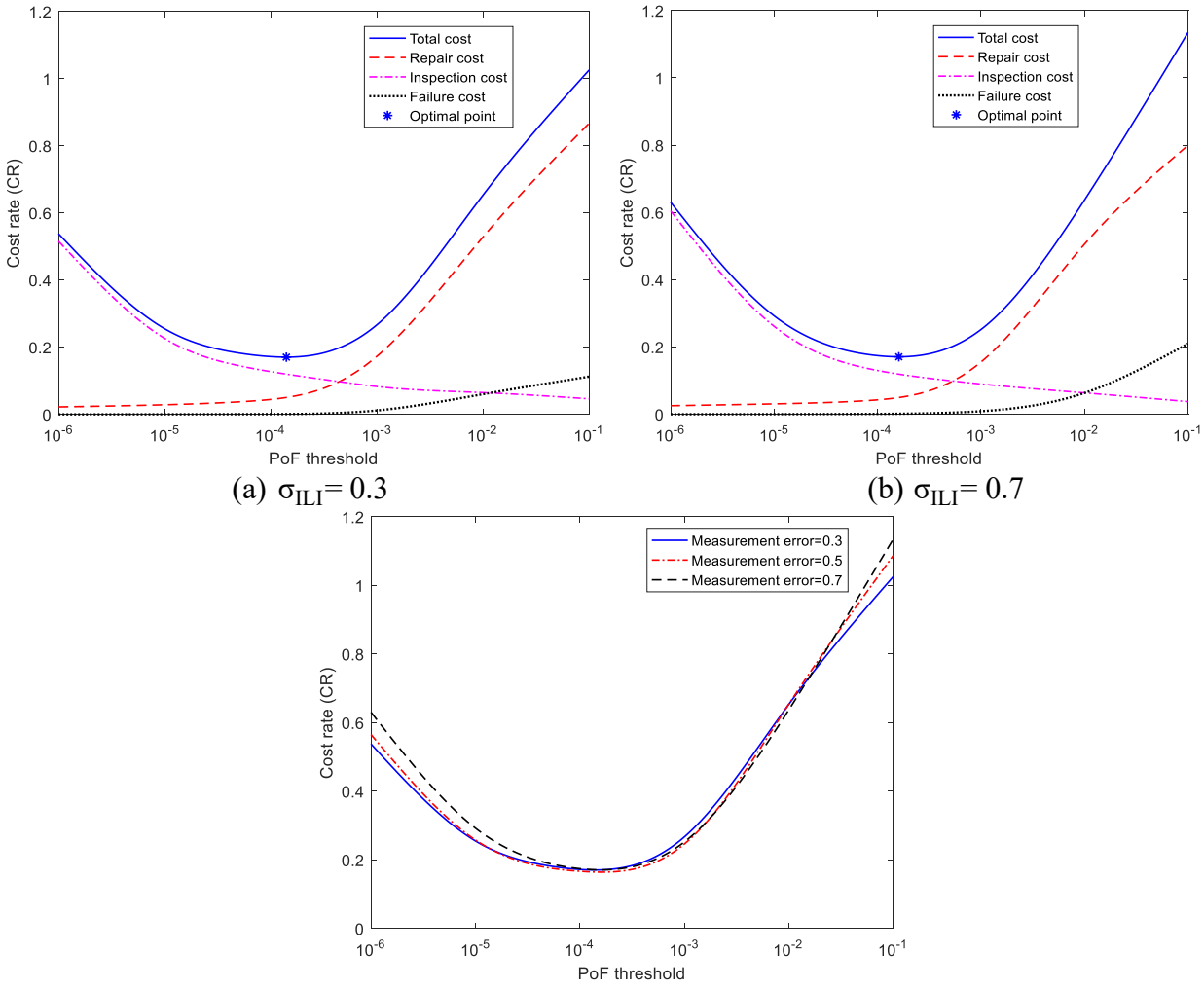

(a) σ_{ILI}= 0.3 (b) σ_{ILI}= 0.7

(c) Comparison results

Figure 4.7 Cost rate vs PoF threshold in term of σ_{ILI} = 0.3, 0.5, 0.7

Three cases are considered in this scenario, namely σ_{ILI} = 0.3, 0.5 and 0.7, respectively. The shapes of the curves for total cost rate and its different components are similar with the change of

ILI tool measurement error. Overall, from the trend of three curves in Figure 4.7c, the total cost rate increases as the measurement error of ILI tool increases. This is mainly because the real corrosion depth could be bigger if the standard deviation of the tool measurement error is bigger, which results in a higher total cost rate. The impact of ILI tool measurement error on the total cost rate and its components are relatively small, and the total cost rate corresponding to different ILI tool measurement error become very close when the PoF threshold is around the optimal solution. This is mainly because the measurement error of ILI tool in this example is relatively small compared to corrosion depth and wall thickness (20.6mm).

4.4.2.5 Summary of the four scenarios

The comparison results of optimal PoF threshold and corresponding cost rate for each scenario are summarized and compared in Table 4.5. The optimal PoF threshold is obtained by finding the lowest total cost rate. Note that in this study, we use the normal safety class and acceptable failure probability is 5×10^{-4}, and in this way, our optimal PoF threshold should be smaller than this value. All the obtained optimal PoF thresholds meet the acceptance criteria in this example. Overall, the optimal PoF threshold for each case is obtained and the minimum and maximum ones are 0.85×10^{-4} and 2.20×10^{-4}, respectively. This means the optimal PoF threshold doesn't change too much with the investigation on these scenarios. That may be because the overall geometry and mechanical properties of the line are same for each scenario. For example, if a different pipeline with different geometry and mechanical properties is used in this example, the optimal PoF thresholds may change to different values. Besides, the total cost rate increases with the increase of the parameters given in all scenarios. The initial defect depths affect the total cost rate the most,

followed by corrosion radial growth rate and the failure cost. It should also be pointed out that a large number of random variables are considered, as listed in Table 4.1, and the variations they introduced may also have impact on the analysis results in this section.

4.4.3 Comparison between the proposed method and the existing fixed interval method

4.4.3.1 Investigation on different cost values

The main difference between the proposed method with the existing fixed interval method is in the design variables. The fixed interval method uses inspection time T as the design variable while in the proposed method, the PoF threshold is used as the design variable. To compare these two methods, we use the same input parameters as the ones used above to obtain the $CR(T)$ curve for fixed interval method. Figure 4.8 shows the plot of total cost rate and optimal point for the baseline. Table 4.6 shows the comparison results of the proposed method and fixed interval method. For pipelines with the same geometry, the inspection cost and failure cost may be different due to different locations and the surrounding environment. Besides, the defect size in the entire line may also vary for different pipeline segments. Therefore, we did investigations on these three parameters and compared our proposed method with the traditional fixed interval method. Ten cases with different d_0, C_{in}, C_f are used for comparison. From Table 4.6, we can find that for all scenarios, the optimal cost rates obtained by the proposed method are smaller than the ones obtained by fixed interval method. The improvement of the proposed method compared with the fixed interval method is in the range of 5.6% to 14.9% in these cases. And typically with a higher cost rate, the improvement is bigger. With the comparisons, we can conclude that the proposed

pipeline re-assessment optimization approach is more cost-effective compared to the traditional fixed interval methods.

Table 4.6 Comparison results of the proposed method and fixed interval method

Parameter Value	Cost rate (Fixed interval method)	Cost rate (Proposed method)	Improvement of proposed method
d_0=(10%~20%)t C_{in}=2.5, C_f=100	0.1782	0.1687	5.6%
d_0=(10%~20%)t C_{in}=2.5, C_f=2000	0.1991	0.1868	6.6%
d_0=(10%~40%)t C_{in}=2.5, C_f=200	0.4942	0.4526	9.1%
d_0=(30%~40%)t C_{in}=2.5, C_f=200	0.7264	0.6453	12.6%
d_0=(10%~20%)t C_{in}=5, C_f=200	0.2712	0.2516	7.8%
d_0=(10%~20%)t C_{in}=15, C_f=200	0.7486	0.6730	11.2%
d_0=(10%~20%)t C_{in}=25, C_f=200	0.9609	0.9060	6.1%
d_0=(30%~40%)t C_{in}=15, C_f=500	2.1364	1.9534	9.4%
d_0=(30%~50%)t C_{in}=5, C_f=200	2.7115	2.4533	10.5%
d_0=(30%~50%)t C_{in}=15, C_f=500	4.4564	3.8780	14.9%

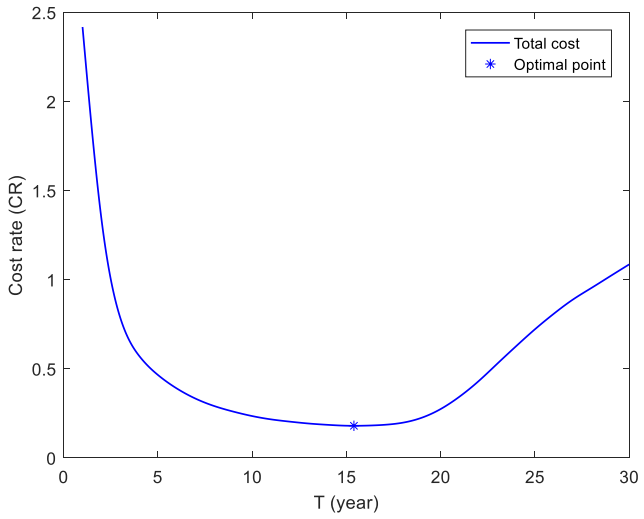

Figure 4.8 Cost rate vs. T for baseline using fixed interval method

4.4.3.2 Investigation on different pipeline geometry

To demonstrate if the proposed model is applicable to other pipelines, we change parameters for geometry and physical properties in Table 4.1, and the new sets of random variables including pipeline diameter, thickness and operating fluid pressure are shown in Table 4.7. For other parameters, we use the baseline parameters, d_0=(10%~20%)t, C_{in}=2.5, C_f=200. And we assume the ILI tool measurement error to be 0.5mm. The plots for cost rates vs. PoF threshold in term of three different sets of pipeline geometry are shown in Figure 4.9. Table 4.8 shows the comparison results of the proposed method and fixed interval method for these three cases. From Table 4.8, we can find that for all these cases, the minimal cost rates obtained by the proposed method are smaller than the ones obtained by fixed interval method by 8.3% to 11.8%, which indicates that the proposed model is applicable to pipelines with different geometry and physical properties.

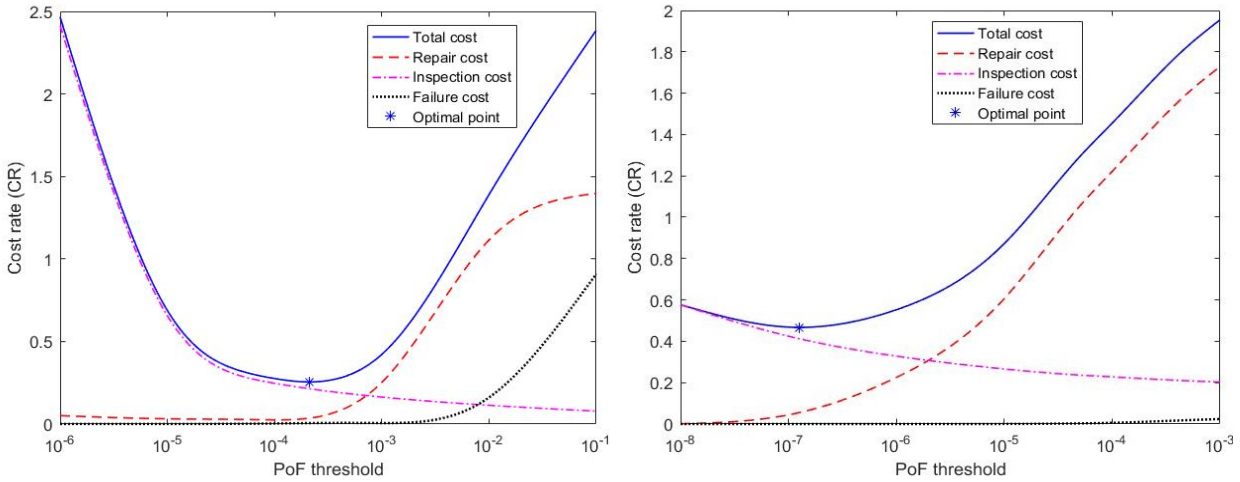

(a) Test 1 (b) Test 2

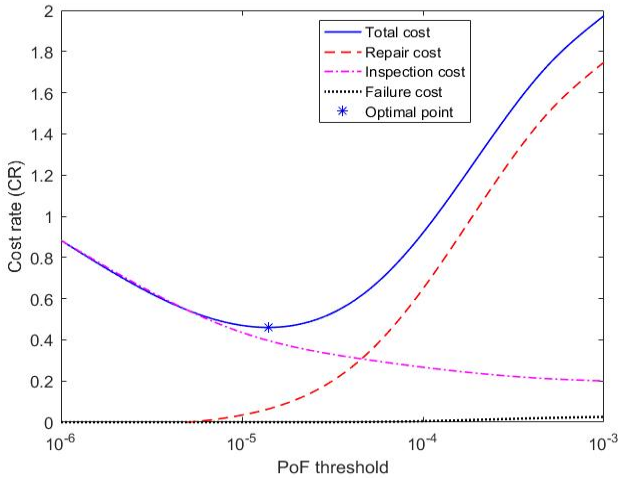

(c) Test 3

Figure 4.9 Cost rate vs PoF threshold in term of different pipeline test sets

Table 4.7 Different pipeline geometry

Test	Pipeline diameter (D) [mm]	Pipeline thickness (t) [mm]	Operating fluid pressure (P_{op}) [MPa]
1	660.4 (std.=13.208)	12.7 (std.=0.254)	5.6 (std.=1.12)
2	508.0 (std.=10.160)	7.9 (std.=0.158)	4.3 (std.=0.86)
3	406.4 (std.=8.128)	7.9 (std.=0.158)	3.9 (std.=0.78)

Table 4.8 Comparison results of the proposed method and fixed interval method

Test	Cost rate (Fixed interval method)	Cost rate (Proposed method)	Improvement of proposed method
1	0.2766	0.2554	8.3%
2	0.5223	0.4671	11.8%
3	0.5134	0.4602	11.6%

4.5 Conclusions

This thesis proposes a method to find the optimal re-assessment policy for pipelines subject to multiple corrosion defects, where the system PoF threshold is used as the decision variable for this optimization problem. Uncertainties from various sources are considered in this study to make an accurate prediction, including uncertainties in pipeline geometry, mechanical properties, defect size, growth rates, and the ones associated with ILI tools. We develop a simulation-based cost evaluation method by using the PoF threshold as the input decision variable. First-order reliability method is used to calculate the PoF to improve efficiency. The optimal PoF threshold can be obtained corresponding to the minimum expected cost rate.

An example is given for illustrating the proposed approach. Sensitivity analysis is performed for four scenarios. The following conclusions can be drawn based on observations and analysis. The optimal PoF threshold doesn't vary too much with the change of failure cost, initial defect depths, radial corrosion growth rate and ILI tool measurement error. The initial defect depths have a remarkable impact on total cost rate, followed by depth growth rate and failure cost. The total cost rate increases with the increase of these parameters.

After obtaining optimal PoF threshold, we could determine the optimal re-assessment interval for a specific pipeline based on this pipeline's current condition and defect information. Specifically, we could generate the degradation model for this pipeline and when the probability of failure reaches the optimal PoF threshold, we perform a next ILI tool run. Besides, we could also use the proposed integrated method in chapter 3 to update the model parameter *m* to make a more accurate prediction and set an optimal reassessment interval.

This approach with the PoF threshold as decision variable can be used to cooperate with the acceptable risk level, and it will help to make decisions with the flexibility of adopting varying re-assessment intervals, rather than being limited to predetermined fixed inspection interval. The uncertainties from all sources are considered here to make a better and more realistic prediction and that support decision making in industry.

5 A method to analyze the impact of in-line inspection on integrity planning of pipelines with cracks

5.1 Introduction

ILI crack detection tools are performed periodically to evaluate the health condition of pipelines with cracks. It is necessary to consider the measurement error of ILI tools in pipeline system integrity management. Cost evaluation and risk analysis need to be investigated with the consideration of the large uncertainties in ILI tools. Due to the nature of statistical tolerance of inspection technology including ILI tools, it is also important to determine the impact of ILI tool inspection specifications on pipeline risks and costs, and thus recommend optimal integrity assessment and risk mitigation activities. By investigating the effect of ILI tool reported tolerance uncertainties on life-cycle costs and re-assessment results, suggestions for future improvement of ILI crack inspection tools can be given. The objective of this chapter is to outline a method used to analyze the impact of ILI tool specifications on pipeline risks, integrity program costs, and thus recommend optimal integrity assessment and risk mitigation activities.

There are many papers in the literature on reliability assessment of pipelines with crack defects. The following models and methodologies are the popular ones used in industry for predicting burst pressure, namely NG-18 method [258]–[260], failure assessment diagram (FAD) Option 3 methods in the standard BS 7910 [156], [261] and Level III of API 579 [155], as well as CorLAS^{TM} [157], [262], [263] model. These methods are compared with experiment results reported in [173]. From the comparison results in [173], we can see that the predicted collapse pressure based on CorLAS^{TM} model and Level 3 FAD for API 579 and Option 3 for BS 7910 are

more accurate, while NG-18 method is more conservative. And with the consideration of accuracy and computation efficiency, we select Level 3 FAD for API 579 for the failure pressure calculation.

Risk-based management for pipelines have been investigated in the literature. Xie and Tian [3] used the PoF threshold as a decision variable to propose a method to determine optimal re-assessment and maintenance schedule for corroded pipelines. Zhang and Zhou [257] developed a stochastic degradation model to determine the optimal inspection time for pipelines with corrosion defects. However, very few studies discussed integrity planning methods for pipelines with crack defects [232]. Uncertainties associated with the reported results from ILI tool need to be considered and investigated within the reliability assessment of pipelines assumed to have crack defects and those are inspected by ILI. Reliability analysis methods for the pipelines with cracks have been reported in a few studies. The effect of different ILI tool measurement error on the reliability analysis results were ignored in these previously reported studies.

In this chapter, reliability assessment for pipelines with single and multiple cracks was performed. The proposed method is based on the use of a Monte Carlo simulation framework, where initial crack defect size and measurement errors are considered as key random variables. Hence the impacts of ILI tool accuracy and initial crack size on when to perform a next ILI tool run was investigated. In addition, a cost evaluation for integrity considerations pipelines with cracks was performed. The investigation results are assessed in a subsequent definition of inspection cost rate (CR_{Insp}) and total integrity cost rate (CR_{Total}) with respect to a range of ILI tool accuracies of reported results.

A set of repair criteria and conditions were present for pipelines with crack defects. A sensitivity analysis was performed considering different inspection costs and relative crack

severity. The non-homogeneous Poisson process was adopted for the generation of new crack defects over time, which results in a varying number of total crack defects during Monte Carlo simulation. Along with the generation of the number of crack defects, other information including crack initiation time, crack length and depth is generated for each defect. The probability of detection was also considered as a function of crack size. Multiple examples are used to investigate the impact of ILI tool accuracy on expected cost rate. Different input parameters such as pressure, failure cost and inspection cost assumptions are considered in these examples. We investigate and compare the optimal inspection intervals and the corresponding total cost rates for different ILI tool accuracies. The proposed method can support integrity management program planning by linking risks with integrity plan costs associated with ILI accuracies.

Section 5.2 presents a description for reliability assessment method for pipelines with crack defects. The parameters selection and the impact of ILI tool accuracy on reliability assessment results for pipelines with single and multiple crack defects are investigated in Section 5.3. Section 5.4 describes the repair criteria and cost evaluation process for crack defects. Section 5.5 investigates the effect of ILI tool accuracy on total cost rate. Section 5.6 presents the steps to evaluate the long-term cost rate and investigates the ILI performance impact on long-term cost rate through several examples. Section 5.7 investigates the impact of different prediction accuracy on total cost rate rates. Section 5.8 gives the conclusions.

5.2 Reliability assessment method description

The proposed reliability assessment method was based on the use of a Monte Carlo simulation framework. The steps for implementing the method are described in this section.

5.2.1 Step 1: Simulation initiation

The initial step was to determine the parameters used for assessing the failure probability of pipelines with a single crack or multiple cracks. In this stage, the current inspection time at the beginning of the inspection cycle was considered (with the predicted re-assessment time as the end of the inspection cycle). Defect information on the size of each defect, namely depth $d_{0,i}$ and length $L_{0,i}$, pipeline geometry (D, t), pipeline mechanical strengths (YS, UTS), were compiled for use in the simulations. In the simulation and reliability calculations, the defect depth was considered as the primary random variable of study. Defect dimensions and depths were set within a framework of measurement uncertainties. For example, the number of detected crack defects is k. The standard deviation of ILI tool measurement error σ_{ILI} is used to representing the ILI tool accuracy. Hence k initial crack defects were generated considering the ILI tool measurement error. The crack depths follow normal distribution N (d_0, σ_{ILI}).

It was noted in the study within reviews of early results, that the methodology could also be adapted for corrosion assessment and other pipeline threats having change or growth mechanisms.

5.2.2 Step 2: Set failure criteria

To assess the reliability of pipelines with cracks, the determination of the failure criteria was set first. There were several failure criteria examples reported in literature, including ones considering the predicted stress intensity factor exceeding the critical stress intensity factor, and as another, the pipeline operating pressure reaching or exceeding the predicted failure pressure.

A reporting threshold was adopted from as reported in literature, for, current ILI tools at a detection level for cracks of length ≥ 25mm and with a depth ≥ 1mm. Noted crack models predict that a crack does not propagate along the crack length direction when the crack length is much longer than the depth. In this context, these above-mentioned failure criteria were then used to determine the critical crack depth with the crack length given.

In this study, the critical crack depth was determined by calculating the following limit state function. With a given burst capacity model, critical crack depth d_c can be derived from Eq. (5-1).

$$\mathrm{LSF}_1\ (P_f) = P_f\ (D, t, YS \text{ or } UTS, d, L) - P_{op}=0 \tag{5-1}$$

where P_f is the burst pressure; P_{op} is the operating pressure; D is the pipeline diameter; t is the pipeline wall thickness; YS and UTS are the pipeline material yield strength and ultimate tensile strength, respectively; L is the axial length of the defect; d is the depth of the defect and T is the elapsed time.

5.2.3 Step 3: Define crack propagation process

Currently, the physics-based crack propagation methods were governed by the Paris' law as used for pipeline fatigue crack growth prediction [6], [13], [14]. The Paris' law as shown as Eq. (5-2), is generally used for describing fatigue crack growth [13], [14], [236], [205]:

$$\mathrm{d}a/\mathrm{d}N = C(\Delta K)^m \tag{5-2}$$

where $\mathrm{d}a/\mathrm{d}N$ is crack growth rate, a is crack depth, N is the number of loading cycles, ΔK is the range of Stress Intensity Factor (SIF). C and m are material-related uncertainty model parameters. Parameters C and m can be estimated via experiments.

API 579 was employed to calculate the SIF at the deepest point of the crack. However, with the use of the standard, computing efficiencies need to be considered due to significant amounts of computation required. A third-order polynomial equation was adopted to fit the original SIF curve with the parameters given. In this way, the computing efficiency was improved to reasonable timeframes. Figure 5.1 shows the comparison of API 579 and the fitted function. The SIF calculations were hence based on the fitted function used in order to improve computing efficiency.

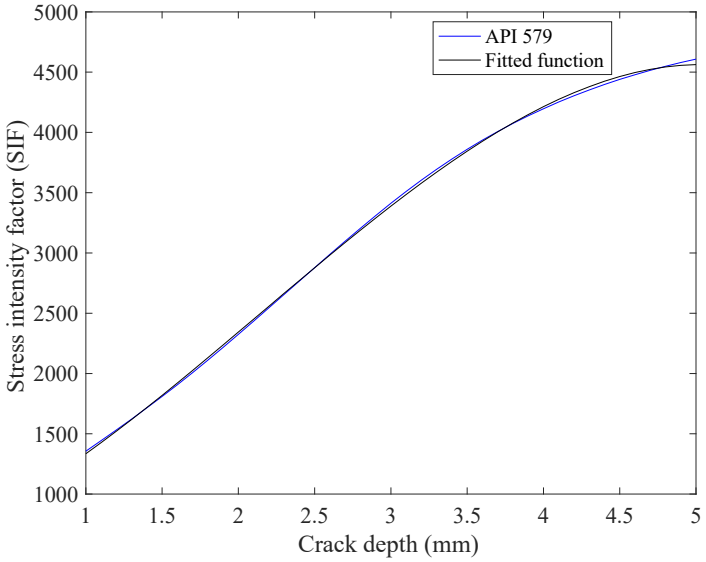

Figure 5.1 Comparison of SIF results between API 579 and fitted function

Next, the following equation Eq. (5-3), was used to obtain the estimated crack depth after a certain number of cycles. Suppose the lifetime of the pipeline is 30 years. It then related ΔN to time and then determine the corresponding crack depth in a given year 1, 2,…, 30.

$$a_{\text{next\_cycle}} = a_{\text{next\_cycle}} + C(\Delta K)^m \Delta N \tag{5-3}$$

5.2.4 Step 4: Failure probability calculation

A re-inspection with an ILI tool was noted to be typically performed when a previously calculated failure probability in time exceeds a preset threshold (such as within an operator's program). For the study, a pipeline with a single crack is considered failed if the crack depth was larger than or equal to the predetermined critical crack depth d_c.

The failure probability of pipeline with a single crack can be determined by Eq. (5-4). The failure probability of pipeline with multiple independent crack defects can be calculated by considering it as a series system with k elements, which is shown in Eq. (5-5).

$$\mathrm{PoF}_{\mathrm{defect}} = \mathrm{Prob}\,(d > d_c) \tag{5-4}$$

$$\mathrm{PoF}_{\mathrm{pipe}} = 1-(1-\mathrm{PoF}_{\mathrm{defect\ 1}})\,(1-\mathrm{PoF}_{\mathrm{defect\ 2}})\ldots\,(1-\mathrm{PoF}_{\mathrm{defect\ k}}) \tag{5-5}$$

The Monte Carlo simulation method was employed to introduce the ability to evaluate the sensitivity of failure probability of pipeline with a single crack defect and with multiple cracks.

Within a Monte Carlo simulation, in each iteration (denoted as i), a set of crack depths was generated as described in Step 1, and then an evaluation of pipeline with cracks exceeding the failure criteria (or not) at any given time T. In other words, if we run N simulation iterations there will be at a time T, N_f number of features exceeding the failure criteria, hence the probability of failure (PoF) of a pipeline with cracks can be estimated:

$$\mathrm{PoF}(T)=N_f/N \tag{5-6}$$

In this way, the relationship between PoF vs. time (T) was generated. The corresponding re-assessment time was then determined to be when PoF exceeded the PoF threshold. In the

following example, the PoF threshold is set to be 10^{-5}, and the next ILI tool run will be performed when PoF(T) is equal to PoF threshold.

5.3 Investigations on reliability assessment results

5.3.1 Parameters selection and determination

For the reliability assessment calculations for pipelines with cracks, the scenario was used as given in Table 5.1.

Table 5.1 Pipe Geometry and Material Properties

Parameters	Values
Diameter (NPS)	20
Diameter	508 mm
Nominal Wall Thickness (WT)	5.7 mm
Modulus	207 GPa (30023 ksi)
Yield Strength	433 MPa (63 ksi)
Ultimate Strength	618 MPa (90 ksi)
Maximum operating pressure	6.8 MPa (986 psi)

With the consideration of prediction accuracy and computation efficiency, Level 3 FAD for API 579 was selected for the reliability assessment. In the example, the crack length is set to be 40mm. So it was reasonable to only consider the growth of crack depth in the degradation process.

With the given parameters and the burst pressure was set to equal the maximum operating pressure, which related to a critical crack depth as equal to 75% *of WT* or =4.275mm in depth.

In the following results, the model parameters in Paris' law, m and C, are assumed to be 3 and 8.6×10^{-19} psi$\sqrt{\text{in}}$ respectively. The PoF threshold value was set to be 10^{-5}. And the number of total trials for Monte Carlo simulations was 10^{7}.

5.3.2 Single crack defect

In this section, the impacts of initial crack depth and ILI tool measurement error on the next inspection time are described.

Using the Monte Carlo simulation method and the Paris' law, the single defect failure probability was computed for same initial crack depth recording from last inspection and different ILI tool accuracies, as well as for cases with different crack depth and the same ILI tool accuracy. Figure 5.2 shows the comparison results for a single depth of d_0=20%*WT* with varying σ_{ILI} while Figure 5.3 shows the comparison results for a single σ_{ILI} with varying d_0=20%*WT* -50%*WT* as examples. We can find from these figures that if we decrease the standard deviation of ILI tool measurement error (increase the measurement accuracy) or initial crack depth, the curve moves to right and down side.

The time to perform the next tool run, i.e. time to reach the threshold 10^{-5}, is summarized in Table 5.2. From the comparison results, it was observed that the number of years to perform the next tool run increased with a more accurate ILI tool if the last reported crack depth was the same. And it decreased when the last reported crack depth increased with the same ILI tool accuracy.

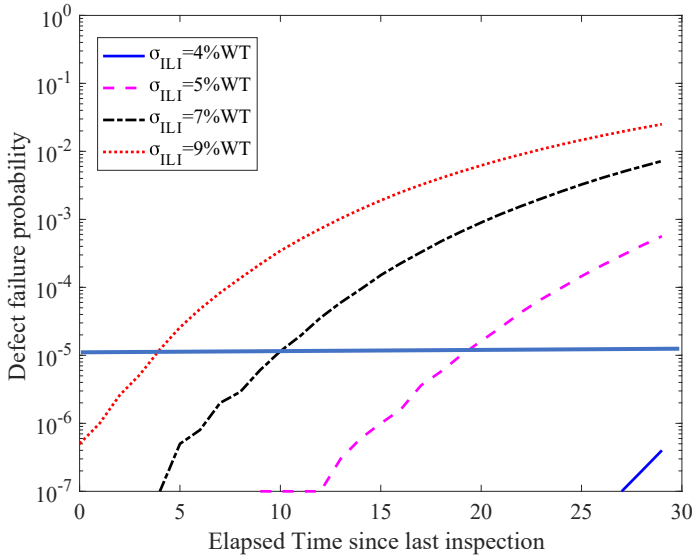

Figure 5.2 Evolution with time of the probability of failure associated with a single defect for d_0=20%t and different ILI tool accuracy using Monte Carlo Method

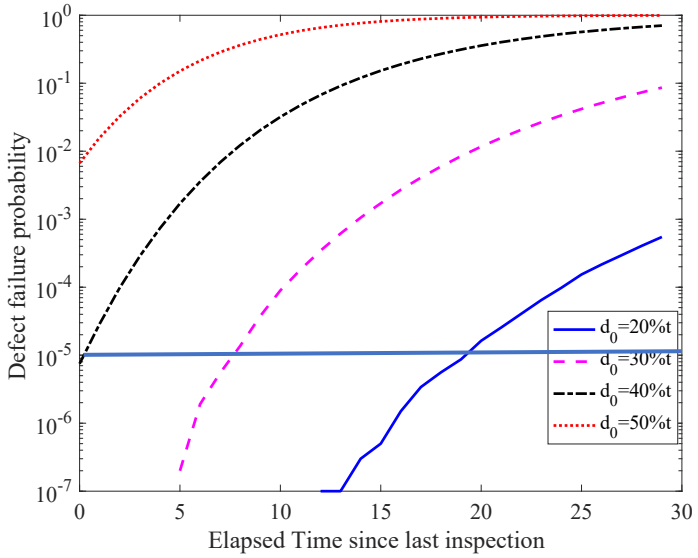

Figure 5.3 Evolution with time of the probability of failure associated with a single defect for σ_{ILI}=5%WT and different d_0 from Monte Carlo simulations

Table 5.2 Comparison results for pipeline with a single crack

Reported initial crack	ILI tool accuracy, σ_{ILI}	Time to reach 10^{-5}
20%	4%	>30
	5%	18.6
	7%	9.8
	9%	4.0
20%	5%	18.6
30%		7.5
40%		1
50%		1

5.3.3 Multiple crack defects

The reliability assessment for a pipeline with multiple cracks is described in this section. Five independent fatigue cracks in the pipeline were considered with the mean values of initial crack depths $d_{0,i}$ of the 5 cracks randomly generated following a uniform distribution within the range 20% to 30% of the wall thickness. For pipelines with multiple defects, a series system was deemed more appropriate because each defect may cause the failure of the pipeline.

Again, utilizing the Monte Carlo simulation method and Paris' law, the pipeline failure probability was computed for different ILI tool accuracies. Figure 5.4 shows the comparison results for σ_{ILI} =4%-9%WT. Horizontal axis indicates the time since last inspection, and the failure probability increases with time for each of the four cases. The reinspection time period, i.e. time to

reach the threshold 10^{-5}, is summarized and compared in Table 5.3. From the comparison results, it was observed that the number of years until a reinspection increased with a more accurate ILI tool.

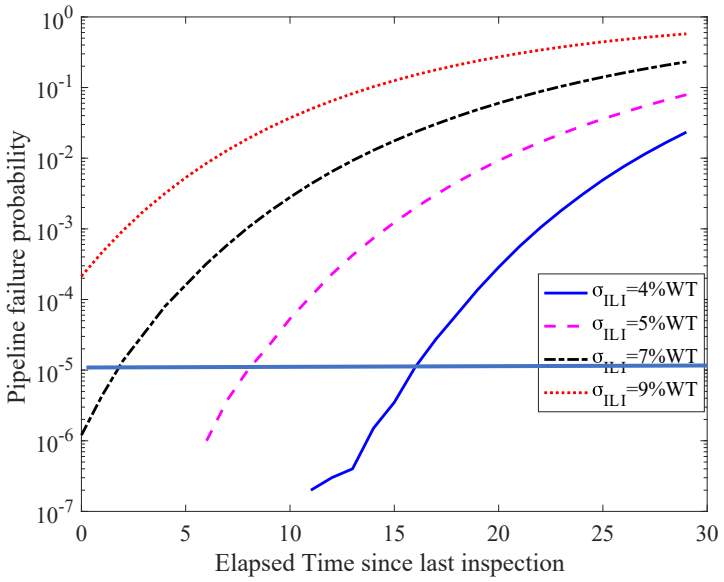

Figure 5.4 Evolution with time of the probability of failure associated with 5 defects for d_0 in the range [20%t, 30%t] and different ILI tool accuracy from Monte Carlo simulations

Table 5.3 Comparison results for pipeline with 5 cracks

Reported initial crack depth, d_0 (%WT)	ILI tool accuracy, σ_{ILI}	Time to reach 10^{-5} (yrs.)
20%~30%	4%	16.1
	5%	7.9
	7%	2.1
	9%	1

5.4 Integrity program cost evaluations

In this section, integrity program cost scenarios for pipeline integrity programs with multiple cracks are described with respect to different crack populations, pipe conditions and ILI accuracies.

5.4.1 Repair criteria

For each crack defect, certain repair criteria can be utilized to determine the corresponding repair actions. Based on the detection results, potential excavations and different repair activities are considered to be performed if a defect met certain criteria. The repair criteria used for this study was based on API 1160 [22]. For example, a crack defect will be repaired immediately or in the near term (within 1 year) after inspection if it meets the repair criteria [22], [206].

Two sets of repair criteria are defined. Repair criteria 1 was defined when at least one of the following two limit state functions was determined as less being than or equal to zero:

$$LSF\,(d) = 0.5t - d \leq 0 \tag{5-7}$$

$$LSF\,(P_f) = P_f - 1.25P_{\text{op}} \leq 0 \tag{5-8}$$

Hence a crack defect will be repaired only when it meets repair criteria 1. However, a crack defect that met repair criteria 1, also was assessed for severity of the defect such to determine whether it meets repair criteria 2 or not.

Repair criteria 2 is described by Eqs. (5-9) and (5-10):

$$LSF\,(d) = 0.7t - d \leq 0 \tag{5-9}$$

$$LSF\,(P_f) = P_f - 1.1P_{\text{op}} \leq 0 \tag{5-10}$$

If the crack defect condition meets repair criteria 2, which means at least one of the limit state functions is smaller than zero, the crack defect was also considered to need to be repaired immediately with a higher repair cost. And if the crack defect did not meet repair criteria 2, excavation and repair activities such as sleeving or recoating were considered to be done within one year but with a lower relative repair cost.

5.4.2 Cost rate calculation

When the probability of failure for a pipeline with cracks reaches the threshold (10^{-5}), it was considered that the next ILI tool run will be performed to affirm the assumed condition of the defect. For the inspection time t^*, the total cost rate is calculated for further comparison and analysis. To calculate the cost rate, the net present value was determined for each Monte Carlo simulation run and set of conditions. The net present value of total cost for pipeline with crack defects was determined as per Eq. (5-11) [3]:

$$PV_{\text{Total},t^*}=PV_{\text{Insp},t^*}+PV_{\text{Fail},t^*}+PV_{\text{Main},t^*}+PV_{\text{Fixed},t^*} \tag{5-11}$$

where PV_{Insp,t^*}, PV_{Fail,t^*}, PV_{Main,t^*}, PV_{Fixed,t^*} are net present values of inspection cost, failure cost, maintenance cost and additional fixed cost for entire line at year t^*.

The inspection cost is given by:

$$PV_{\text{Insp},\,t^*}=\frac{C_{\text{in}}}{(1+r)^{t^*}} \tag{5-12}$$

where C_{in} is the inspection cost; r is the discounted cash rate. In this study, ILI tools with different ILI tool accuracies were considered to calculate and compare the inspection and total cost rates.

The subsequent failure cost is given by

$$PV_{\text{fail, t}^*} = \frac{C_{\text{fa}}}{(1+r)^{t^*}} \times \text{PoF}_{\text{pipe}} \tag{5-13}$$

where PoF_{pipe} is the probability of failure for pipeline; C_{fa} is the failure cost which includes economic loss and other costs due to damage to population and environment. The maintenance cost is given by:

$$PV_{\text{Main, t}^*} = \frac{\sum_{j=1}^{k}(C_{\text{main}} \times \text{PoR}(j))}{(1+r)^{t^*}} \tag{5-14}$$

where C_{main} is the repair cost; k is the number of crack defects; PoR(j) is the probability of repair for defect j. The probability of repair for each defect is calculated by using the corresponding repair criteria introduced above.

5.5 Investigation on the total cost rate with different ILI measurement errors

In this section, an example is provided to describe the impact of ILI tool accuracy on inspection and total cost rates. The geometry and material properties of pipeline are shown in Table 5.1. The summary of baseline costs relative to a given ILI inspection is shown in Table 5.4.

For UT cracking inspection, the standard deviation was equal to 0.5mm (relative cost = 1) as the baseline level. Recoating and repair sleeve installation of the pipeline were two alternative options for repair actions, at relatively low relative costs to the inspection for the purposes of this study. The failure costs were divided into two types, immediate cleanup/repair and other damages.

Table 5.4 Summary of baseline costs for Total Cost Rate of an integrity program.

Cost item	Relative cost
In-line inspection C_{in}	1
Excavation C_{ev}	0.14
Recoating C_{rc}	0.04
Sleeving C_{rs}	0.07
Failure cost - immediate cleanup/repair C_{f1}	4
Failure cost - other damages C_{f2}	60
Fixed cost (labor, transportation, etc.) C_{fi}	0.05

The inspection cost C_{in} increased when the accuracy of ILI tool improved. Based on the results in Figure 5.3 and Figure 5.4, the re-assessment time such that PoF reaches 10^{-5}, increased as the ILI tool accuracy improved. The relationship between inspection cost and ILI tool accuracy are shown in Table 5.5 considering two assumption scenarios.

Within inspection cost assumption case 1, the inspection cost was 15% higher for each improved increment of 0.1mm of the standard deviation of ILI tool (σ_{ILI}). Within inspection case assumption 2, a larger differential cost (exponential cost increase) was assumed for more accurate ILI tool performance, as shown in Table 5.5.

With each Monte Carlo simulation run, the total net present value $PV_{Total,i}$ and total time T_i were calculated. The following two equations were then used to calculate the inspection cost rate (Eq. (5-15)) and total cost rate (Eq. (5-16)), respectively:

$$CR_{Insp} = \frac{\sum_{i=1}^{N} \frac{C_{in}}{(1+r)^{T_i}}}{\sum_{i=1}^{N} T_i} \tag{5-15}$$

$$CR_{\text{Total}} = \frac{\sum_{i=1}^{N} PV_i}{\sum_{i=1}^{N} T_i} \tag{5-16}$$

The corresponding re-assessment time (PoF reaches 10^{-5}) is calculated by taking the average of each re-assessment time as per Eq. (5-17):

$$\overline{T} = \frac{\sum_{i=1}^{N} T_i}{N} \tag{5-17}$$

Five crack defects were considered in the following examples. The feature population of the following cases is a normal distribution with the mean is 21%*WT* (1.2mm) and standard deviation is 1.7%*WT* (0.1mm). These five crack defects were randomly sampled using the above-mentioned normal distribution to generate in the pipeline. Two discount cash rates were considered as r=0 (no time-weighted value) and 0.14 (time-weighted value), respectively.

The comparison results for relative inspection and total cost rates under Assumption 1 and 2 are shown in Table 5.5 and 5.6, respectively. The first column shows ILI tool accuracy as a percentage of the wall thickness (*WT*). The second column shows inspection cost relative to the baseline inspection cost, at 9%*WT*. Table 5.5 shows costs with Assumption case 1, where inspection cost is subject to moderate change with respect to ILI tool accuracy. While with Assumption case 2, shown in Table 5.6, the inspection cost changes more dramatically with tool accuracy. The last two columns show the inspection cost rate and total cost rate, defined in equations (5-15) and (5-16), respectively. The lower the cost rates, the more attractive the condition can be considered to be. The minimum values for inspection and total cost rates are highlighted as bold in these tables.

Table 5.5 Comparison results for inspection and Total Cost Rates with different Discount Cash Rates per Cost Assumption Case 1 (15% per 0.1mm std. difference)

(a) r=0

ILI tool accuracy, σ_{ILI} (% WT)	Cost Assumption (as multiple)	Time to reach 10^{-5} (yrs.)	Inspection cost rate, CR_{Insp}	Total cost rate, CR_{Total}
4%	**1.52**	**28.8**	**0.0530**	**0.0548**
5%	1.33	15.5	0.0867	0.0899
7%	1.15	7.7	0.1511	0.1575
9%	1	2.4	0.4268	0.4489
11%	0.87	1.0	0.8700	0.9310
12%	0.75	1.0	0.7500	0.8564

(b) r=0.14

ILI tool accuracy, σ_{ILI} (%WT)	Cost Assumption (as multiple)	Time to reach 10^{-5} (yrs.)	Inspection cost rate, CR_{Insp}	Total cost rate, CR_{Total}
4%	**1.52**	**28.8**	**0.0012**	**0.0016**
5%	1.33	15.5	0.0114	0.0129
7%	1.15	7.7	0.0551	0.0597
9%	1	2.4	0.3116	0.3313
11%	0.87	1.0	0.7632	0.8222
12%	0.75	1.0	0.6579	0.7499

Table 5.6 Comparison results for Inspection and Total cost rates with different Discount Cash Rates per Cost Assumption Case 2 (exponential increase with std. difference)

(a) r=0

ILI tool accuracy, σ_{ILI} (%WT)	Cost Assumption (as multiple)	Time to reach 10^{-5} (yrs.)	Inspection cost rate, CR_{Insp}	Total cost rate, CR_{Total}
4%	50	28.8	1.7434	1.7452
5%	8	15.5	0.5215	0.5247
7%	2.5	7.7	0.4344	0.4411
9%	1	2.4	0.4268	0.4489
11%	0.5	1.0	0.5000	0.5599
12%	**0.25**	**1.0**	**0.2500**	**0.3852**

(b) r=0.14

ILI tool accuracy, σ_{ILI} (%WT)	Cost Assumption (as multiple)	Time to reach 10^{-5} (yrs.)	Inspection cost rate, CR_{Insp}	Total cost rate, CR_{Total}
4%	**50**	**28.8**	**0.0400**	**0.0404**
5%	8	15.5	0.0684	0.0699
7%	2.5	7.7	0.1584	0.1781
9%	1	2.4	0.3116	0.3313
11%	0.5	1.0	0.4386	0.4976
12%	0.25	1.0	0.2193	0.3113

From the comparison results in Table 5.6, we can find that for both r=0 and 0.14, when ILI tool accuracy is σ_{ILI} =4%WT (0.2mm), the lowest inspection and total cost rates were achieved (as

expected). For Assumption 2 with r=0 (Table 5.6), the time value of money is reflected directly within the exponential differences of the inspection cost in comparison to a non-zero discount cash rate. Also notably beyond the extreme inspection cost scenario (best accuracy), the cost rate is similar amongst remaining accuracies. However, for the r=0.14 discounted cash rate scenario as in Table 5.5, the inspection and total cost rates both decrease with an increase of ILI tool accuracy. In this example, the PoF acceptability threshold was set to be 10^{-5}, which resulted in a relatively low maintenance and failure cost rate for each case.

The comparison results are plotted in Figure 5.5 for inspection cost rate and total cost rate, where the horizontal axis is the tool accuracy in terms of *WT* percentage. From Figure 5.5, it was observed that with inspection cost assumption case 1, the trends for r=0 and r=0.14 were similar as well as for the practical business case of r=0.14 within assumption case 2. Notably in all of these cases, even with notably higher inspection cost rates, the lower Total cost rates were achieved with increased accuracy.

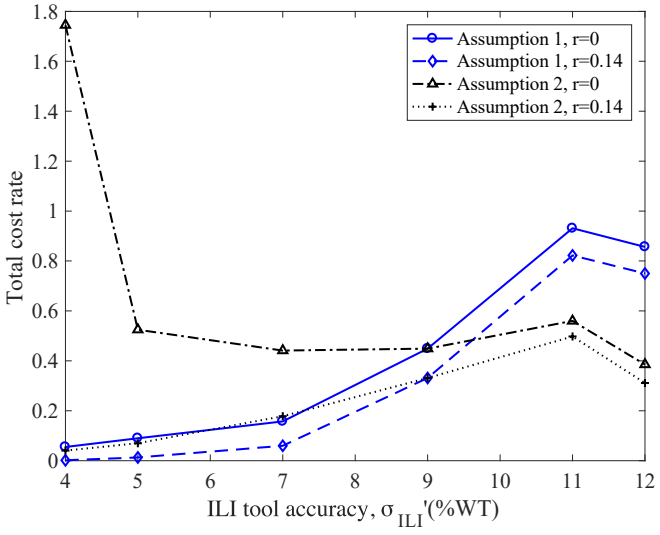

Figure 5.5 Total cost rate comparison results for different ILI tool accuracies

In context for the non-reality case of r=0 in assumption case 2, it reflected that without a time-value to cost, and for inspection costs of similar magnitude to outright failure, a calculable threshold value of inspection accuracy can be determined as non-viable and that otherwise inspection accuracy differences did not show influence in resulting Total cost rates.

The decrease in Total cost rate as shown in Figure 5.5 between 11% *WT* and 12% *WT* was observed to be due to the timescale effect relative to the cost multiples vs accuracy differences, the repair response criteria and the initial case condition as a relatively thin nominal wall thickness of 5.7mm, such that there was not a time value "benefit" in detecting the immediate failure criteria conditions. For example, as can be observed in Table 5.5a and Table 5.5b, Time to reach 10^{-5} for both the 11% *WT* and 12% *WT* cases are 1.0 year.

Table 5.7 Comparison results for inspection and Total Cost Rates with different Discount Cash Rates per Cost Assumption Case 1 (PoF threshold=10^{-4})

ILI tool accuracy, σ_{ILI} (%*WT*)	Cost Assumption (as multiple)	Time to reach 10^{-4} (yrs.)	Inspection cost rate, CR_{Insp}	Total cost rate, CR_{Total}
4%	**1.52**	**29.9**	**0.0010**	**0.0011**
5%	1.33	20.2	0.0051	0.0062
7%	1.15	13.8	0.0137	0.0156
9%	1	7.2	0.0541	0.0593
11%	0.87	2.4	0.2646	0.2982
12%	0.75	1.1	0.5908	0.7499

Next a less conservative case was also considered, where the PoF threshold equals to 10^{-4}, to further examine the total cost rate trend. The discount cost rate is set to be 0.14, and Assumption

1 is used. The comparison results are shown in Table 5.7. With the comparison between Table 5.5b and Table 5.7, it can be found that as the PoF threshold increases from 10^{-5} to 10^{-4}, the re-assessment time is getting bigger for all different ILI tool accuracies, and the corresponding inspection and total cost rates decrease for all cases. The Total cost rate shows a monotonically increasing trend, and the re-assessment time decreases as ILI tool accuracy decreases from 11% *WT* and 12% *WT*.

5.6 Investigation on long-term cost rate

In this section, we investigate the impact of ILI tool accuracy on long-term cost rate considering new anomaly initiation and continuous growth. In Section 5.5 presented earlier, it is assumed that the crack size distributions at the beginning of an inspection cycle are known, and such distributions are the same at the beginning of different inspection cycles, which is the case for stable operations. In this section, we introduce new defect generation, and a crack defect can grow continuously across multiple inspection cycles before maintenance actions are taken. The non-homogeneous Poisson process was introduced to generate the number of crack defects over the long-term interval instead of the fixed number used in Section 5.5. Besides, the probability of detection was also considered when evaluating the cost rates. Examples will be presented and results will be discussed.

5.6.1 Long-term cost rate evaluation

The procedure for the long-term cost rate evaluation is presented in this section.

5.6.1.1 Step 1: Crack defects generation

Because each crack defect is independent of time, we adopt non-homogeneous Poisson process to generate the crack defects over the period from zero to a given year T. Let i be the label of a defect. In this step, we calculate the expected total number of crack defects, and generate the information (crack depth c_i, crack length d_i, crack initiation time t_i) associated with defect i. The expected number of crack defects over the time period from zero to T, $\Lambda(T)$, can be calculated using the following equation: $\Lambda(T)=\int_0^T \lambda(\tau)d\tau$ [257]. $\lambda(\tau)$ is the instantaneous generation rate and it is calculated as: $\lambda(\tau)=\lambda_0\tau^b$, where λ_0 and b can be determined based on historical data. Due to the assumption we made that the generation of crack defects is independent of time, we assume b is equal to zero. And λ_0 is assumed to be 2 for the following examples. After calculating the expected number of crack defects, we could use Poisson probability mass function to generate the total number of crack defects (n_T) generated in the time interval.

$$n_T \sim f\left(N(T)\middle|\Lambda(T)\right)=\frac{\Lambda(T)^{N(T)}e^{-\Lambda(T)}}{N(T)!} \quad (5\text{-}18)$$

With the generation of total number of crack defects (n_T), for each defect i, crack length c_i is randomly generated within the range [10, 50], crack depth d_i is randomly generated within the range [1, 1.1], and the initiation time t_i is randomly generated within the range [0, 30] for the following examples.

5.6.1.2 Step 2: Crack defect growth and decision making at the end of an inspection interval

Let T_I be the inspection interval, we grow each defect year by year until it fails or reaches T_I in this step. If a crack defect meets failure criteria, we consider it as a failure. The failure cost is

calculated at that moment. For this failed pipeline joint, we replace it and re-generate crack defects using the generation mechanism described in Step 1. When the time reaches inspection interval T_I, we first need to check if the ILI tool detects this defect or not. Here, the probability of detection of ILI tools is introduced and assumed to be a function of the crack depth, which is defined as follows [82]:

$$PoD(d)=1-\exp(-2.303d) \tag{5-19}$$

From the equation above, we can find that the detection ability of ILI crack detection tool increases as crack depth increases. For defect *i*, to check if it is detected or not, we generate a random number from a uniform distribution between zero and one, and compare it with $PoD(d)$. If this random number is smaller, we consider it is successfully detected. The measurement error of ILI tool is then considered to determine the ILI reported crack depth and length for each detected defect. If the crack meets the repair criteria, we calculate the corresponding repair and excavation cost. We assume the repair is a perfect repair, and delete the *i*th defect. If it is not detected or does not meet repair criteria, this defect will continue to grow in the next cycle, and we move on to the next crack defect.

5.6.1.3 Step 3: Cost rate calculation

In an inspection cycle, we calculate the inspection, repair, failure, additional fixed and total cost rate. Then we consider calculating a long-term cost rate. In this step, we use long-term run rather than 30 years to calculate the cost rate. This is because considering crack defects generation mechanism and probability of detection will cause more uncertainties. The long-term methodology will deal with these uncertainties and produce more accurate results compared with

a traditional method. Let T_{life} be the total long-term life, and the number of inspection interval can be calculated as T_{life}/T. With a given inspection interval, we run the calculation procedure till T reaches T_{life}. After calculating cost rate for each inspection interval, the expected cost rate can be obtained through taking the average of cost rates. In this way, total cost rates will finally converge to a certain value as T_{life} increases. A more reliable and accurate result will be obtained with the use of long-term methodology compared with a small value of pipeline life (30 years). Figure 5.6 shows an example of the comparison of the expected cost rates associated with different long-term life. We can find that expected cost rates increase as T_{life} increase from 0 to around 100 years, and they fluctuate a lot when T_{life} between 100 and 700 years. When the total long-term life is bigger than 700 years, the expected cost rates become steady and approach a certain value (0.72). In the following examples, we set T_{life} to be 1000 years for long-term cost rate calculation.

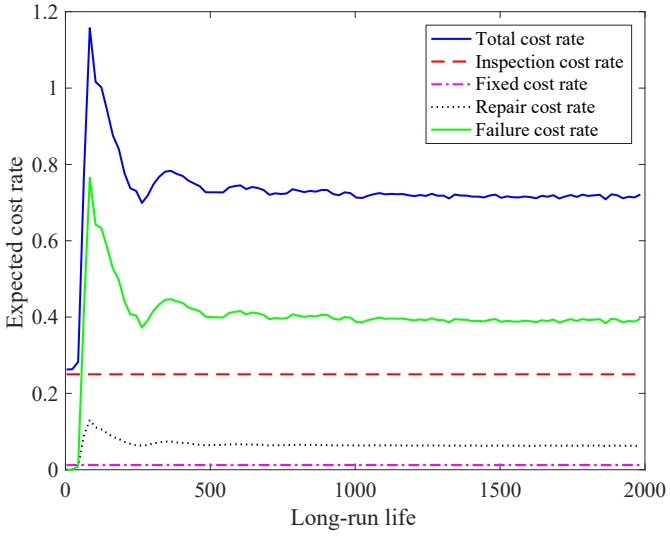

Figure 5.6 Comparison of the expected cost rates associated with different long-term life

5.6.2 Examples

We use the same geometry and material property of pipelines as those discussed in Section 5.5 for the following examples. Five cases with different input parameters including pressure, discount rate and failure cost were performed to investigate the impact of ILI tool accuracy on the results. The optimal inspection intervals and the corresponding total cost rates were then obtained and compared for different ILI tool accuracies. Sensitivity analysis for pressure and failure cost were performed in this section.

The pipe geometry and material properties used for long-term examples are shown in Table 5.1. The relative cost for different cost items we use are shown in Table 5.4. Two different failure costs are studied and compared here, and 4 and 60 represent minor and major failure costs respectively. Internal pressure affects the growth rates per year for crack defects. We select pressure 2MPa and 5MPa to perform the sensitivity analysis. The discount rate is assumed to be 0. The list of cases we studied is shown in Table 5.8. For each case, six different standard deviations of measurement error of ILI tools are investigated here. The inspection cost assumption associated with different measurement error of ILI tools are described in Table 5.5 (Cost Assumption Case 1) in Section 5.5. The discount rate was assumed to be 0 for cases 1 to 4. And it was assumed to be 0.14 for case 5. We also considered a 1000 years long-term life for this case. We limit the discounting (i.e. 14%) to one inspection cycle of pipe life during the simulation, no matter when the cycle starts. That is, only discount the cost to the beginning of the inspection interval of that particular pipe. This is because if we discount the cost to time 0, the future cycles are discounted too much, which does not seem reasonable. Through investigating these five cases with different failure cost, pressure, and inspection cost assumption, we can give parametric analysis and draw conclusions regarding the impact of ILI tool performance.

Table 5.8 List of cases

Case	Failure cost C_f	Pressure	Discount rate r_d	Inspection cost assumption
1	4	2	0	1
2	4	5	0	1
3	60	5	0	1
4	4	5	0	2
5	4	5	0.14	1

We follow the above-described evaluation approach and use Monte Carlo simulation method to obtain the expected inspection, repair, failure, fixed and total cost rates. The inspection interval varies from 1 to 30 with an increment of 1 year, and the long-term life is set to be 1000 years. The plots for comparison of the expected cost rates associated with different cost items for cases 1 to 5 are shown in Figures 5.7, 5.9, 5.11, 5.13, 5.15, respectively. For each case, six values of standard deviation of measurement error of ILI tools (σ_{ILI}) were considered, i.e. σ_{ILI}=4%*WT*, 5%*WT*, 7%*WT*, 9%*WT*, 11%*WT*, 12%*WT*, respectively. The expected total cost rates corresponding to different standard deviations of measurement error of ILI tools for cases 1 to 5 are depicted in Figures 5.8, 5.10, 5.12, 5.14, 5.16, respectively. The comparison results for optimal solutions with different ILI tool accuracies for cases 1 to 5 are summarized in Tables 5.9 to 5.13 respectively. Optimal inspection intervals and corresponding total cost rates are shown and compared in these tables.

The curves show the trends in total cost rates and their component cost rates. We use spline interpolation functions as fitted functions and then find the minimum points as the optimal points,

which are labeled in the following figures. The optimal point can then give us the optimal inspection interval and its corresponding expected total cost rate. The results shown in Figure 5.7 indicate that the inspection cost rate has the highest contribution to total cost rate when inspection interval is smaller than a specific value, for example, it is around 12 for Figure 5.7a. After that intersection point between inspection cost rate and failure cost rate, the failure cost rate contributes more than other components. Overall, the inspection and failure cost rates are two important cost components compared with others. The inspection cost rate is getting smaller while failure cost rate is getting bigger as inspection interval increases. The reason for inspection cost rate decrease is that the basic inspection tool run cost is a constant value and the denominator (interval) is getting bigger. As inspection interval increases, crack defects are more likely to fail, and therefore the failure cost rate is getting bigger, which is expected. Note that there are some small peaks and valleys in both failure cost rate curves and the total cost rate curves. This is mainly because that the annual failure probabilities fluctuate a bit when inspection interval is big.

From the results shown in Table 5.9, as σ_{ILI} decreases which means we increase the ILI tool accuracy, the optimal inspection interval is getting bigger and the corresponding total cost rate is getting smaller. The comparison results suggest that the most accurate ILI tool ($\sigma_{ILI} = 4\%WT$) gives the smallest expected total cost rate. Results shown in Figure 5.8 suggest that a bigger σ_{ILI} gives a smaller total cost rate as long as inspection interval is smaller than the optimal inspection interval. And when inspection interval is bigger than the optimal one, a curve associated with a higher σ_{ILI} becomes the higher one.

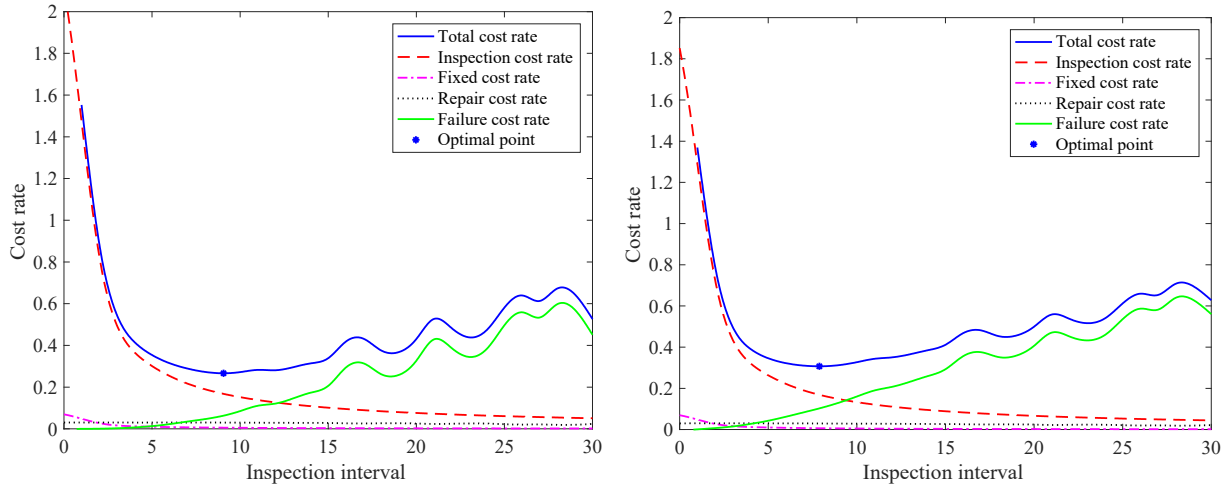

(a) σ_{ILI} =4%WT (b) σ_{ILI} =5%WT

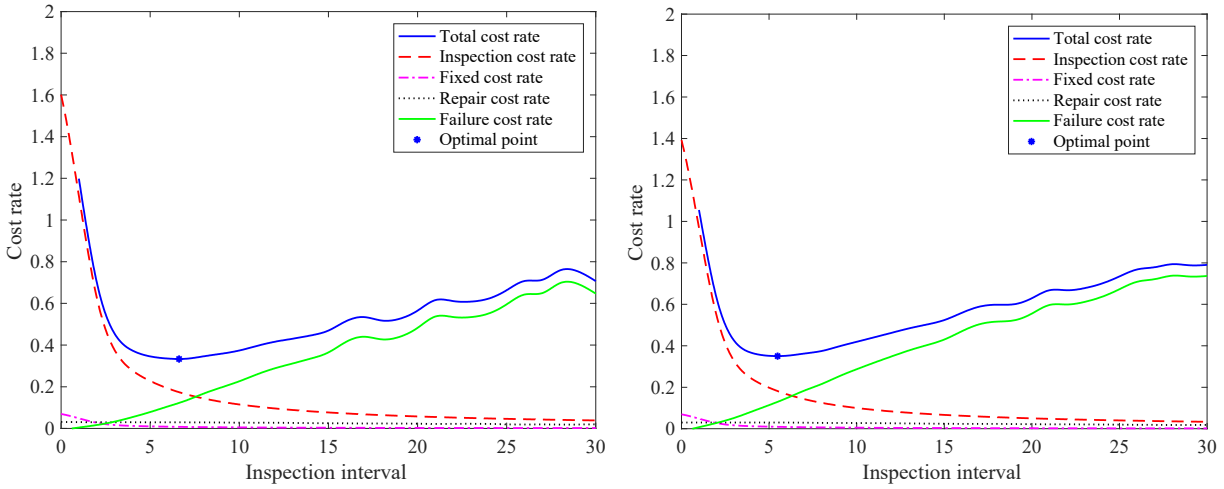

(c) σ_{ILI} =7%WT (d) σ_{ILI} =9%WT

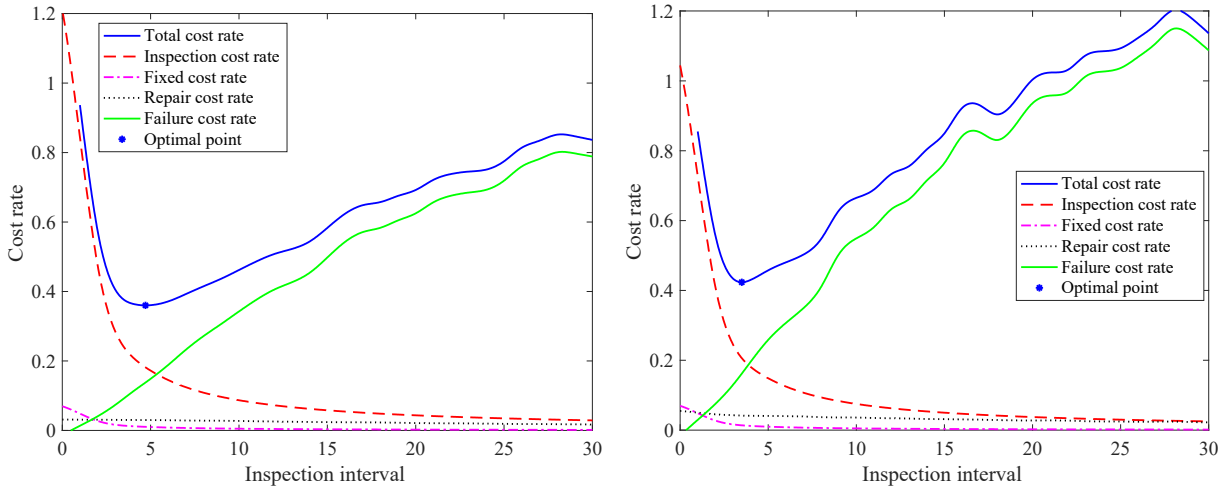

(e) σ_{ILI} =11%WT (f) σ_{ILI} =12%WT

Figure 5.7 Comparison of the expected cost rates associated with different cost items (Case 1)

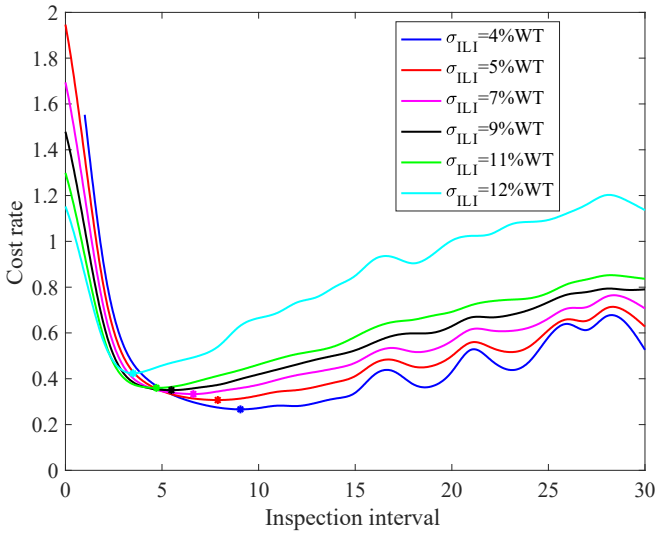

Figure 5.8 Comparison of the expected total cost rates associated with different standard deviation of measurement error of ILI tools (Case 1)

Table 5.9 Comparison of optimal solutions with different standard deviations (Case 1)

ILI tool accuracy, σ_{ILI} (%WT)	Optimal inspection interval	Total cost rate
4%	9.0577	0.2664
5%	7.8848	0.3070
7%	6.6213	0.3331
9%	5.4850	0.3502
11%	4.7089	0.3600
12%	3.4994	0.4235

The values of total cost rates and their components for different tool accuracy for Case 2 are plotted in Figure 5.9. The characteristics of these curves are similar to those in Figure 5.7. However, these curves have steeper slopes. The comparisons of optimal solutions with different standard deviations for Case 2 are summarized in Table 5.10. We can draw similar conclusions as those based on Table 5.9: the higher σ_{ILI} is, the shorter optimal inspection interval and bigger total cost rate are except for σ_{ILI}=12%*WT*. Compared with Case 1, with the increase of pressure, the effects of σ_{ILI} on optimal inspection interval and total cost rate decrease. The comparison results shown in Figure 5.10 suggest that these curves have similar shapes including small peaks and valleys. The curve corresponding to a higher σ_{ILI} gives slight bigger values compared with a lower one.

The results shown in Figure 5.11 illustrate the total cost rates and their components for different σ_{ILI} with the input parameters from Case 3. With a much higher failure cost (60) compared with the previous cases, as expected, the failure cost rates increase faster and have the highest contribution to total cost rates. And other cost rates are negligible compared with failure cost rates for this case. The total cost rates in Figures 5.11c-5.11f are almost monotonically decreasing with some small peaks and valleys. Therefore, the optimal inspection intervals are 1 for these situations.

The impact of σ_{ILI} on total cost rates are illustrated in Table 5.9 and Figure 5.12. From the comparison results in Table 5.9, the optimal inspection interval decreases and remains the same after it reaches 1 as σ_{ILI} increases. The total cost rate keeps increasing when σ_{ILI} is increasing. So the total cost rate corresponding to σ_{ILI}=4%*WT* has the smallest value. Figure 5.12 indicates that a higher σ_{ILI} leads to a higher total cost rate. This is mainly because the failure probability corresponding to a higher σ_{ILI} is bigger, which leads to a higher failure cost rate and total cost rate.

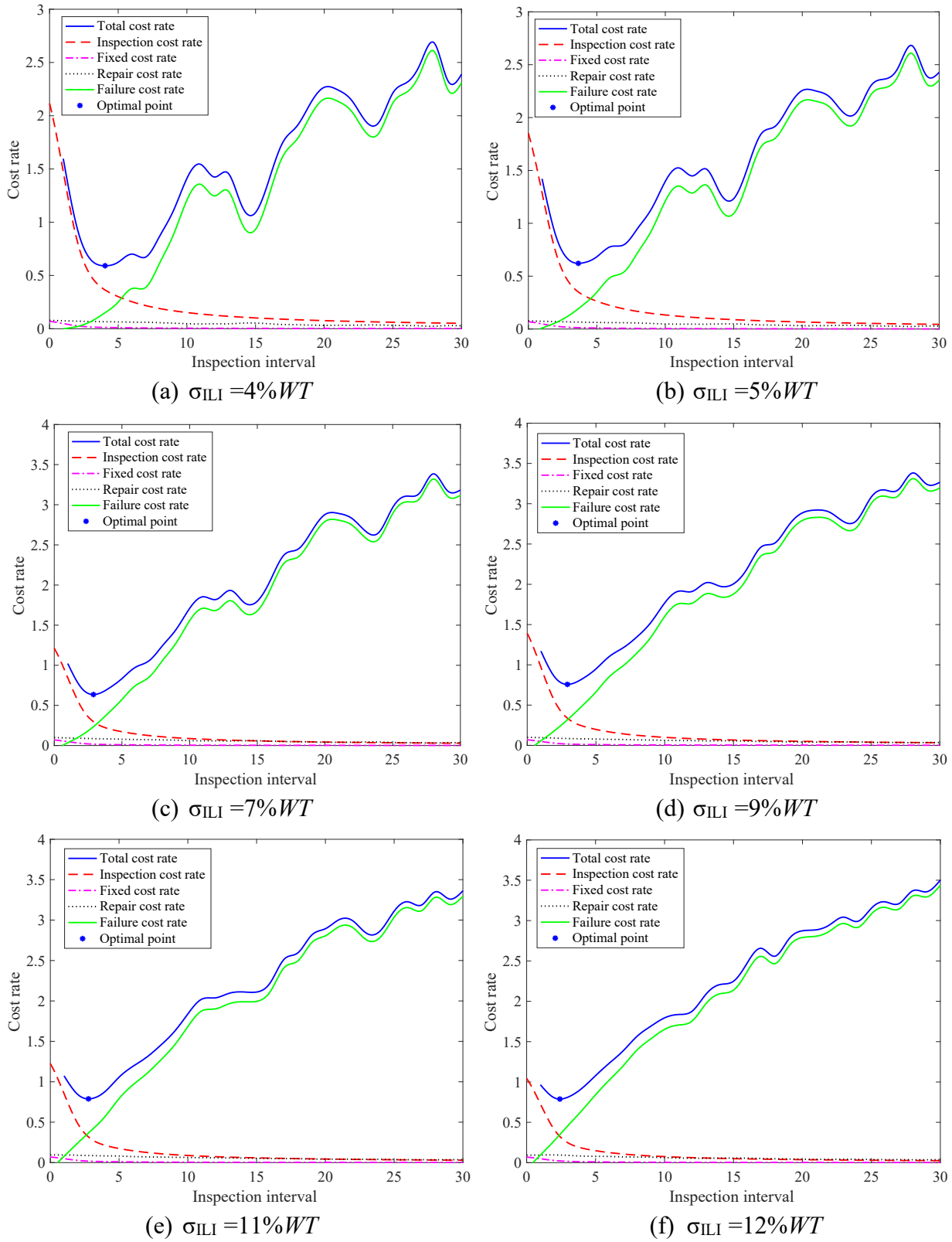

(a) σ_{ILI} =4%WT (b) σ_{ILI} =5%WT

(c) σ_{ILI} =7%WT (d) σ_{ILI} =9%WT

(e) σ_{ILI} =11%WT (f) σ_{ILI} =12%WT

Figure 5.9 Comparison of the expected cost rates associated with different cost items (Case 2)

Table 5.10 Comparison of optimal solutions with different standard deviations (Case 2)

ILI tool accuracy, σ_{ILI} (%WT)	Optimal inspection interval	Total cost rate
4%	4.0453	0.5912
5%	3.5954	0.6279
7%	2.9412	0.6351
9%	2.9266	0.7574
11%	2.7768	0.7884
12%	2.4094	0.7792

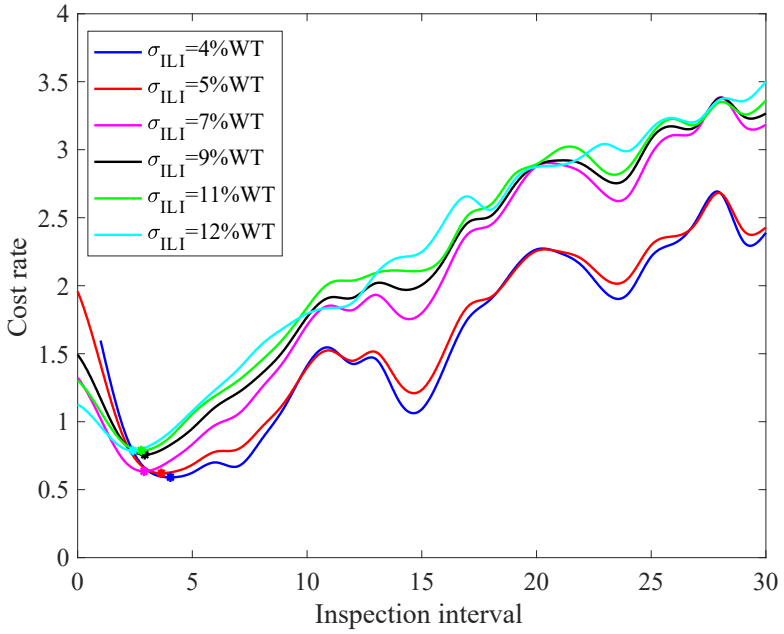

Figure 5.10 Comparison of the expected total cost rates associated with different standard deviations of measurement error of ILI tools (Case 2)

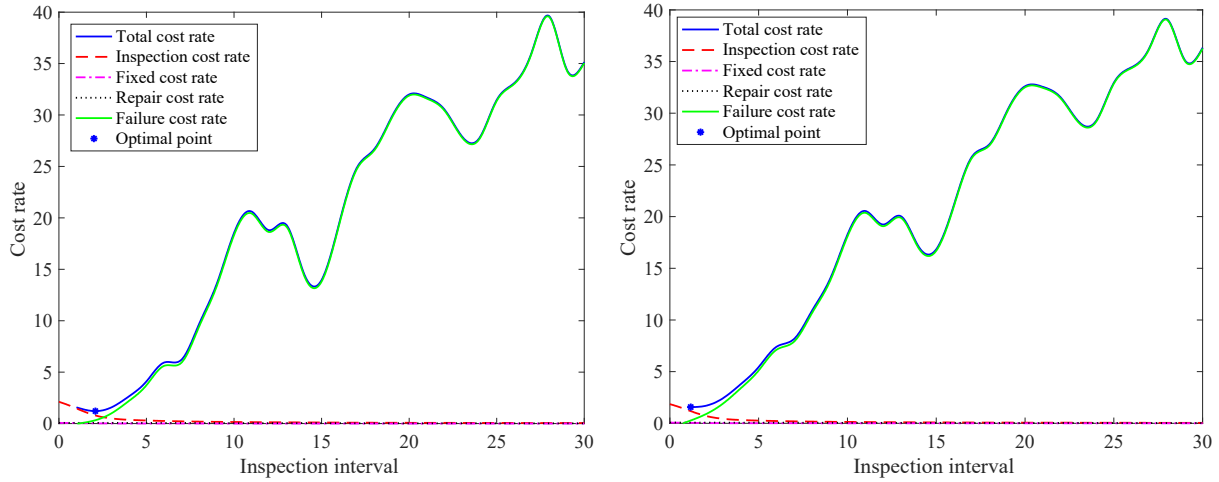

(a) σ_{ILI} =4%WT (b) σ_{ILI} =5%WT

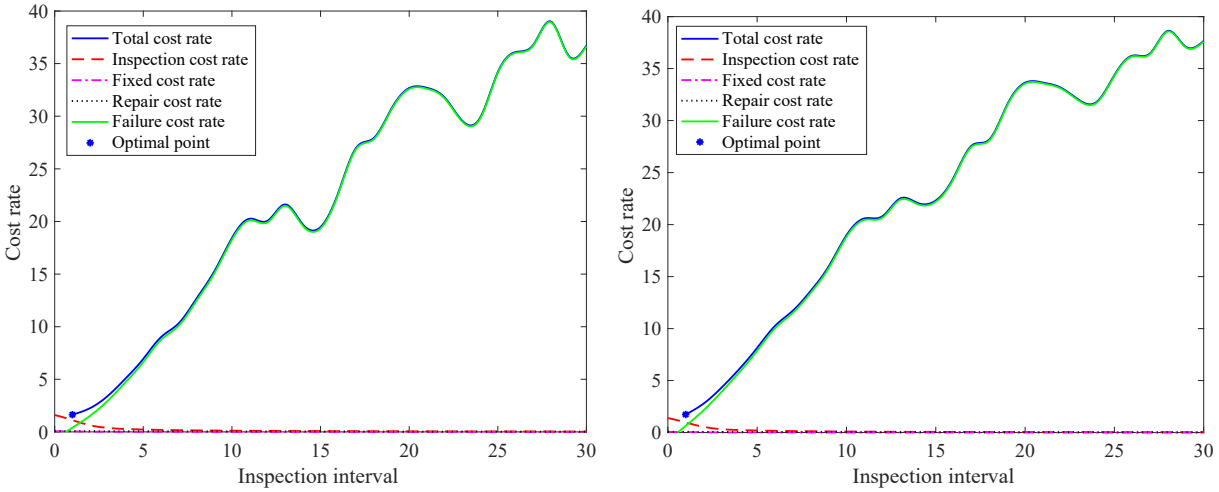

(c) σ_{ILI} =7%WT (d) σ_{ILI} =9%WT

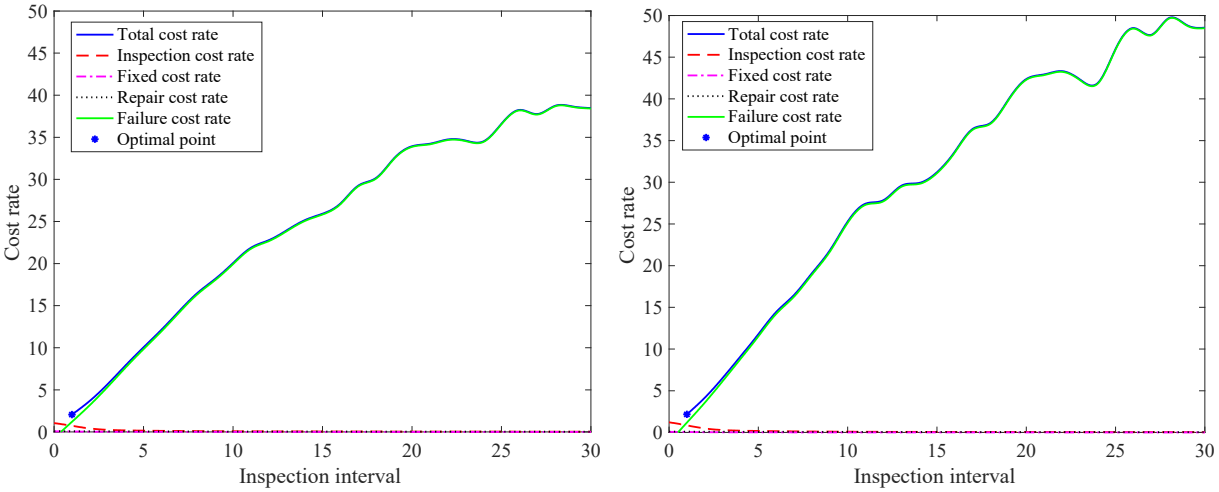

(e) σ_{ILI} =11%WT (f) σ_{ILI} =12%WT

Figure 5.11 Comparison of the expected cost rates associated with different cost items (Case 3)

Table 5.11 Comparison of optimal solutions with different standard deviations (Case 3)

ILI tool accuracy, σ_{ILI} (%*WT*)	Optimal inspection interval	Total cost rate
4%	2.0848	1.2136
5%	1.1762	1.5732
7%	1.0001	1.6382
9%	1.0000	1.7387
11%	1.0000	2.0584
12%	1.0000	2.1666

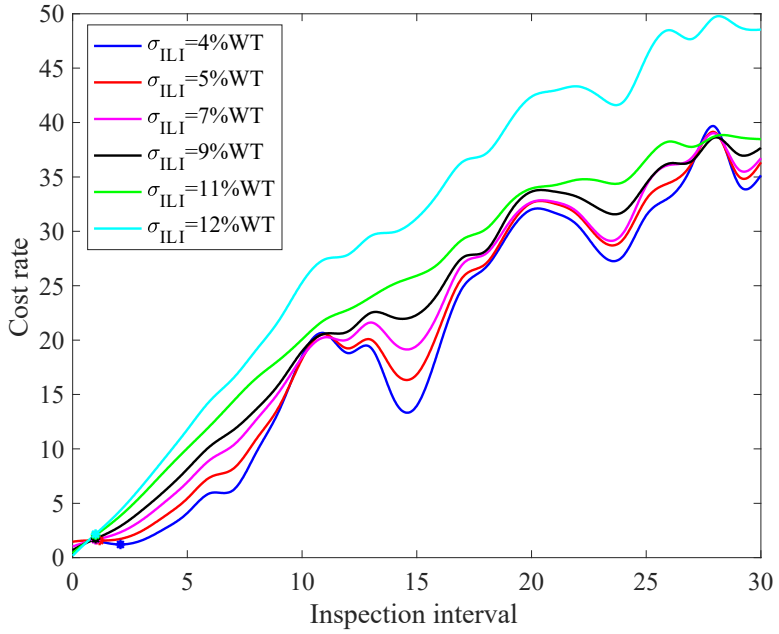

Figure 5.12 Comparison of the expected total cost rates associated with different standard deviations of measurement error of ILI tools (Case 3)

The values of cost rates as functions of inspection interval and σ_{ILI} with the consideration of cost assumption 2 are depicted in Fig 5.13 (Case 4). The shapes of these curves are a bit different from Case 2. The inspection and failure cost rates are the dominant ones among all cost rates components. And other cost rates are negligible compared with inspection and failure cost rates so that the optimal points are around the intersection points of green and red curves. The corresponding comparison results are given in Fig 5.14. The curves are moving down as σ_{ILI} increases when inspection interval is small. This can be explained that for small inspection interval, the inspection cost rate has the highest contribution and inspection cost decreases as σ_{ILI} increases, resulting in a lower expected inspection cost rate and total cost rate. Table 5.12 suggests that the optimal inspection interval increases a lot as σ_{ILI} decreases and the total cost rate decreases as σ_{ILI} increases, which is completely different from other cases. And this indicates that the inspection costs assumption has a big impact on cost rates. This is mainly because inspection cost increases a lot as σ_{ILI} decreases, resulting in a higher inspection cost rate and total cost rate.

Table 5.12 Comparison of optimal solutions with different standard deviations (Case 4)

ILI tool accuracy, σ_{ILI} (%*WT*)	Optimal inspection interval	Total cost rate
4%	23.8151	3.9779
5%	7.2197	1.7368
7%	4.2908	0.9926
9%	2.9266	0.7574
11%	2.4132	0.5410
12%	1.3654	0.4481

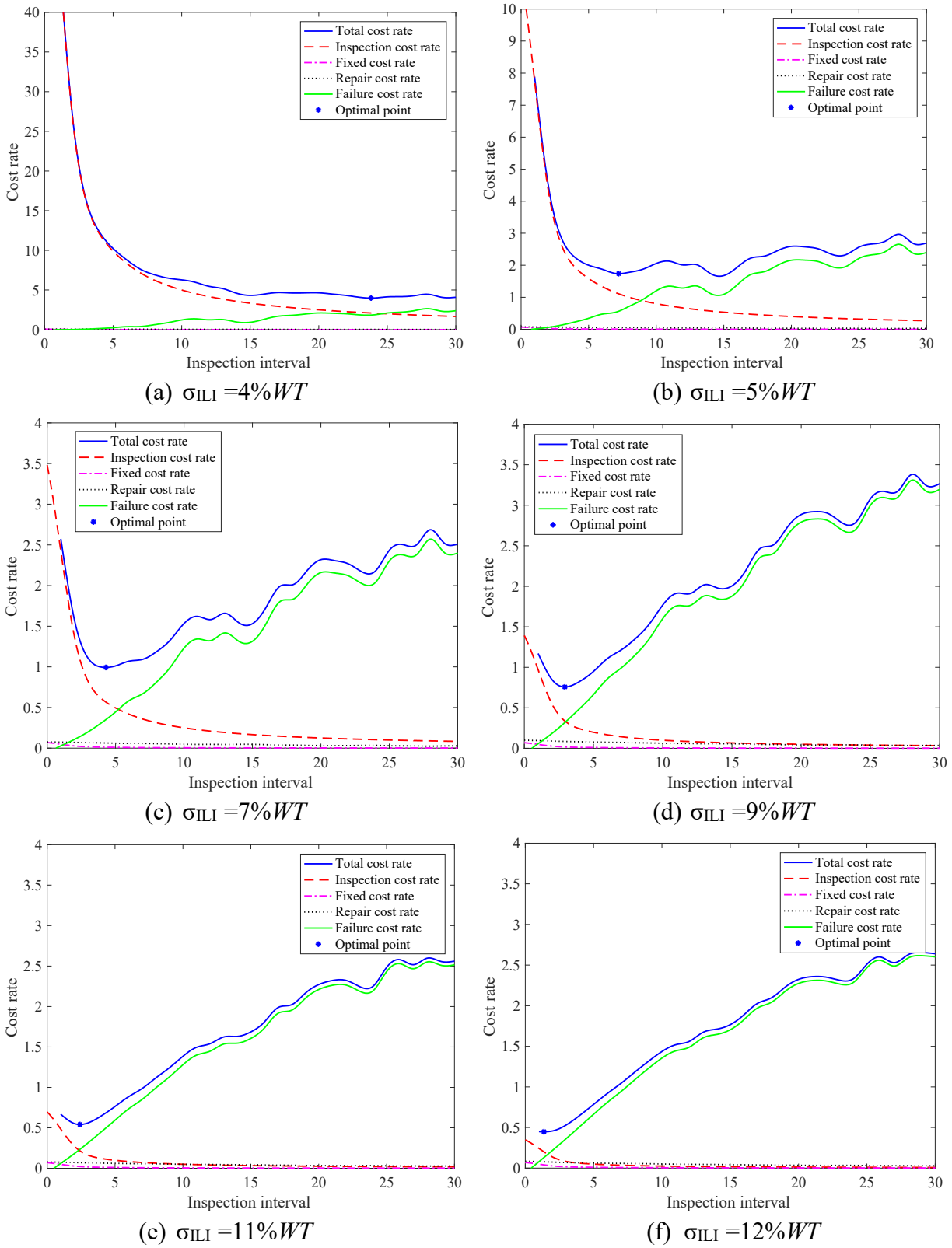

(a) σ_{ILI} =4%WT (b) σ_{ILI} =5%WT

(c) σ_{ILI} =7%WT (d) σ_{ILI} =9%WT

(e) σ_{ILI} =11%WT (f) σ_{ILI} =12%WT

Figure 5.13 Comparison of the expected cost rates associated with different cost items (Case 4)

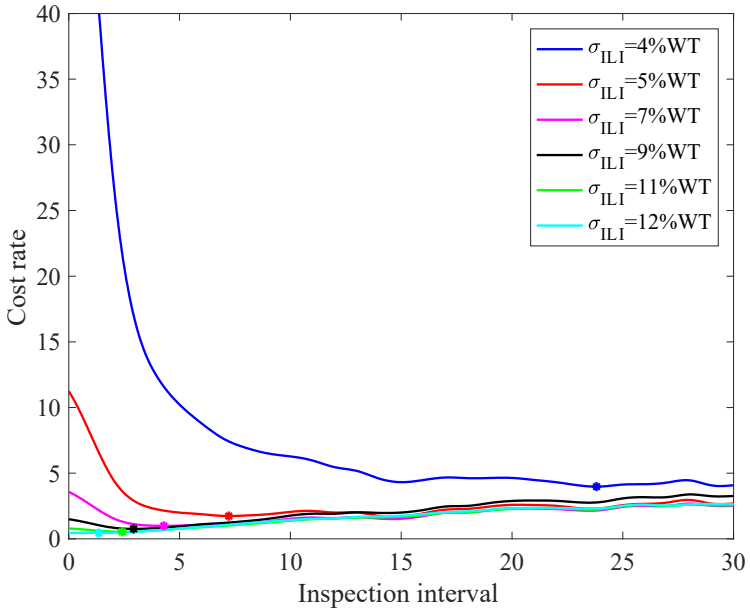

Figure 5.14 Comparison of the expected total cost rates associated with different standard deviations of measurement error of ILI tools (Case 4)

The shapes of curves for the last case are shown in Figure 5.15. Overall, the total cost rates decrease before the optimal points and fluctuate a bit after those points. The comparison results shown in Table 5.13 indicate that a higher σ_{ILI} gives a bigger total cost rate. And a higher σ_{ILI} gives a smaller inspection interval correspondingly. We can see from this table that a relatively small increment in optimal inspection interval gives a large increment in total cost rate. This is mainly because of the consideration of discount rate. Figure 5.16 shows the comparison of expected total cost rates associated with σ_{ILI}. As reflected in Figure 5.16, a higher σ_{ILI} gives a higher total cost rate. This is mainly attributed to that a higher σ_{ILI} leads to a higher failure probability and failure cost rate affects the total cost rate a lot, and therefore a higher failure cost rate and total cost rate.

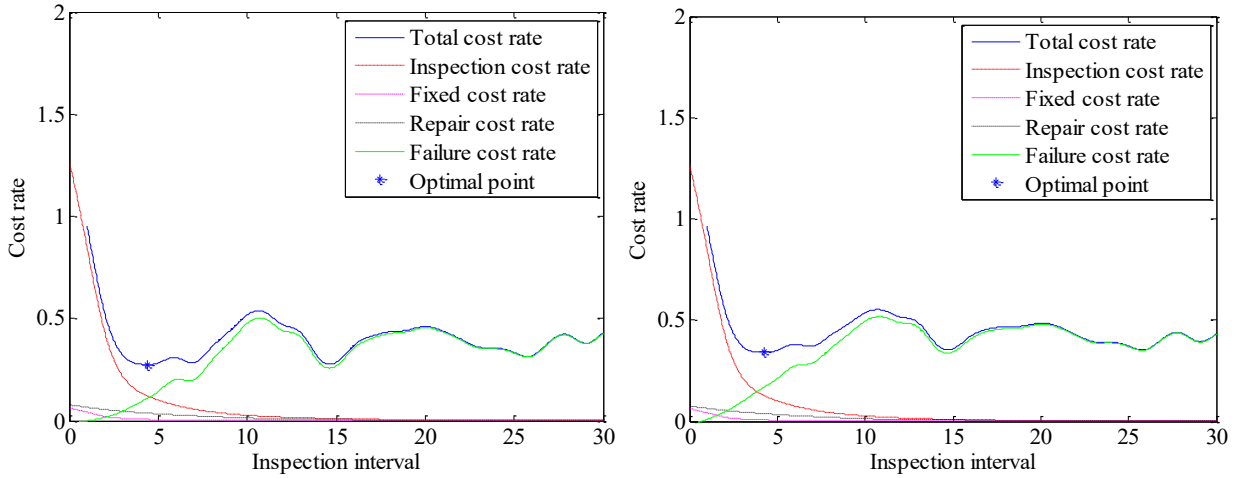

(a) σ_{ILI} =4%WT (b) σ_{ILI} =5%WT

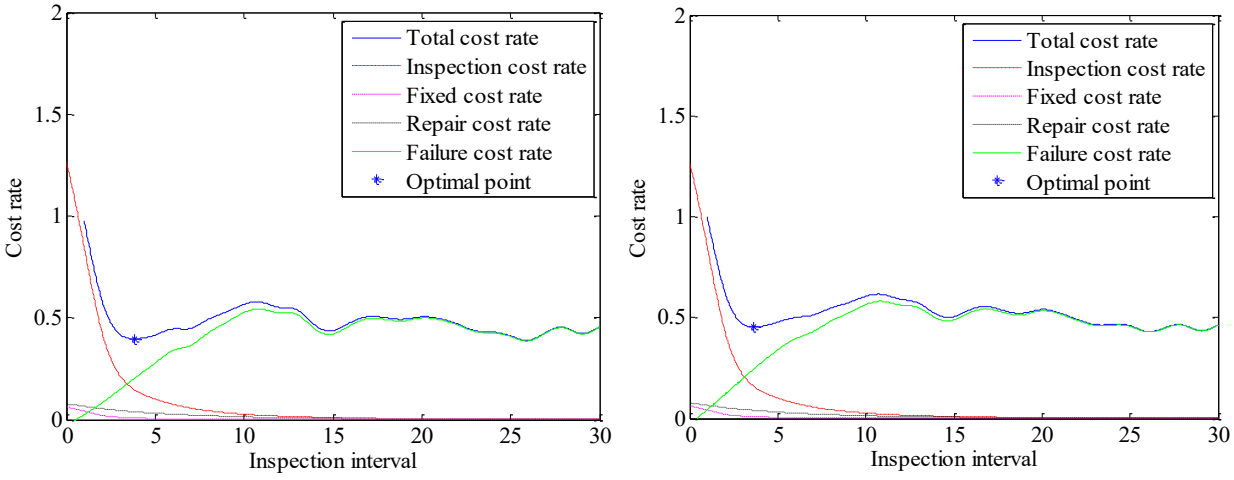

(c) σ_{ILI} =7%WT (d) σ_{ILI} =9%WT

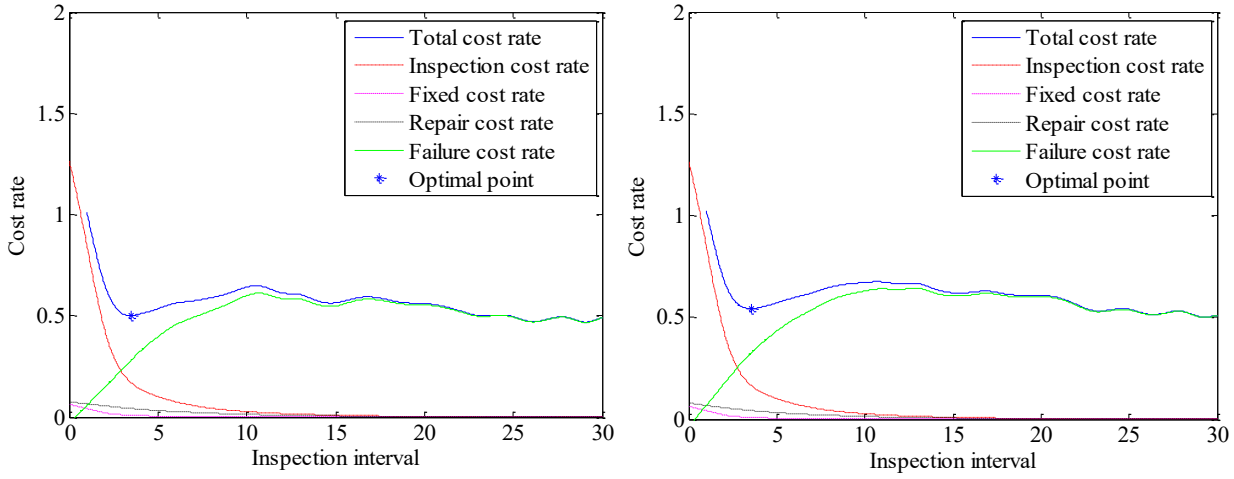

(e) σ_{ILI} =11%WT (f) σ_{ILI} =12%WT

Figure 5.15 Comparison of the expected cost rates associated with different cost items (Case 5)

Table 5.13 Comparison of optimal solutions with different standard deviations (Case 5)

ILI tool accuracy, σ_{ILI} (%*WT*)	Optimal inspection interval	Total cost rate
4%	20.9171	0.0021
5%	20.7593	0.0022
7%	20.5282	0.0025
9%	18.9630	0.0031
11%	18.0679	0.0094
12%	17.9984	0.0424

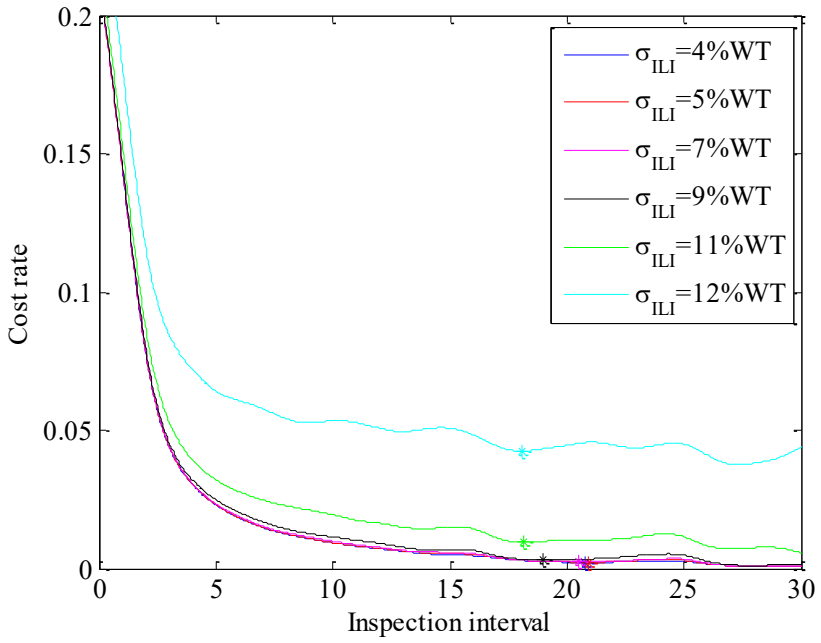

Figure 5.16 Comparison of the expected total cost rates associated with different standard deviations of measurement error of ILI tools (Case 5)

Figure 5.17 shows the effect of pressure and failure cost on the results with σ_{ILI} =9%*WT*. The total cost rates increase as the pressure increase, and so does the failure cost. The optimal points move to the left as these parameters increase. This can be explained by that a higher pressure leads to a higher probability of failure with the same inspection interval. And a higher failure cost directly affects failure cost rate and total cost rate. Therefore, there is a positive correlation between the increase in these parameters and the increase in total cost rate.

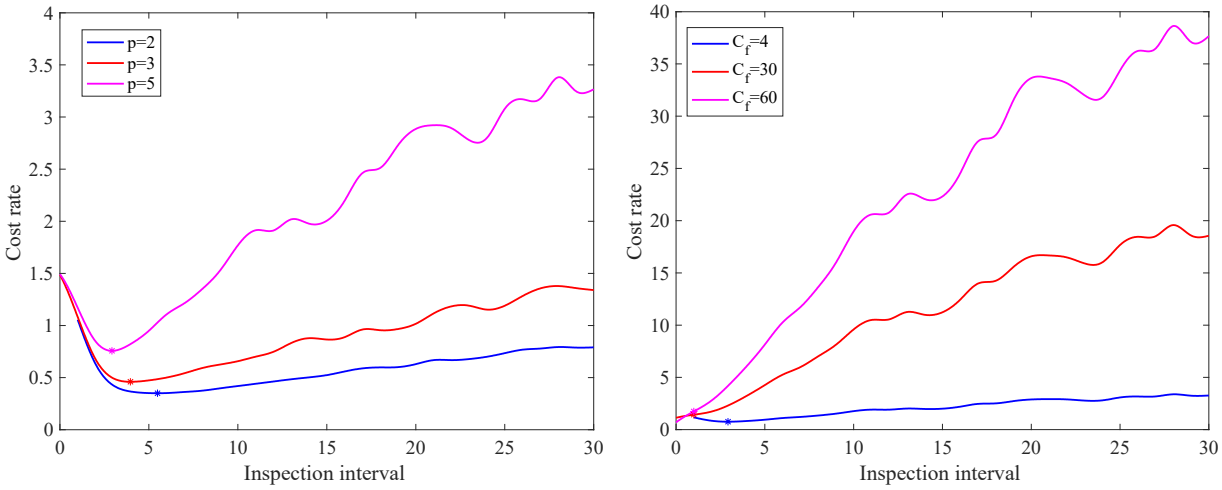

(a) Pressure (b) Failure cost

Figure 5.17 Expected total cost rate vs the inspection interval in term of pressure and failure cost

5.7 Investigation on the total cost rate with different prediction accuracies

In general, we can expect less downtime and failure with a more advanced prediction model. This could lead to a potential cost-saving benefit with less failure cost. And if we have the perfect

inspection tool and prediction model, we would have no prediction error in this ideal case. Researchers and engineers try to improve the prediction accuracy, and that would lead to less failure and a potential more cost-effective integrity program.

In chapter 3, the prediction accuracy for pipelines with crack defects is improved by using the proposed integrated method. It is also important that we investigate the impact of the prediction accuracy on the total cost rate. The prediction accuracy can be improved by improving the ILI tool accuracy and/or the model accuracy. In this chapter, the total cost rate decreases with the increase of ILI tool accuracy. As for the model accuracy, we use the standard deviation of model parameter *m* as prediction error to quantify the cost-saving benefits with improved prediction accuracy. This can be achieved because we have proved that a smaller standard deviation of *m* leads to a more accurate RUL prediction in chapter 3.

Table 5.14 Comparison of optimal solutions with different standard deviations of parameter *m*

Standard deviation of parameter *m*, σ_m	Optimal inspection interval	Total cost rate
0.1	2.7585	0.8149
0.05	3.2213	0.5222
0.01	3.5582	0.4632
0	3.6021	0.4472

Four σ_m are used to represent the prediction accuracy and they are 0.1, 0.05, 0.01, and 0 respectively. The results of the investigation on different σ_m are shown in Table 5.14 and Figure 5.18. Table 5.14 suggests that the optimal inspection interval increases and the total cost rate decreases as σ_m decreases. And this indicates that a reduced prediction error leads to a less total

cost rate as expected. Figure 5.18 gives the comparison of cost rate items associated with σ_m. We can find that the failure cost and inspection cost rates contribute most to the total cost rate. The inspection cost rate curves are exactly the same for different σ_m. As for failure cost rate, it increases with a bigger σ_m, and finally leads to a bigger total cost rate.

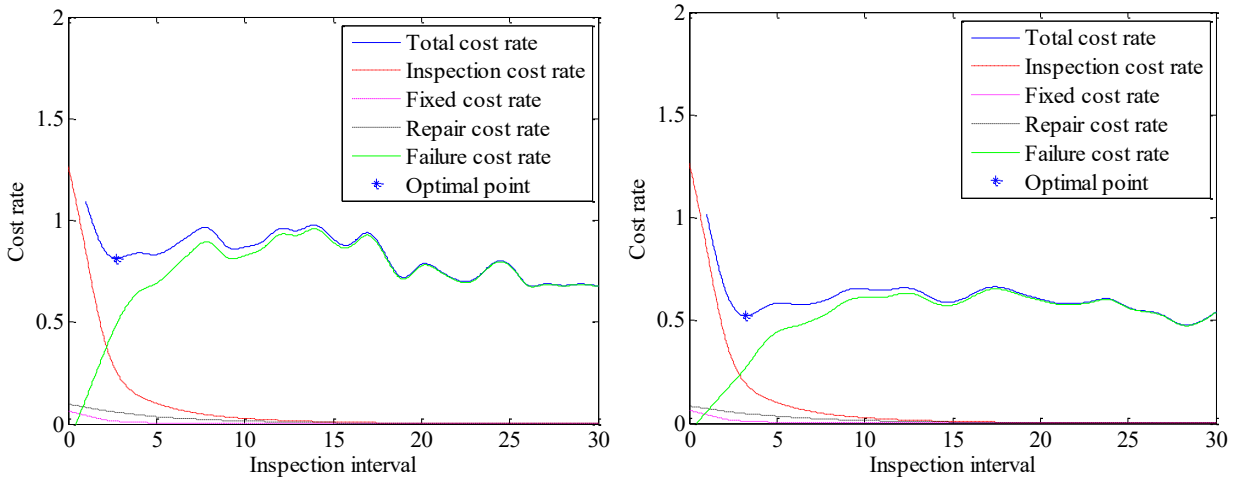

(a) $\sigma_m = 0.1$ (b) $\sigma_m = 0.05$

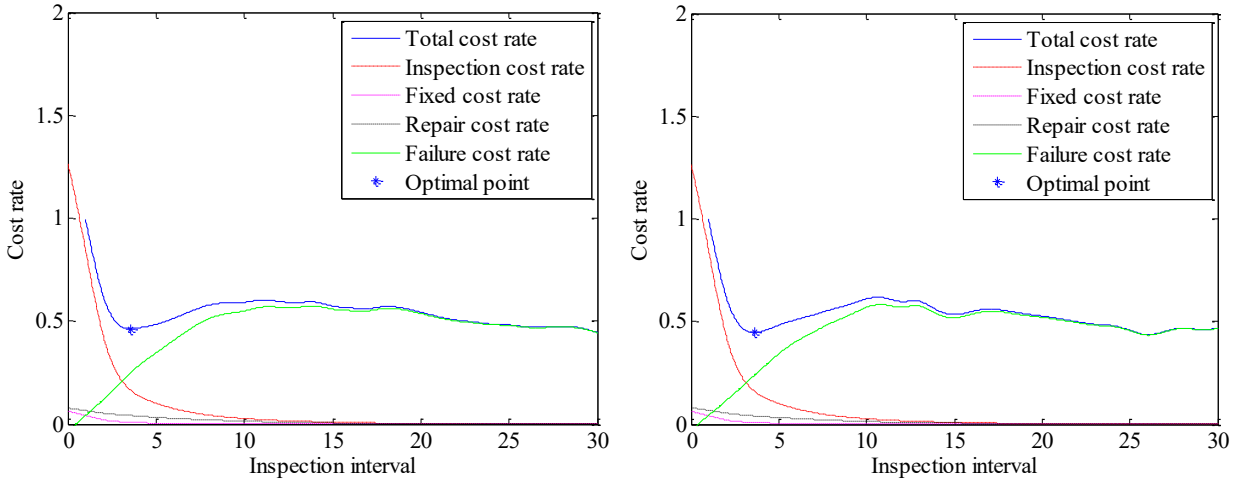

(c) $\sigma_m = 0.01$ (d) $\sigma_m = 0$

Figure 5.18 Comparison of the expected cost rates associated with different cost items (different σ_m)

Figure 5.19 shows the comparison of expected total cost rates associated with σ_m. Overall, a higher σ_m gives a higher total cost rate when the inspection interval remains the same. The curve for σ_m=0.01 is very close to the no prediction error case (σ_m=0). And a relatively small reduction of prediction error from σ_m=0.1 to 0.05 affects the total cost rate results a lot.

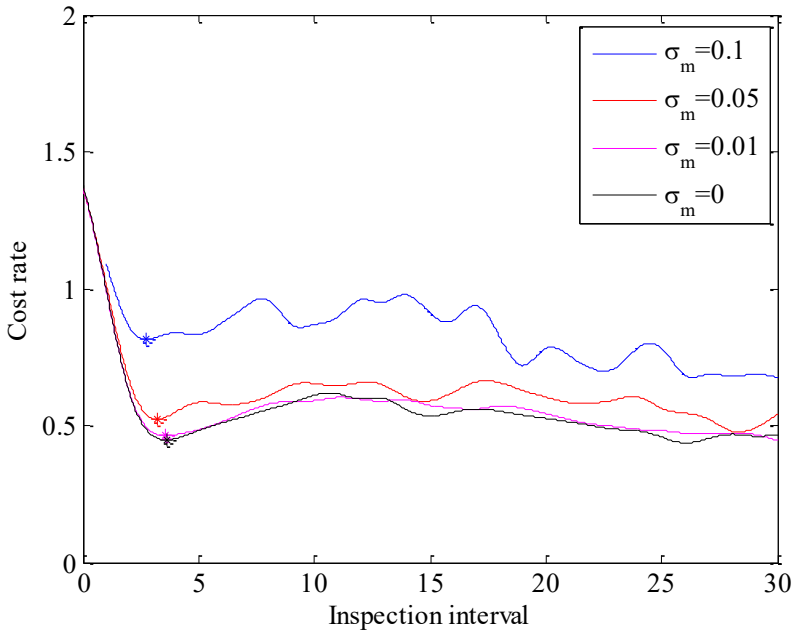

Figure 5.19 Expected total cost rate vs the inspection interval in term of σ_m

5.8 Conclusions

In this chapter, a reliability assessment study was completed for pipelines with single and multiple crack defects. A method was presented for analyzing the impact of ILI tool accuracy on integrity planning for pipelines with crack defects through two aspects, pipeline reliability as measured by PoF (Probability of Failure) and integrity costs (as determined by a Total cost rate). The Monte Carlo simulation technique was employed to evaluate the cost rates. Besides, we investigated the

impact of ILI tool accuracy on long-term cost rate. The crack defect generation mechanism was introduced instead of a fixed number of crack defects. The non-homogeneous Poisson process and the probability of detection were considered to evaluate the long-term total cost rate. Five cases with different input parameters including pressure, failure cost and inspection costs assumption were considered for long-term cost rates evaluation. The optimal inspection intervals and the corresponding total cost rates for different tool accuracies and different input parameters were then obtained and compared.

The examples and case studies in this chapter investigated the impact of ILI tool accuracy and initial crack size including the consideration of when to perform a next tool run after an initial run. The impact of ILI tool accuracy on integrity program costs for pipelines with crack defects, was presented with different assumptions particularly on inspection cost rate factors. The comparison results of different ILI tool accuracies on long-term cost rates were investigated. Furthermore, the comparison results among different cases were also discussed. The following conclusions can be drawn based on the studies:

(1) The time to perform the next tool run increased with a more accurate ILI tool for a pipeline with single or multiple crack defects. And it decreased with a higher initial crack depth for pipeline with a single crack defect.

(2) Relatively small improvements in relative ILI accuracy (tolerance) can greatly improve the cost-effectiveness of an integrity program.

(3) The assumption of the relationship between inspection cost and ILI tool accuracy affects the inspection and total cost rates, yet with lower total cost rates for higher accuracy ILI inspection are achieved, even at higher cost assumptions.

(4) The use and selection of a non-zero discounted cash rate was also prominent in the future cost evaluation results

(5) Cost rates were influenced by the relative levels of ILI accuracy, actual absolute pipe wall thickness and timeline to reach repair condition criteria.

(6) For Cases 1, 2, 3 and 5 discussed in Section 5.6, a higher σ_{ILI} leads to a lower optimal inspection interval and a bigger total cost rate with a few exceptions.

(7) For Case 4 discussed in Section 5.6, a higher σ_{ILI} leads to a lower optimal inspection interval and a lower total cost rate. This means that the inspection cost assumption greatly affects the trends of results regarding different σ_{ILI}.

(8) The total cost rates increase as the pressure or failure cost increases if we keep other parameters unchanged. The optimal inspection intervals decrease as these parameters increase.

(9) The total cost rates decrease as the prediction accuracy of a pipeline integrity program increases.

6 Conclusions and future work

In recent years, remaining useful life prediction and risk analysis has attracted great attention to the management of public safety and financial risks in the pipeline industry. The purposes of this thesis are to develop more accurate RUL prognostics methods and to establish more effective RBIM models for pipelines that address reliability targets for the safe operation of pipelines while also addressing life-cycle costs in common financial terms. There is a great value to keep making huge efforts in the area of pipeline integrity management. In this chapter, we conclude the study in the thesis, and suggest several potential works in the future.

6.1 Conclusions

Integrity has been the top priority for the pipeline industry, and plays a critical role for the oil and gas industry as a whole. Significant advances are needed in pipeline integrity management to develop more effective methods, models and technologies to accurately monitor and predict pipeline conditions, extend the lifetimes of pipelines and prevent potential ruptures and the resulting consequences. In this thesis, three main steps of a pipeline integrity program have been discussed. Key ILI techniques along with their performance and applications have been reviewed. Data-driven methods and physics-based model for predicting pipeline defect growth have been discussed in details. Risk-based inspection and maintenance methods and models have also been presented. In-line inspection, defect prediction and risk-based planning, which are three main steps of pipeline integrity management, actually form a closed loop. Plan, schedule, execute, analyze

and improve are the elements of the loop of the activities need to be performed to manage pipeline integrity.

The main objectives of pipeline integrity management are listed as follows:

(a) Identify and assess defects and threats to safety in the design, construction and operation of pipelines.

(b) Ensure the safety of the population, prevent failures that could cause damages to the surrounding environment.

(c) Allocate available resources to pipeline integrity activities such as inspection and maintenance as efficient and effective as possible.

(d) Reduce high costs, high risks and unnecessary shutdown while ensuring the system reliability reaches a suitable level and complying with regulatory codes.

In conclusion, this research work makes significant contributions to pipeline integrity management. This thesis aims to improve the prognostics accuracy and cost-effectiveness of a pipeline integrity program. The contributions for the proposed three topics of this thesis are summarized as follows.

(1) An integrated prognostics approach for pipeline fatigue crack growth prediction utilizing ILI data

Currently, there are large measurement uncertainties in the existing ILI crack detection tools. The fixed model parameters are used for the current physics-based prognostics methods for pipelines with fatigue cracks. They result in uncertainty that is managed through the use of conservative safety factors such as adding depth uncertainty to the measured depth in deciding integrity management and risk mitigation strategies. In this thesis, an integrated approach is proposed for

pipeline fatigue crack growth prediction utilizing ILI data including consideration of crack depth measurement uncertainty. This approach is done by integrating the physical models, including the stress analysis models, the crack growth model, and the ILI data. The finite element (FE) model of a cracked pipe is built to obtain SIF. ILI data is utilized to update the model parameter so that a more accurate pipeline RUL prediction can be achieved. Time-varying loading conditions are considered in the proposed integrated method by using rainflow counting method. The proposed integrated prognostics approach is compared with the existing physics-based method using examples based on simulated data. Field data provided by a Canadian pipeline operator is also employed for the validation of the proposed method. The examples and case studies in this topic demonstrate the limitations of the existing physics-based method, and the promise of the proposed method for achieving accurate fatigue crack growth prediction as continuous improvement of ILI technologies further reduce ILI measurement uncertainty.

(2) Risk-based pipeline re-assessment optimization considering corrosion defects

Inspections or assessments are performed periodically to assess the health conditions of pipelines. Existing methods for determining the optimal inspection interval mainly used constant fixed re-assessment interval as the decision variable during the whole service. However, pipelines with different defect sizes at the current inspection point lead to different future defect growth and failure probability, and it is more reasonable to apply different re-assessment intervals depending on pipeline health conditions. This thesis proposes a method to find the optimal re-assessment intervals for pipelines with corrosion defects. The PoF threshold is used as the decision variable for this optimization problem. An accurate and realistic prediction is achieved by considering uncertainties from various sources. A simulation-based cost evaluation approach is developed for

a given re-assessment policy defined by the PoF threshold. First-order reliability method is used to improve the calculation efficiency. Examples are given to demonstrate the proposed approach, and sensitivity studies are performed. The results show that the proposed method performs better than the fixed interval methods.

(3) A method to analyze the impact of in-line inspection on integrity planning of pipelines with cracks

An efficient and effective integrity planning method can address the most significant risk and optimize operational and maintenance costs. In this thesis, a method is presented for analyzing the impact of ILI tool accuracy on integrity planning for pipelines for fatigue cracks. Crack inspection and threat of fatigue cracking was used as the working case for the analysis although the approach could potentially be used for any pipeline threat type. The proposed method is based on a Monte Carlo simulation framework. And initial crack defect size and ILI measurement errors are used as input random variables for this method.

The integrity (severity) assessment of the crack population scenarios used the CorLAS^{TM} burst pressure model and the Paris' law crack growth model. The subsequent pipeline reliability assessments also considered single and multiple cracks scenarios. Using a reliability / probability of failure (PoF) approach, the impact of ILI tool accuracy and initial crack size on when to set reinspection and re-assessment intervals was investigated.

Furthermore, integrity program cost scenarios for pipeline integrity programs with multiple cracks was also evaluated with respect to different (crack) populations, pipe conditions and ILI accuracies. A sensitivity analysis was performed considering different inspection costs, maintenance costs and relative crack severity for pipelines with financial metrics. Various

scenarios were discussed regarding maintenance and inspection planning and a “total cost rate” for different situations.

The impact of ILI tool accuracy on long-term cost rate was also investigated considering new defect generation and continuous growth. The non-homogeneous Poisson process was employed to generate new crack defects, and probability of detection was also considered in cost evaluation. Examples were used to investigate the effect of ILI tool accuracy considering different input parameters such as pressure, failure cost and inspection costs assumption. The optimal inspection intervals and the corresponding total cost rates with respect to different ILI tool accuracies and different input parameters were obtained and compared. The proposed method can support integrity management program planning by linking risks with integrity plan costs associated with ILI accuracies, and optimal re-assessment intervals.

6.2 Future work

In-line inspection sensor technologies and pipeline integrity practices must continue to evolve, especially for crack detection tools. More reliable and effective signal processing and data analysis methods need to be developed for noise removal in ILI data and accurate defect evaluation. Prognostics approaches and models need to be further improved. Balancing the ILI tool run times with costs also need to be further investigated. Different pipeline integrity management frameworks need to be further developed regarding different types of defects. Effective validation methods and technologies also need to be established. Specifically, with standing on my current research stage, the following research directions need to be further investigated in pipeline integrity management.

(1) Pipeline system assessment

Pipeline integrity management can also be performed on a large scale, i.e. pipeline system. In industry, corrosion and crack defects can occur in a pipeline system at the same time. The interaction of different types of defects will be considered in the pipeline system assessment. Existing qualitative and quantitative risk analysis methods for pipeline system will be studied. A method for risk and reliability assessment of the pipeline system will be proposed considering the condition monitoring data and structure of the pipeline system. Risk-cost optimization of pipeline system will be investigated.

The aim of the topic is to develop a common scientific methodology for the assessment of reliability, costs and risks of the pipeline systems. First, we need to assess in terms of likelihood and consequence all reasonably expected hazards to public safety and environment. Then, we will identify the major failure mechanisms and study and assess different types of defects based on the first three topics. Finally, an optimized and cost-effective inspection plan will be established to ensure the integrity of pipeline system. In addition, sensitivity analysis will also be performed for different threats (such as corrosion, crack, third party damage, etc.) to the pipeline system. Group inspection and maintenance activities will be considered in the proposed pipeline system assessment framework since it has the potential to reduce the inspection and maintenance costs and service interruptions. In cost evaluation, we need to consider the dependency on the costs of dealing with multiple defects and multiple pipe segments, and plan to deal with this challenge based on condition-based models developed for multi-component systems. The performance of this proposed idea will be compared with the performance of the existing methods. The method proposed in this topic will be ready to be used in practical activities.

(2) RUL prediction and RBIM for pipelines with crack defects under big shocks

In this thesis, RUL prediction and RBIM are performed for pipelines with crack defects under normal operational condition. Even with the consideration of varying internal pressure, the overall assumption is that the pipeline does not suffer big shocks from outside. The aim of this topic is to make RUL prediction and to present an assessment of risk for pipelines with crack defects posed by dropped objects. The research on the impact of big shocks on RUL prediction and RBIM for pipelines will be conducted in future work.

(3) Risk-based management for pipelines with crack defects considering multiple uncertainty sources

In Section 5, we only considered two important random variables, the population of initial crack depths and ILI tool measurement error. However, in reality, the model parameters for Paris' law, the mechanical properties and geometry parameters for pipelines keep changing all the time. The uncertainties from these sources will be considered to make a better decision on when to reinspection and re-assessment. The life cycle cost results will be compared with Section 5. Sensitivity analysis will be performed on these important parameters.

References

[1] M. Xie and Z. Tian, "A review on pipeline integrity management utilizing in-line inspection data," *Eng. Fail. Anal.*, vol. 92, pp. 222–239, Oct. 2018.

[2] M. Xie, S. Bott, A. Sutton, A. Nemeth, and Z. Tian, "An integrated prognostics approach for pipeline fatigue crack growth prediction utilizing inline inspection data," *J. Press. Vessel Technol.*, vol. 140, no. 3, p. 031702, 2018.

[3] M. Xie and Z. Tian, "Risk-based pipeline re-assessment optimization considering corrosion defects," *Sustain. Cities Soc.*, vol. 38, pp. 746–757, 2018.

[4] M. Xie, Z. Tian, J. Sutherland, B. Fang, and B. Gu, "A Method to Analyze the Impact of Inline Inspection Accuracy on Integrity Management Program Planning of Pipelines," in *2018 12th International Pipeline Conference*, 2018, p. V001T03A051–V001T03A051.

[5] Z. Tian, "An artificial neural network method for remaining useful life prediction of equipment subject to condition monitoring," *J. INTELLIGENT Manuf.*, vol. 23, no. 2, SI, pp. 227–237, Apr. 2012.

[6] M. Mohitpour, A. Murray, M. McManus, and I. Colquhoun, *Pipeline Integrity Assurance: A Practical Approach*. New York: American Society of Mechanical Engineers, 2010.

[7] M. Zarea, M. Piazza, G. Vignal, C. Jones, J. Rau, and R. Wang, "Review of R&D In support of mechanical damage threat management in onshore transmission pipeline operations," in *Proceedings of the 9th International Pipeline Conference, 2012, vol. 2*, New York, USA, 2013, pp. 569–582.

[8] Pipeline Research Council International, *Year in Review*. 2014.

[9] K. Reber, M. Beller, and A. O. Barbian, "Run Comparisons: Using in-line Inspection Data for the Assessment of Pipelines," p. 8, 2006.

[10] A. C. Palmer and R. A. King, *Subsea pipeline engineering*. PennWell Books, 2004.

[11] G. A. Antaki, *Piping and pipeline engineering: design, construction, maintenance, integrity, and repair*. CRC Press, 2003.

[12] Y. Bai and Q. Bai, "Chapter 11 - LCC Modeling for Pipeline Design," in *Subsea Pipeline Integrity and Risk Management*, Boston: Gulf Professional Publishing, 2014, pp. 247–270.

[13] A. Nielsen, J. Mallet-Paret, and K. Griffin, "Probabilistic modeling of crack threats and the effects of mitigation," in *Proceedings of the Biennial International Pipeline Conference*, 2014, vol. 3.

[14] A. Sutton, Y. Hubert, S. Textor, and S. Haider, "Allowable pressure cycling limits for liquid pipelines," in *Proceedings of the Biennial International Pipeline Conference, IPC*, 2014, vol. 2.

[15] A. K. S. Jardine, D. Lin, and D. Banjevic, "A review on machinery diagnostics and prognostics implementing condition-based maintenance," *Mech. Syst. Signal Process.*, vol. 20, no. 7, pp. 1483–1510, Oct. 2006.

[16] S. Dresie, “Implementing an Integrated Pipeline Integrity Management System (PIMS): Case Study,” in *2012 9th International Pipeline Conference*, 2012, pp. 283–292.

[17] V. Semiga, S. Tiku, and A. Dinovitzer, “Pipeline Mechanical Damage Integrity Management Framework,” in *2012 9th International Pipeline Conference*, 2012, pp. 445–452.

[18] M. R. Shaik, “Pipeline Integrity Assessment: Methodology,” in *ASME 2015 India International Oil and Gas Pipeline Conference*, 2015, p. V001T03A001–V001T03A001.

[19] F. I. Khan, M. M. Haddara, and S. K. Bhattacharya, “Risk-Based Integrity and Inspection Modeling (RBIIM) of Process Components/System,” *Risk Anal.*, vol. 26, no. 1, pp. 203–221, Feb. 2006.

[20] C. R. Alexander, “Evaluating damaged subsea pipelines using an engineering-based integrity management program,” in *ASME International Offshore Pipeline Forum, Houston, TX, ASME Paper No. IOPF2009-6002*, 2009.

[21] C. A. Paul, “Managing integrity programmes in a litigious society.,” *J. Pipeline Eng.*, vol. 7, no. 1, 2008.

[22] A. P. I. Standard, “1160 Managing System Integrity for Hazardous Liquid Pipelines,” *Firs Ed. Novemb.*, 2001.

[23] F. Varela, M. Yongjun Tan, and M. Forsyth, “An overview of major methods for inspecting and monitoring external corrosion of on-shore transportation pipelines,” *Corros. Eng. Sci. Technol.*, vol. 50, no. 3, pp. 226–235, May 2015.

[24] L. Manian and A. Hodgdon, “Pipeline integrity assessment and management,” *Mater. Perform.*, vol. 44, no. 2, pp. 18–22, 2005.

[25] L. G. Rankin, “Pipeline integrity information integration,” *Mater. Perform.*, vol. 43, no. 6, pp. 56–60, 2004.

[26] A. Young and A. Lockey, “The assessment of pipeline integrity in geohazard areas using ILI data,” in *ASME 2013 International Pipeline Geotechnical Conference*, 2013, p. V001T02A008–V001T02A008.

[27] J. R. Walker, P. Mallaburn, and D. Balmer, “Inline Inspection: Both Effective Data Collection and Interpretation Needed to Achieve High Quality Reporting Results,” in *2010 8th International Pipeline Conference*, 2010, pp. 187–196.

[28] L. Cartz, *Nondestructive testing: radiography, ultrasonics, liquid penetrant, magnetic particle, eddy current*. Materials Park, OH: ASM International, 1995.

[29] N. B. S. Gloria, M. C. L. Areiza, I. V. J. Miranda, and J. M. A. Rebello, “Development of a magnetic sensor for detection and sizing of internal pipeline corrosion defects,” *NDT E Int.*, vol. 42, no. 8, pp. 669–677, Dec. 2009.

[30] R. C. Ireland and C. R. Torres, “Finite element modelling of a circumferential magnetiser,” *Sens. Actuators Phys.*, vol. 129, no. 1–2, pp. 197–202, May 2006.

[31] G. Kopp and H. Willems, “Sizing limits of metal loss anomalies using tri-axial MFL measurements: A model study,” *NDT E Int.*, vol. 55, pp. 75–81, Apr. 2013.

[32] P. Yeung, R. Sporns, S. Clouston, G. A. Coleman, S. Miller, and C. Mieila, “Maximizing MFL ILI Sizing Confidence and Accuracy Using High-Resolution Field Measurement Data,” in *2012 9th International Pipeline Conference*, 2012, pp. 217–227.

[33] S. Miller and S. Clouston, “Optimizing magnetic fluxleakage inspection sizing model performance using highresolution non-destructive examination data.,” *J. Pipeline Eng.*, vol. 11, no. 2, 2012.

[34] B. Mao, Y. Lu, P. Wu, B. Mao, and P. Li, “Signal processing and defect analysis of pipeline inspection applying magnetic flux leakage methods,” *Intell. Serv. Robot.*, vol. 7, no. 4, pp. 203–209, Oct. 2014.

[35] S. Saha, S. Mukhopadhyay, U. Mahapatra, S. Bhattacharya, and G. P. Srivastava, “Empirical structure for characterizing metal loss defects from radial magnetic flux leakage signal,” *NDT E Int.*, vol. 43, no. 6, pp. 507–512, Sep. 2010.

[36] S. Kathirmani, A. K. Tangirala, S. Saha, and S. Mukhopadhyay, “Online data compression of MFL signals for pipeline inspection,” *NDT E Int.*, vol. 50, pp. 1–9, Sep. 2012.

[37] A. Joshi, L. Udpa, S. Udpa, and A. Tamburrino, “Adaptive Wavelets for Characterizing Magnetic Flux Leakage Signals From Pipeline Inspection,” *IEEE Trans. Magn.*, vol. 42, no. 10, pp. 3168–3170, Oct. 2006.

[38] M. Afzal and S. Udpa, “Advanced signal processing of magnetic flux leakage data obtained from seamless gas pipeline,” *NDT E Int.*, vol. 35, no. 7, pp. 449–457, Oct. 2002.

[39] Fengzhu Ji, Shiyu Sun, Changlong Wang, Haipeng Zhang, and Dongyan Liu, “Applications of adaptive fuzzy lifting wavelet transform in MFL signal processing,” *Insight Non-Destr. Test. Cond. Monit.*, vol. 52, no. 1, pp. 16–19, Jan. 2010.

[40] A. A. Carvalho, J. M. A. Rebello, L. V. S. Sagrilo, C. S. Camerini, and I. V. J. Miranda, “MFL signals and artificial neural networks applied to detection and classification of pipe weld defects,” *NDT E Int.*, vol. 39, no. 8, pp. 661–667, Dec. 2006.

[41] L. Chen, X. Li, G. Qin, and Q. Lu, “Signal processing of magnetic flux leakage surface flaw inspect in pipeline steel,” *Russ. J. Nondestruct. Test.*, vol. 44, no. 12, pp. 859–867, Dec. 2008.

[42] D. Mukherjee, S. Saha, and S. Mukhopadhyay, “An adaptive channel equalization algorithm for MFL signal,” *NDT E Int.*, vol. 45, no. 1, pp. 111–119, Jan. 2012.

[43] F. Caleyo, L. Alfonso, J. H. Espina-Hernández, and J. M. Hallen, “Criteria for performance assessment and calibration of in-line inspections of oil and gas pipelines,” *Meas. Sci. Technol.*, vol. 18, no. 7, pp. 1787–1799, Jul. 2007.

[44] H. Goedecke, “Ultrasonic or MFL inspection: Which technology is better for you,” *Pipeline Gas J.*, vol. 230, no. 10, pp. 34–41, 2003.

[45] H. Lei, Z. Huang, W. Liang, Y. Mao, and P. W. Que, “Ultrasonic pig for submarine oil pipeline corrosion inspection,” *Russ. J. Nondestruct. Test.*, vol. 45, no. 4, pp. 285–291, Apr. 2009.

[46] T. Hennig and G. Lokwani, “Latest Generation of ILI Tools for High Resolution Ultrasonic Inspection and Integrity Assessment,” in *ASME 2015 India International Oil and Gas Pipeline Conference*, 2015, p. V001T03A002–V001T03A002.

[47] T. Hrncir *et al.*, “A case study of the crack sizing performance of the ultrasonic phased array combined crack and wall loss inspection tool on the centennial pipeline, the defect evaluation, including the defect evaluation, field feature verification and tool performance validation (performed by Marathon Oil, DNV and GE Oil & Gas),” in *2010 8th International Pipeline Conference*, 2010, pp. 137–143.

[48] Y. Ying *et al.*, “Toward Data-Driven Structural Health Monitoring: Application of Machine Learning and Signal Processing to Damage Detection,” *J. Comput. Civ. Eng.*, vol. 27, no. 6, pp. 667–680, 2013.

[49] D. Bo, Z. Huiping, S. Sha, D. Jinxi, X. Zurong, and T. Dongliang, “An Ultrasonic In-line Inspection System on Crude Oil Pipelines,” in *2007 Chinese Control Conference*, 2007, pp. 199–203.

[50] S. Song and P. Que, “Wavelet based noise suppression technique and its application to ultrasonic flaw detection,” *Ultrasonics*, vol. 44, no. 2, pp. 188–193, 2006.

[51] L. Angrisani and P. Daponte, “Thin thickness measurements by means of a wavelet transform-based method,” *Measurement*, vol. 20, no. 4, pp. 227–242, 1997.

[52] F. W. Margrave, K. Rigas, D. A. Bradley, and P. Barrowcliffe, “The use of neural networks in ultrasonic flaw detection,” *Measurement*, vol. 25, no. 2, pp. 143–154, 1999.

[53] T. Chen, P. Que, and Q. Liu, “Pipeline defects diagnosis based on feature extraction and neural-network fusion,” *Russ. J. Nondestruct. Test.*, vol. 42, no. 5, pp. 340–344, 2006.

[54] O. Martinez, M. Parrilla, M. A. G. Izquierdo, and L. G. Ullate, “Application of digital signal processing techniques to synthetic aperture focusing technique images,” *Sens. Actuators Phys.*, vol. 76, no. 1–3, pp. 448–456, Aug. 1999.

[55] H. Ravanbod, “Application of neuro-fuzzy techniques in oil pipeline ultrasonic nondestructive testing,” *NDT E Int.*, vol. 38, no. 8, pp. 643–653, Dec. 2005.

[56] H. Ravanbod and A. Jalali, “Configurable ultrasonic flaw classification of oil pipelines: Part I: image acquisition, preprocessing and flaw area and volume estimation,” *Nondestruct. Test. Eval.*, vol. 23, no. 1, pp. 43–55, Mar. 2008.

[57] B. Shakibi, F. Honarvar, M. D. C. Moles, J. Caldwell, and A. N. Sinclair, “Resolution enhancement of ultrasonic defect signals for crack sizing,” *NDT E Int.*, vol. 52, pp. 37–50, Nov. 2012.

[58] F. Cau, A. Fanni, A. Montisci, P. Testoni, and M. Usai, “Artificial neural networks for non-destructive evaluation with ultrasonic waves in not accessible pipes,” in *Fourtieth IAS Annual Meeting. Conference Record of the 2005 Industry Applications Conference, 2005.*, 2005, vol. 1, pp. 685-692 Vol. 1.

[59] F. Cau, A. Fanni, A. Montisci, P. Testoni, and M. Usai, “A signal-processing tool for non-destructive testing of inaccessible pipes,” *Eng. Appl. Artif. Intell.*, vol. 19, no. 7, pp. 753–760, Oct. 2006.

[60] H. Chen, M. J. Zuo, X. Wang, and M. R. Hoseini, “An adaptive Morlet wavelet filter for time-of-flight estimation in ultrasonic damage assessment,” *Measurement*, vol. 43, no. 4, pp. 570–585, May 2010.

[61] S. Iyer, S. K. Sinha, B. R. Tittmann, and M. K. Pedrick, “Ultrasonic signal processing methods for detection of defects in concrete pipes,” *Autom. Constr.*, vol. 22, pp. 135–148, Mar. 2012.

[62] J. Saniie, E. Oruklu, and S. Yoon, “System-on-chip design for ultrasonic target detection using split-spectrum processing and neural networks,” *IEEE Trans. Ultrason. Ferroelectr. Freq. Control*, vol. 59, no. 7, pp. 1354–1368, Jul. 2012.

[63] R. Murayama, S. Makiyama, M. Kodama, and Y. Taniguchi, “Development of an ultrasonic inspection robot using an electromagnetic acoustic transducer for a Lamb wave and an SH-plate wave,” *Ultrasonics*, vol. 42, no. 1–9, pp. 825–829, Apr. 2004.

[64] H.-J. Salzburger, F. Niese, and G. Dobmann, “Emat Pipe Inspection with Guided Waves,” *Weld. World*, vol. 56, no. 5–6, pp. 35–43, May 2012.

[65] S. Tappert, D. L. Allen, A. Mann, M. Balzer, and G. Van Boven, “Inline Inspection for Cracks in Gas Pipelines: Enhancements Derived From 5 Years’ Operational Experience,” in *2008 7th International Pipeline Conference*, 2008, pp. 161–167.

[66] R. Kania *et al.*, “Validation of EMAT technology for gas pipeline crack inspection,” in *2012 9th International Pipeline Conference*, 2012, pp. 73–77.

[67] M. Hilvert and T. Beuker, “High-Resolution EMAT as a Diagnostic Tool for Analysis of SCC and Crack-Like Pipelines Defects,” p. V001T04A005, Apr. 2015.

[68] M. Hirao and H. Ogi, “An SH-wave EMAT technique for gas pipeline inspection,” *NDT E Int.*, vol. 32, no. 3, pp. 127–132, Apr. 1999.

[69] J. Tucker Raymond W., S. W. Kercel, and V. K. Varma, “Characterization of gas pipeline flaws using wavelet analysis,” 2003, vol. 5132, pp. 485–493.

[70] P. Mazal and Česka Společnost pro Nedestruktivní Testování, Eds., *Defektoskopie 2004: sborník příspěvk°u ; 34. mezinárodní konference, 03. - 05. listopad 2004, Špindler°uv Mlýn, Czech Republic*. Brno: Univ. of Technology, Faculty of Mechanical Engineering, 2004.

[71] J.-H. Lee, S. Han, J. Ahn, D.-H. Kim, and H. Moon, “Two-module robotic pipe inspection system with EMATs,” *ResearchGate*, vol. 13, no. 6, pp. 1041–1063, Jun. 2014.

[72] S. W. Kercel, J. Tucker Raymond W., and V. K. Varma, “Pipeline flaw detection with wavelet packets and GAs,” 2003, vol. 5103, pp. 217–226.

[73] A. O. Bolshakov, J. Zhao, E. J. Domangue, V. S. Dubinsky, and D. J. Patterson, “APPLICATION OF SPECIAL FILTERING TECHNIQUES IN THE ANALYSIS OF EMAT DATA,” in *AIP Conference Proceedings*, 2009, vol. 1096, pp. 596–603.

[74] G. A. Coleman, “Self Excited Eddy Currents for the Detection of SCC,” in *2008 7th International Pipeline Conference*, 2008, pp. 463–469.

[75] M. Mohitpour, *Pipeline integrity assurance : a practical approach /*. New York : ASME, c2010.

[76] H. Wang, A. Yajima, R. Y. Liang, and H. Castaneda, "A Bayesian model framework for calibrating ultrasonic in-line inspection data and estimating actual external corrosion depth in buried pipeline utilizing a clustering technique," *Struct. Saf.*, vol. 54, pp. 19–31, May 2015.

[77] R. McNealy, R. McCann, M. Van Hook, A. Stiff, and R. Kania, "In-Line Inspection Performance III: Effect of In-Ditch Errors in Determining ILI Performance," in *2010 8th International Pipeline Conference*, 2010, pp. 469–473.

[78] G. Desjardins, R. Nickle, and M. Read, "The Pipeline Pigging and Integrity Management Conference," 2007.

[79] R. G. Mora, A. Murray, J. Paviglianiti, and S. Abdollahi, "Dealing with uncertainty in pipeline integrity and rehabilitation," in *2008 7th International Pipeline Conference*, 2008, pp. 611–619.

[80] R. McCann, R. McNealy, and H. Haines, "A Bayesian Approach to Assessment of In-Line-Inspection Tool Performance," pp. 39–49, Sep. 2012.

[81] G. A. Coleman and S. J. Miller, "ILI tool tolerance and repeatability effect on corrosion growth rates," in *2010 8th International Pipeline Conference*, 2010, pp. 549–556.

[82] R. H. Adianto, J. B. Skow, and J. Sutherland, "The Benefits of Accurate ILI Performance on Pipeline Integrity Programs for Axial Crack and Metal Loss Corrosion Threats," in *2016 11th International Pipeline Conference*, 2016, p. V001T03A075–V001T03A075.

[83] T. L. Anderson and D. J. Revelle, "Advanced assessment of pipeline integrity using ILI data," *J. Pipeline Eng.*, vol. 9, no. 1, p. 29, 2010.

[84] C. Alexander, "Evaluating damage to on-and offshore pipelines using data acquired using ILI.," *J. Pipeline Eng.*, vol. 8, no. 1, 2009.

[85] A. Lockey and A. Young, "Predicting pipeline performance in geohazard areas using ILI mapping techniques," in *2012 9th International Pipeline Conference*, 2012, pp. 491–499.

[86] K. W. Ferguson, "Operator Assessment of ILI Defects," in *2006 International Pipeline Conference*, 2006, pp. 799–804.

[87] S. Brockhaus *et al.*, "In-line inspection (ILI) methods for detecting corrosion in underground pipelines," in *Underground Pipeline Corrosion*, Elsevier, 2014, pp. 255–285.

[88] P. H. Vieth, "Assessment criteria for ILI metal-loss data: B31G and RSTRENG," *J. PIPELINE Integr.*, vol. 1, no. 3, pp. 165–169, 2002.

[89] M. Lecchi, "Evaluation of predictive assessment reliability on corroded transmission pipelines," *J. Nat. Gas Sci. Eng.*, vol. 3, no. 5, pp. 633–641, Oct. 2011.

[90] N. Bates, D. Lee, and C. Maier, "A Review of Crack Detection in-Line Inspection Case Studies," in *2010 8th International Pipeline Conference*, 2010, pp. 197–208.

[91] M. Slaughter, K. Spencer, J. Dawson, and P. Senf, “Comparison of multiple crack detection in-line inspection data to assess crack growth,” in *2010 8th International Pipeline Conference*, 2010, pp. 397–406.

[92] J. E. Marr, E. Sanjuan, G. Rosea, J. Sutherland, and A. Mann, “Validation of the latest generation EMAT ILI technology for SCC management.,” *J. Pipeline Eng.*, vol. 11, no. 1, 2012.

[93] A. D. Batte, R. R. Fessler, J. E. Marr, and S. C. Rapp, “A new joint-industry project addressing the integrity management of SCC in gas transmission pipelines.,” *J. Pipeline Eng.*, vol. 11, no. 2, 2012.

[94] J. Marr *et al.*, “Combining EMAT ILI and multiple data sets for crack detection in natural gas pipelines to reduce validation costs,” *Pipeline Pigging Integr. Technol. J Tiratsoo*, pp. 161–168, 2013.

[95] S. Limon-Tapia, D. Katz, T. Beuker, C. Döscher, and B. Brown, “A framework for managing the threat of SCC and other forms of cracking in pipelines using in-line inspection tools,” in *2008 7th International Pipeline Conference*, 2008, pp. 191–197.

[96] A. Nielsen, J. Mallet-Paret, and K. Griffin, “Probabilistic Modeling of Crack Threats and the Effects of Mitigation,” in *2014 10th International Pipeline Conference*, 2014, p. V003T12A021–V003T12A021.

[97] C. R. Schneider, A. Muhammed, and R. M. Sanderson, “Predicting the remaining lifetime of in-service pipelines based on sample inspection data,” *Insight-Northamp.- Eur. Issues*, vol. 43, no. 2, pp. 102–104, 2001.

[98] A. Senouci, M. Elabbasy, E. Elwakil, B. Abdrabou, and T. Zayed, “A model for predicting failure of oil pipelines,” *Struct. Infrastruct. Eng.*, vol. 10, no. 3, pp. 375–387, Mar. 2014.

[99] L. Shilin, L. Tingquan, and C. Yanhua, “Application of Artificial Neural Network to Modeling of Pipeline Damage Prediction,” 2009, pp. 499–502.

[100] L. H. Lee, R. Rajkumar, L. H. Lo, C. H. Wan, and D. Isa, “Oil and gas pipeline failure prediction system using long range ultrasonic transducers and Euclidean-Support Vector Machines classification approach,” *Expert Syst. Appl.*, vol. 40, no. 6, pp. 1925–1934, May 2013.

[101] D. Isa and R. Rajkumar, “Pipeline defect prediction using support vector machines,” *Appl. Artif. Intell.*, vol. 23, no. 8, pp. 758–771, Oct. 2009.

[102] Y. Liu, H. Hu, and D. Zhang, “Probability Analysis of Damage to Offshore Pipeline by Ship Factors,” *Transp. Res. Rec. J. Transp. Res. Board*, vol. 2326, pp. 24–31, Dec. 2013.

[103] A. Cosham and P. Hopkins, “An overview of the pipeline defect assessment manual (PDAM),” in *4th International Pipeline Technology Conference, May*, 2004, pp. 9–13.

[104] L. Cortese, T. Coppola, F. Campanelli, F. Campana, and M. Sasso, “Prediction of ductile failure in materials for onshore and offshore pipeline applications,” *Int. J. Damage Mech.*, vol. 23, no. 1, pp. 104–123, Jan. 2014.

[105] J. L. Alamilla, M. A. Espinosa-Medina, and E. Sosa, “Modelling steel corrosion damage in soil environment,” *Corros. Sci.*, vol. 51, no. 11, pp. 2628–2638, Nov. 2009.

[106] R. E. Ricker, “Analysis of Pipeline Steel Corrosion Data From NBS (NIST) Studies Conducted Between 1922–1940 and Relevance to Pipeline Management,” *J. Res. Natl. Inst. Stand. Technol.*, vol. 115, no. 5, p. 373, 2010.

[107] T. A. Netto, U. S. Ferraz, and S. F. Estefen, “The effect of corrosion defects on the burst pressure of pipelines,” *J. Constr. Steel Res.*, vol. 61, no. 8, pp. 1185–1204, Aug. 2005.

[108] H. S. da Costa Mattos, L. M. Paim, and J. M. L. Reis, “Analysis of burst tests and long-term hydrostatic tests in produced water pipelines,” *Eng. Fail. Anal.*, vol. 22, pp. 128–140, Jun. 2012.

[109] A. N. S. Institute, *Manual for Determining the Remaining Strength of Corroded Pipelines: A Supplement to ASME B31 Code for Pressure Piping*. American Society of Mechanical Engineers, 1991.

[110] J. F. Kiefner and P. H. Vieth, “A Modified Criterion for Evaluating the Remaining Strength of Corroded Pipe,” Battelle Columbus Div., OH (USA), PR-3-805, Dec. 1989.

[111] D. Ritchie and S. Last, “Burst criteria of corroded pipelines-defect acceptance criteria,” in *Proceedings of the EPRG/PRC 10th Biennial Joint Technical Meeting on Line Pipe Research*, 1995.

[112] W. Wang, M. Q. Smith, C. H. Popelar, and J. A. Maple, “New rupture prediction model for corroded pipelines under combined loadings,” in *The 1998 International Pipeline Conference, IPC. Part 1(of 2)*, 1998, pp. 563–572.

[113] D. N. Veritas, “Recommended Practice DNV-RP-F101 Corroded Pipelines,” *Hovik Nor.*, vol. 11, 2004.

[114] D. N. Veritas, *DNV-RP-F101–Corroded Pipelines*. Norway, 1999.

[115] D. S. Cronin and R. J. Pick, “A new multi-level assessment procedure for corroded line pipe,” in *Proceedings of the Third International Pipeline Conference (IPC 2000), Calgary, Alberta, Canada, American Society of Mechanical Engineers*, 2000, pp. 801–808.

[116] B. N. Leis, D. R. Stephens, and others, “An alternative approach to assess the integrity of corroded line pipe-part I: current status,” in *The Seventh International Offshore and Polar Engineering Conference*, 1997.

[117] B. N. Leis, D. R. Stephens, and others, “An alternative approach to assess the integrity of corroded line pipe-part II: Alternative criterion,” in *The Seventh International Offshore and Polar Engineering Conference*, 1997.

[118] D. R. Stephens, B. N. Leis, M. D. Kurre, and others, “Development of an alternative criterion for residual strength of corrosion defects in moderate-to high-toughness pipe,” in *Proc. Int. Pipeline Conf*, 2000, vol. 2, pp. 781–792.

[119] J. F. Kiefner, W. Maxey, R. Eiber, and A. Duffy, “Failure stress levels of flaws in pressurized cylinders,” in *Progress in flaw growth and fracture toughness testing*, ASTM International, 1973.

[120] A. Cosham, P. Hopkins, and K. A. Macdonald, “Best practice for the assessment of defects in pipelines – Corrosion,” *Eng. Fail. Anal.*, vol. 14, no. 7, pp. 1245–1265, Oct. 2007.

[121] F. Caleyo, J. L. González, and J. M. Hallen, "A study on the reliability assessment methodology for pipelines with active corrosion defects," *Int. J. Press. Vessels Pip.*, vol. 79, no. 1, pp. 77–86, Jan. 2002.

[122] G. R. Engelhardt, R. C. Woollam, and D. D. Macdonald, "Deterministic Prediction of Localized Corrosion Damage in Oil and Gas Pipelines," *ECS Trans.*, vol. 50, no. 31, pp. 141–153, May 2013.

[123] S.-X. Li *et al.*, "A method of probabilistic analysis for steel pipeline with correlated corrosion defects," *Corros. Sci.*, vol. 51, no. 12, pp. 3050–3056, Dec. 2009.

[124] R. E. Melchers, *Structural reliability analysis and prediction*. John Wiley & Son Ltd, 1999.

[125] O. Larin, E. Barkanov, and O. Vodka, "Prediction of reliability of the corroded pipeline considering the randomness of corrosion damage and its stochastic growth," *Eng. Fail. Anal.*, vol. 66, pp. 60–71, Aug. 2016.

[126] H. Zhang, K. Liao, and Y. Li, "Computation Model of the Failure Probability and Reliability for the Submarine Oil and Gas Pipeline with Corrosion Defects," 2011, pp. 694–697.

[127] A. P. Teixeira, C. Guedes Soares, T. A. Netto, and S. F. Estefen, "Reliability of pipelines with corrosion defects," *Int. J. Press. Vessels Pip.*, vol. 85, no. 4, pp. 228–237, Apr. 2008.

[128] J. M. Race, S. J. Dawson, L. M. Stanley, and S. Kariyawasam, "Development of a predictive model for pipeline external corrosion rates," *J. Pipeline Eng.*, vol. 6, no. 1, p. 13, 2007.

[129] K. Spencer, S. Kariyawasam, C. Tetreault, and J. Wharf, "A Practical Application to Calculating Corrosion Growth Rates by Comparing Successive ILI Runs From Different ILI Vendors," in *2010 8th International Pipeline Conference*, 2010, pp. 467–473.

[130] S. Zhang and W. Zhou, "System reliability of corroding pipelines considering stochastic process-based models for defect growth and internal pressure," *Int. J. Press. Vessels Pip.*, vol. 111–112, pp. 120–130, Nov. 2013.

[131] M. Al-Amin, W. Zhou, S. Zhang, S. Kariyawasam, and H. Wang, "Hierarchical Bayesian corrosion growth model based on in-line inspection data," *J. Press. Vessel Technol.*, vol. 136, no. 4, p. 041401, 2014.

[132] S. Zhang, W. Zhou, and H. Qin, "Inverse Gaussian process-based corrosion growth model for energy pipelines considering the sizing error in inspection data," *Corros. Sci.*, vol. 73, pp. 309–320, Aug. 2013.

[133] F. A. V. Bazán and A. T. Beck, "Stochastic process corrosion growth models for pipeline reliability," *Corros. Sci.*, vol. 74, pp. 50–58, Sep. 2013.

[134] W. Zhou, "System reliability of corroding pipelines," *Int. J. Press. Vessels Pip.*, vol. 87, no. 10, pp. 587–595, Oct. 2010.

[135] A. Valor, F. Caleyo, L. Alfonso, D. Rivas, and J. M. Hallen, "Stochastic modeling of pitting corrosion: A new model for initiation and growth of multiple corrosion pits," *Corros. Sci.*, vol. 49, no. 2, pp. 559–579, Feb. 2007.

[136] J. L. Alamilla and E. Sosa, “Stochastic modelling of corrosion damage propagation in active sites from field inspection data,” *Corros. Sci.*, vol. 50, no. 7, pp. 1811–1819, Jul. 2008.

[137] Z. Weiguo, L. Dongjing, W. Hai, and P. Xinxin, “Remaining-Life Prediction and Reliability Assessment of Buried Gas Pipelines under Corrosion and Alternating Loads,” *J. Pipeline Syst. Eng. Pract.*, vol. 6, no. 1, p. 05014002, Feb. 2015.

[138] B. Medjo, M. Rakin, M. Arsic, Ž. Šarkocevic, M. Zrilic, and S. Putic, “Determination of the load carrying capacity of damaged pipes using local approach to fracture,” *Mater. Trans.*, vol. 53, no. 1, pp. 185–190, 2012.

[139] K. Das, D. Basu, and T. Mintz, “Comparative Assessment of Turbulence Models for Prediction of Flow-Induced Corrosion Damages,” in *ASME 2011 Pressure Vessels and Piping Conference*, 2011, pp. 51–60.

[140] H. Wang, A. Yajima, R. Y. Liang, and H. Castaneda, “Bayesian Modeling of External Corrosion in Underground Pipelines Based on the Integration of Markov Chain Monte Carlo Techniques and Clustered Inspection Data: Bayesian modeling of external corrosion in underground pipelines,” *Comput.-Aided Civ. Infrastruct. Eng.*, vol. 30, no. 4, pp. 300–316, Apr. 2015.

[141] E. Zdravecká, J. Slota, and J. Tkáčová, “Erosive failure of steel pipeline by solid pulverized particles,” *Eng. Fail. Anal.*, vol. 46, pp. 18–25, Nov. 2014.

[142] M. Parsi, K. Najmi, F. Najafifard, S. Hassani, B. S. McLaury, and S. A. Shirazi, “A comprehensive review of solid particle erosion modeling for oil and gas wells and pipelines applications,” *J. Nat. Gas Sci. Eng.*, vol. 21, pp. 850–873, Nov. 2014.

[143] J. I. Ukpai, R. Barker, X. Hu, and A. Neville, “Determination of particle impacts and impact energy in the erosion of X65 carbon steel using acoustic emission technique,” *Tribol. Int.*, vol. 65, pp. 161–170, Sep. 2013.

[144] A. Gnanavelu, N. Kapur, A. Neville, and J. F. Flores, “An integrated methodology for predicting material wear rates due to erosion,” *Wear*, vol. 267, no. 11, pp. 1935–1944, Oct. 2009.

[145] P. Tang *et al.*, “Failure analysis and prediction of pipes due to the interaction between multiphase flow and structure,” *Eng. Fail. Anal.*, vol. 16, no. 5, pp. 1749–1756, Jul. 2009.

[146] J. Chen, Y. Wang, X. Li, R. He, S. Han, and Y. Chen, “Erosion prediction of liquid-particle two-phase flow in pipeline elbows via CFD–DEM coupling method,” *Powder Technol.*, vol. 275, pp. 182–187, May 2015.

[147] B. Pinheiro, J. Lesage, I. Pasqualino, and N. Benseddiq, “Assessment of Fatigue Damage Initiation in Oil and Gas Steel Pipes,” in *ASME 2011 30th International Conference on Ocean, Offshore and Arctic Engineering*, 2011, pp. 35–44.

[148] M. Zheng, J. H. Luo, X. W. Zhao, Z. Q. Bai, and R. Wang, “Effect of pre-deformation on the fatigue crack initiation life of X60 pipeline steel,” *Int. J. Press. Vessels Pip.*, vol. 82, no. 7, pp. 546–552, Jul. 2005.

[149] N. I. I. Mansor, S. Abdullah, A. K. Ariffin, and J. Syarif, “A review of the fatigue failure mechanism of metallic materials under a corroded environment,” *Eng. Fail. Anal.*, vol. 42, pp. 353–365, Jul. 2014.

[150] B. de C. Pinheiro and I. P. Pasqualino, “Fatigue analysis of damaged steel pipelines under cyclic internal pressure,” *Int. J. Fatigue*, vol. 31, no. 5, pp. 962–973, May 2009.

[151] S. W. Hong, J. M. Koo, C. S. Seok, J. W. Kim, J. H. Kim, and S. K. Hong, “Fatigue life prediction for an API 5L X42 natural gas pipeline,” *Eng. Fail. Anal.*, vol. 56, pp. 396–402, Oct. 2015.

[152] P. C. Paris and F. Erdogan, “A critical analysis of crack propagation laws,” *J. Basic Eng.*, vol. 85, no. 4, pp. 528–533, 1963.

[153] D.-J. Shim and G. Wilkowski, “Bulging Factor for Axial Surface Cracks in Pipes,” in *2014 10th International Pipeline Conference*, 2014, p. V003T07A014–V003T07A014.

[154] M. Ben Amara, G. Pluvinage, J. Capelle, and Z. Azari, “Crack Tip Opening Angle as a Fracture Resistance Parameter to Describe Ductile Crack Extension and Arrest in Steel Pipes under Service Pressure,” *Phys. Mesomech.*, vol. 18, no. 4, pp. 355–369, Oct. 2015.

[155] T. L. Anderson and D. A. Osage, “API 579: a comprehensive fitness-for-service guide,” *Int. J. Press. Vessels Pip.*, vol. 77, no. 14, pp. 953–963, 2000.

[156] B. S. Institution, *Guide on methods for assessing the acceptability of flaws in metallic structures*. British Standard Institution, 1999.

[157] C. E. Jaske, *CorLAS 1.0 User Manual: Computer Program for Corrosion-Life Assessment of Piping and Pressure Vessels*. Version, 1996.

[158] C. Popelar, A. R. Rosenfield, and M. F. Kanninen, “Steady-state crack propagation in pressurized pipelines,” *J. Press. Vessel Technol.*, vol. 99, no. 1, pp. 112–121, 1977.

[159] F. Oikonomidis, A. Shterenlikht, and C. E. Truman, “Prediction of crack propagation and arrest in X100 natural gas transmission pipelines with the strain rate dependent damage model (SRDD). Part 1: A novel specimen for the measurement of high strain rate fracture properties and validation of the SRDD model parameters,” *Int. J. Press. Vessels Pip.*, vol. 105–106, pp. 60–68, May 2013.

[160] F. Oikonomidis, A. Shterenlikht, and C. E. Truman, “Prediction of crack propagation and arrest in X100 natural gas transmission pipelines with a strain rate dependent damage model (SRDD). Part 2: Large scale pipe models with gas depressurisation,” *Int. J. Press. Vessels Pip.*, vol. 122, pp. 15–21, Oct. 2014.

[161] P. S. Yu and C. Q. Ru, “A Strain Rate-Dependent Finite Element Model of Drop-Weight Tear Tests for Pipeline Steels,” in *2014 10th International Pipeline Conference*, 2014, p. V003T07A002–V003T07A002.

[162] M. Iranpour and F. Taheri, “Applicability of equivalent constant amplitude loading for assessing the fatigue life of pipelines and risers and the influence of compressive stress cycles,” *J. Press. Vessel Technol.*, vol. 135, no. 2, p. 021703, 2013.

[163] M. Iranpour and F. Taheri, “Influence of the Peak Tensile Overload Cycles on the Fatigue Crack Growth of Aluminum Alloy Under Spectrum Loading,” *J. Mater. Eng. Perform.*, vol. 22, no. 11, pp. 3490–3499, Nov. 2013.

[164] R. L. Amaro, E. S. Drexler, and A. J. Slifka, “Fatigue crack growth modeling of pipeline steels in high pressure gaseous hydrogen,” *Int. J. Fatigue*, vol. 62, pp. 249–257, May 2014.

[165] R. L. Amaro, N. Rustagi, K. O. Findley, E. S. Drexler, and A. J. Slifka, “Modeling the fatigue crack growth of X100 pipeline steel in gaseous hydrogen,” *Int. J. Fatigue*, vol. 59, pp. 262–271, Feb. 2014.

[166] A. S. Sekhar, “Multiple cracks effects and identification,” *Mech. Syst. Signal Process.*, vol. 22, no. 4, pp. 845–878, May 2008.

[167] S. J. Polasik and C. E. Jaske, “Effective Modeling of Fatigue Crack Growth In Pipelines,” in *ASME 2012 Pressure Vessels and Piping Conference*, 2012, pp. 927–933.

[168] F. Hadjoui, M. Benachour, and M. Benguediab, “Fatigue Crack Growth on Double Butt Weld with Toe Crack of Pipelines Steel,” *Mater. Sci. Appl.*, vol. 03, no. 09, pp. 596–599, 2012.

[169] A. Nonn and C. Kalwa, “Simulation of ductile crack propagation in high-strength pipeline steel using damage models,” in *2012 9th International Pipeline Conference*, 2012, pp. 597–603.

[170] J. Kumar, S. Ahmad, C. K. Mukhopadhyay, T. Jayakumar, and V. Kumar, “Acoustic emission studies for characterization of fatigue crack growth behavior in HSLA steel,” *Nondestruct. Test. Eval.*, vol. 31, no. 1, pp. 77–96, Jan. 2016.

[171] A. J. Slifka *et al.*, “Fatigue crack growth of two pipeline steels in a pressurized hydrogen environment,” *Corros. Sci.*, vol. 78, pp. 313–321, Jan. 2014.

[172] Q. Jin, Z. Y. Sun, and W. N. Guo, “Experimental and Finite Element Study on the Fatigue Growth of a Semi-Elliptical Surface Crack in a X80 Pipeline Steel Specimen,” *Appl. Mech. Mater.*, vol. 580–583, pp. 3026–3029, Jul. 2014.

[173] A. Hosseini, D. Cronin, A. Plumtree, and R. Kania, “Experimental testing and evaluation of crack defects in line pipe,” in *2010 8th International Pipeline Conference*, 2010, pp. 275–285.

[174] D. A. Pumpyanskyi *et al.*, “Crack Propagation and Arrest in X70 1420x21, 6mm Pipes for New Generation of Gas Transportation System,” in *2008 7th International Pipeline Conference*, 2008, pp. 365–370.

[175] M. B. Chen and Y. R. Jiang, “Fatigue Crack Propagation Analysis of X60 Pipeline Steel Pipelines with Defects,” *Adv. Mater. Res.*, vol. 284–286, pp. 1148–1151, Jul. 2011.

[176] M. R. Naniwadekar, S. S. Naik, and S. K. Maiti, “On prediction of crack in different orientations in pipe using frequency based approach,” *Mech. Syst. Signal Process.*, vol. 22, no. 3, pp. 693–708, Apr. 2008.

[177] D. An, J.-H. Choi, and N. H. Kim, “Identification of correlated damage parameters under noise and bias using Bayesian inference,” *Struct. Health Monit.*, p. 1475921711424520, 2011.

[178] J. Hu, Y. Tian, H. Teng, L. Yu, and M. Zheng, "The probabilistic life time prediction model of oil pipeline due to local corrosion crack," *Theor. Appl. Fract. Mech.*, vol. 70, pp. 10–18, Apr. 2014.

[179] B. T. Lu, F. Song, M. Gao, and M. Elboujdaini, "Crack growth prediction for underground high pressure gas lines exposed to concentrated carbonate–bicarbonate solution with high pH," *Eng. Fract. Mech.*, vol. 78, no. 7, pp. 1452–1465, May 2011.

[180] A. Imanian and M. Modarres, "A Thermodynamic Entropy Approach to Reliability Assessment with Applications to Corrosion Fatigue," *Entropy*, vol. 17, no. 10, pp. 6995–7020, Oct. 2015.

[181] M. Chookah, M. Nuhi, and M. Modarres, "A probabilistic physics-of-failure model for prognostic health management of structures subject to pitting and corrosion-fatigue," *Reliab. Eng. Syst. Saf.*, vol. 96, no. 12, pp. 1601–1610, Dec. 2011.

[182] C. E. Jaske and J. Beavers, "Fitness-for-service assessment for pipelines subject to stress-corrosion cracking," *Corros. Prev. Control*, vol. 47, no. 1, pp. 15–16, 2000.

[183] Y. Bai and Q. Bai, "Chapter 3 - Dented Pipelines," in *Subsea Pipeline Integrity and Risk Management*, Boston: Gulf Professional Publishing, 2014, pp. 51–71.

[184] E. R. Lancaster and S. C. Palmer, "Burst pressures of pipes containing dents and gouges," *Proc. Inst. Mech. Eng. Part E J. Process Mech. Eng.*, vol. 210, no. 1, pp. 19–27, 1996.

[185] M. Allouti, C. Schmitt, G. Pluvinage, J. Gilgert, and S. Hariri, "Study of the influence of dent depth on the critical pressure of pipeline," *Eng. Fail. Anal.*, vol. 21, pp. 40–51, Apr. 2012.

[186] H. Ghaednia, S. Das, R. Wang, and R. Kania, "Effect of Dent Depth on the Burst Pressure of NPS30 X70 Pipes With Dent-Crack Defect," in *2014 10th International Pipeline Conference*, 2014, p. V002T06A044–V002T06A044.

[187] A. Rafi, J. Silva, S. Kenno, S. Das, R. Kania, and R. Y. Wang, "Strength of Line Pipe With Dent and Crack Defect," in *2010 8th International Pipeline Conference*, 2010, pp. 151–157.

[188] K. A. Macdonald and A. Cosham, "Best practice for the assessment of defects in pipelines – gouges and dents," *Eng. Fail. Anal.*, vol. 12, no. 5, pp. 720–745, Oct. 2005.

[189] A. Cosham and P. Hopkins, "The effect of dents in pipelines—guidance in the pipeline defect assessment manual," *Int. J. Press. Vessels Pip.*, vol. 81, no. 2, pp. 127–139, Feb. 2004.

[190] P. A. Ivanov *et al.*, "Magnetic flux leakage modeling for mechanical damage in transmission pipelines," *IEEE Trans. Magn.*, vol. 34, no. 5, pp. 3020–3023, 1998.

[191] B. Bolton, V. Semiga, A. Dinovitzer, S. Tiku, and C. Alexander, "Towards a Validated Pipeline Dent Integrity Assessment Model," pp. 893–903, Jan. 2008.

[192] E. Dama, S. A. Karamanos, and A. M. Gresnigt, "Failure of Locally Buckled Pipelines," *J. Press. Vessel Technol.*, vol. 129, no. 2, p. 272, 2007.

[193] B. Bolton, V. Semiga, S. Tiku, A. Dinovitzer, and J. Zhou, "Full scale cyclic fatigue testing of dented Pipelines and development of a Validated Dented Pipe Finite Element Model," in *2010 8th International Pipeline Conference*, 2010, pp. 863–872.

[194] M. Azadeh and F. Taheri, "On the response of dented stainless-steel pipes subject to cyclic bending moments and its prediction," *Thin-Walled Struct.*, vol. 99, pp. 12–20, Feb. 2016.

[195] D. B. Noronha, R. R. Martins, B. P. Jacob, and E. de Souza, "Procedures for the strain based assessment of pipeline dents," *Int. J. Press. Vessels Pip.*, vol. 87, no. 5, pp. 254–265, May 2010.

[196] G. Goodfellow, S. Turner, J. Haswell, and R. Espiner, "An Update to the UKOPA Pipeline Damage Distributions," in *2012 9th International Pipeline Conference*, 2012, pp. 541–547.

[197] S. M. Hsu, M. C. Shen, and A. W. Ruff, "Wear prediction for metals," *Tribol. Int.*, vol. 30, no. 5, pp. 377–383, 1997.

[198] S. El-Hussein, J. J. Harrigan, and A. Starkey, "Finite element simulation of guided waves in pipelines for long range monitoring against third party attacks," *J. Phys. Conf. Ser.*, vol. 628, p. 012039, Jul. 2015.

[199] A. S. Oddy and J. M. J. McDill, "Burnthrough prediction in pipeline welding," *Int. J. Fract.*, vol. 97, no. 1–4, pp. 249–261, 1999.

[200] X.-C. Niu, J.-M. Gong, Y. Jiang, and J.-T. Bao, "Creep damage prediction of the steam pipelines with high temperature and high pressure," *Int. J. Press. Vessels Pip.*, vol. 86, no. 9, pp. 593–598, Sep. 2009.

[201] R. T. Hill and A. D. Director, "Pipeline risk analysis," in *Institution of Chemical Engineers Symposium Series*, 1993, vol. 130, pp. 657–657.

[202] P. Dey, M. T. Tabucanon, and S. O. Ogunlana, "Planning for project control through risk analysis: a petroleum pipeline-laying project," *Int. J. Proj. Manag.*, vol. 12, no. 1, pp. 23–33, 1994.

[203] A. S. Akintoye and M. J. MacLeod, "Risk analysis and management in construction," *Int. J. Proj. Manag.*, vol. 15, no. 1, pp. 31–38, 1997.

[204] Z.-G. Zhao, A.-L. Yao, and X.-F. Zhao, "Study of quality evaluation of oil and gas pipeline risk analysis," *Anquan Yu Huanjing XuebaoJournal Saf. Environ.*, vol. 5, no. 5, pp. 28–32, 2005.

[205] S. Bott and R. Sporns, "The Benefits and Limitations of Using Risk Based Probabilistic and Deterministic Analysis for Monitoring and Mitigation Planning," in *2008 7th International Pipeline Conference*, 2008, pp. 797–807.

[206] W. Zhou and M. A. Nessim, "Optimal design of onshore natural gas pipelines," *J. Press. Vessel Technol.*, vol. 133, no. 3, p. 031702, 2011.

[207] C.-H. Chien and C.-H. Chen, "Reliability Analysis of Pressure Vessels in Lubricant Process Unit for Risk Based Inspection," in *ASME 2008 Pressure Vessels and Piping Conference*, 2008, pp. 1427–1435.

[208] V. V. Kuznetsov, M. G. Malyukova, and S. A. Timashev, “Bayesian reassessment of the number of flaws in a pipeline,” *Russ. J. Nondestruct. Test.*, vol. 48, no. 5, pp. 309–318, May 2012.

[209] S. B. Cunha, “Comparison and analysis of pipeline failure statistics,” in *2012 9th International Pipeline Conference*, 2012, pp. 521–530.

[210] K. McCallum *et al.*, “Localized Corrosion Risk Assessment Using Markov Analysis,” *Corrosion*, vol. 70, no. 11, pp. 1114–1127, Nov. 2014.

[211] J. N. Mihell and C. Rout, “Risk Assessment of Modern Pipelines,” in *2012 9th International Pipeline Conference*, 2012, pp. 497–503.

[212] P. Tuft, N. Yoosef-Ghodsi, and J. Bertram, “Benchmarking pipeline risk assessment processes,” in *2012 9th International Pipeline Conference*, 2012, pp. 477–486.

[213] A. W. Dawotola, T. B. Trafalis, Z. Mustaffa, P. H. A. J. M. van Gelder, and J. K. Vrijling, “Risk-Based Maintenance of a Cross-Country Petroleum Pipeline System,” *J. Pipeline Syst. Eng. Pract.*, vol. 4, no. 3, pp. 141–148, 2013.

[214] Y. Bai, M. Ashri, M. F. Badaruddin, X. Bai, and S. L. He, “Risk Based Inspection (RBI) for Subsea Equipments,” in *ASME 2010 29th International Conference on Ocean, Offshore and Arctic Engineering*, 2010, pp. 527–534.

[215] S. K. Sinha and R. A. McKim, “Probabilistic based integrated pipeline management system,” *Tunn. Undergr. Space Technol.*, vol. 22, no. 5–6, pp. 543–552, Sep. 2007.

[216] K. F. Tee, L. R. Khan, H. P. Chen, and A. M. Alani, “Reliability based life cycle cost optimization for underground pipeline networks,” *Tunn. Undergr. Space Technol.*, vol. 43, pp. 32–40, Jul. 2014.

[217] Y. Sahraoui, R. Khelif, and A. Chateauneuf, “Maintenance planning under imperfect inspections of corroded pipelines,” *Int. J. Press. Vessels Pip.*, vol. 104, pp. 76–82, Apr. 2013.

[218] M. Stephens, M. Nessim, and A. van Roodselaar, “Reliability-Based Corrosion Management: The Impact of Maintenance and Implications for the Time to Next Inspection,” in *2010 8th International Pipeline Conference*, 2010, pp. 595–604.

[219] H. P. Hong, “Inspection and maintenance planning of pipeline under external corrosion considering generation of new defects,” *Struct. Saf.*, vol. 21, no. 3, pp. 203–222, Sep. 1999.

[220] P. J. Moreno *et al.*, “Development and Application of Local Corrosion Growth Rates for Pipeline Integrity Assessments,” in *NACE International, Proceedings of Corrosion 2012 Conference*, 2012.

[221] W. J. S. Gomes, A. T. Beck, and T. Haukaas, “Optimal inspection planning for onshore pipelines subject to external corrosion,” *Reliab. Eng. Syst. Saf.*, vol. 118, pp. 18–27, Oct. 2013.

[222] W. J. S. Gomes and A. T. Beck, “Optimal inspection planning and repair under random crack propagation,” *Eng. Struct.*, vol. 69, pp. 285–296, Jun. 2014.

[223] B. Kamsu-Foguem, "Information structuring and risk-based inspection for the marine oil pipelines," *Appl. Ocean Res.*, vol. 56, pp. 132–142, Mar. 2016.

[224] S.-W. Tien, W.-T. Hwang, and C.-H. Tsai, "Study of a risk-based piping inspection guideline system," *ISA Trans.*, vol. 46, no. 1, pp. 119–126, Feb. 2007.

[225] M. J. Kallen and J. M. van Noortwijk, "Optimal maintenance decisions under imperfect inspection," *Reliab. Eng. Syst. Saf.*, vol. 90, no. 2–3, pp. 177–185, Nov. 2005.

[226] M. Singh and T. Markeset, "A methodology for risk-based inspection planning of oil and gas pipes based on fuzzy logic framework," *Eng. Fail. Anal.*, vol. 16, no. 7, pp. 2098–2113, Oct. 2009.

[227] P. K. Dey, "Decision Support System for Inspection and Maintenance: A Case Study of Oil Pipelines," *IEEE Trans. Eng. Manag.*, vol. 51, no. 1, pp. 47–56, Feb. 2004.

[228] W. K. Muhlbauer, *Pipeline risk management manual*, 2nd ed. Houston: Gulf Pub. Co, 1996.

[229] Z. Tian, T. Jin, B. Wu, and F. Ding, "Condition based maintenance optimization for wind power generation systems under continuous monitoring," *Renew. Energy*, vol. 36, no. 5, pp. 1502–1509, May 2011.

[230] Z. Tian and H. Liao, "Condition based maintenance optimization for multi-component systems using proportional hazards model," *Reliab. Eng. Syst. Saf.*, vol. 96, no. 5, pp. 581–589, May 2011.

[231] J. K. Seo, Y. Cui, M. H. Mohd, Y. C. Ha, B. J. Kim, and J. K. Paik, "A risk-based inspection planning method for corroded subsea pipelines," *Ocean Eng.*, vol. 109, pp. 539–552, Nov. 2015.

[232] R. R. Fessler and S. Rapp, "Method for Establishing Hydrostatic Re-Test Intervals for Pipelines with Stress-Corrosion Cracking," in *2006 International Pipeline Conference*, 2006, pp. 259–263.

[233] M. Zarea, M. Piazza, G. Vignal, C. Jones, J. Rau, and R. Wang, "Review of r&d in support of mechanical damage threat management in onshore transmission pipeline operations," in *2012 9th International Pipeline Conference*, 2012, pp. 569–582.

[234] A. Ganji and L. Jowkarshorijeh, "Advance first order second moment (AFOSM) method for single reservoir operation reliability analysis: a case study," *Stoch. Environ. Res. Risk Assess.*, vol. 26, no. 1, pp. 33–42, Jan. 2012.

[235] R. Rackwitz and B. Flessler, "Structural reliability under combined random load sequences," *Comput. Struct.*, vol. 9, no. 5, pp. 489–494, Nov. 1978.

[236] F. Zhao, Z. Tian, and Y. Zeng, "Uncertainty Quantification in Gear Remaining Useful Life Prediction Through an Integrated Prognostics Method," *IEEE Trans. Reliab.*, vol. 62, no. 1, pp. 146–159, Mar. 2013.

[237] F. Zhao, Z. Tian, E. Bechhoefer, and Y. Zeng, "An integrated prognostics method under time-varying operating conditions," *IEEE Trans. Reliab.*, vol. 64, no. 2, pp. 673–686, 2015.

[238] M. Roshanfar and M. H. Salimi, “Comparing of methods of cycle calculating and counting to the rain flow method,” 2015.

[239] NIST, Materials Reliability Division, “Mechanical Properties and Crack Behavior in Line Pipe Steels,” *DOT Q. Rep.*, 2007.

[240] H. M. Al-Muslim and A. F. M. Arif, “Effect of geometry, material and pressure variability on strain and stress fields in dented pipelines under static and cyclic pressure loading using probability analysis,” in *Proceedings of the ASME International Pipeline Conference 2010, VOL 1*, New York, NY 10016-5990 USA, 2010, pp. 381–395.

[241] J. Silva, H. Ghaednia, and S. Das, “Fatigue life assessment for NPS30 steel pipe,” in *Proceedings of the 9th International Pipeline Conference*, New York, NY 10016-5990 USA, 2012, pp. 619–624.

[242] D. Shim and G. Wilkowski, “Bulging factor for axial surface cracks in pipes,” presented at the The 10th International Pipeline Conference, 2014.

[243] J. Newman and I. Raju, “An empirical stress-intensity factor equation for the surface crack,” *Eng. Fract. Mech.*, vol. 15, no. 1–2, pp. 185–192, 1981.

[244] Michael Baker Jr., *OPS TTO5 – Low Frequency ERW and Lap Welded Longitudinal Seam Evaluation*. 2004.

[245] M. Chookah, M. Nuhi, and M. Modarres, “A probabilistic physics-of-failure model for prognostic health management of structures subject to pitting and corrosion-fatigue,” *Reliab. Eng. Syst. Saf.*, vol. 96, no. 12, pp. 1601–1610, Dec. 2011.

[246] Q. Jin, Z. Sun, and W. Guo, “Experimental and finite element study on the fatigue growth of a semi-elliptical surface crack in aX80 pipeline steelspecimen,” in *Advances in Civil and Industrial Engineering Iv*, vol. 580–583, G. Li, C. Chen, B. Jiang, and Q. Shen, Eds. 2014, pp. 3026–3029.

[247] A. Carpinteri and R. Brighenti, “Circumferential surface flaws in pipes under cyclic axial loading,” *Eng. Fract. Mech.*, vol. 60, no. 4, pp. 383–396, Jul. 1998.

[248] A. Carpinteri, “Shape change of surface cracks in round bars under cyclic axial loading,” *Int. J. Fatigue*, vol. 15, no. 1, pp. 21–26, Jan. 1993.

[249] F. Zhao, Z. Tian, and Y. Zeng, “A stochastic collocation approach for efficient integrated gear health prognosis,” *Mech. Syst. Signal Process.*, vol. 39, no. 1–2, pp. 372–387, Sep. 2013.

[250] Z. Y. Han and W. G. Weng, “Comparison study on qualitative and quantitative risk assessment methods for urban natural gas pipeline network,” *J. Hazard. Mater.*, vol. 189, no. 1–2, pp. 509–518, May 2011.

[251] F. Li, L. Ma, Y. Sun, and J. Mathew, “Optimized Group Replacement Scheduling for Water Pipeline Network,” *J. Water Resour. Plan. Manag.*, vol. 142, no. 1, p. 04015035, Jan. 2016.

[252] S. Zhang and W. Zhou, “System reliability of corroding pipelines considering stochastic process-based models for defect growth and internal pressure,” *Int. J. Press. Vessels Pip.*, vol. 111–112, pp. 120–130, Nov. 2013.

[253] X. Li, G. Chen, and H. Zhu, “Quantitative risk analysis on leakage failure of submarine oil and gas pipelines using Bayesian network,” *Process Saf. Environ. Prot.*, vol. 103, pp. 163–173, Sep. 2016.

[254] W. A. Fuller, *Measurement error models*, vol. 305. John Wiley & Sons, 2009.

[255] J. L. Jaech, *Statistical analysis of measurement errors*, vol. 2. John Wiley & Sons Incorporated, 1985.

[256] Y. Bai and Q. Bai, “Chapter 9 - Risk-Based Inspection,” in *Subsea Pipeline Integrity and Risk Management*, Boston: Gulf Professional Publishing, 2014, pp. 213–232.

[257] S. Zhang and W. Zhou, “Cost-based optimal maintenance decisions for corroding natural gas pipelines based on stochastic degradation models,” *Eng. Struct.*, vol. 74, pp. 74–85, Sep. 2014.

[258] W. A. Maxey, J. F. Kiefner, R. J. Eiber, and A. R. Duffy, “Ductile fracture initiation, propagation, and arrest in cylindrical vessels,” in *Fracture Toughness: Part II*, ASTM International, 1972.

[259] R. J. Eiber, *The Effects of Dents on Failure Characteristics of Line Pipe*. American Gas Assn, 1981.

[260] J. F. Kiefner, W. Maxey, R. Eiber, and A. Duffy, “Failure stress levels of flaws in pressurized cylinders,” in *Progress in flaw growth and fracture toughness testing*, ASTM International, 1973.

[261] B. BSI, *7910: 2013+ A1: 2015: Guide to Methods for Assessing the Acceptability of Flaws in Metallic Structures*. December, 2013.

[262] C. E. Jaske and J. A. Beavers, “Review and proposed improvement of a failure model for SCC of pipelines,” in *1998 2nd International Pipeline Conference*, 1998, pp. 439–445.

[263] C. E. Jaske and J. A. Beavers, “Development and evaluation of improved model for engineering critical assessment of pipelines,” in *2002 4th International Pipeline Conference*, 2002, pp. 1459–1466.

[264] F. Zhao, Z. Tian, and Y. Zeng, “Uncertainty quantification in gear remaining useful life prediction through an integrated prognostics method,” *IEEE Trans. Reliab.*, vol. 62, no. 1, pp. 146–159, Mar. 2013.

[265] S. Bott and R. Sporns, “The benefits and limitations of using risk based probabilistic and deterministic analysis for monitoring and mitigation planning,” in *Proceedings of the Biennial International Pipeline Conference, IPC*, 2009, vol. 2, pp. 797–807.